ECN-102

ECN-102

ECN

OCTOBER 1981

THERMOCHEMICAL INVESTIGATIONS ON INTERMETALLIC UMe_3 COMPOUNDS (ME = Ru, Rh, Pd)

BY
G. WIJBENGA

Thesis Amsterdam University, 9 December 1981

Netherlands Energy Research Foundation

Netherlands Energy Research Foundation ECN

P.O. Box 1

1755 ZG Petten (NH)

The Netherlands

Telephone (0)2246 - 6262

Telex 57211

ECN-102

OCTOBER 1981

THERMOCHEMICAL INVESTIGATIONS ON INTERMETALLIC UMe_3 COMPOUNDS (Me = Ru, Rh, Pd)

BY
G. WIJBENGA

Thesis Amsterdam University, 9 December 1981

CONTENTS

CHAPTER I

INTRODUCTION

I.1. FISSION PRODUCTS IN NUCLEAR FUEL

This thesis describes an investigation into the high-temperature thermodynamic properties of the intermetallic compounds of uranium with the light platinum metals, ruthenium, rhodium and palladium. These intermetallic compounds are of technological importance because they are formed during fission of nuclear fuel in a reactor.
In mixed uranium-plutonium oxide fuel, $(U,Pu)C_2$, these compounds have been identified as face-centered cubic $(U,Pu)Me_3$ phases (Me = Ru, Rh and Pd) [1]. The importance of $(U,Pu)Me_3$ phases in reactor technology is that considerable plutonium enrichment [1,5] has been found in these phases compared to the U/Pu ratio in mixed oxide fuels. In addition, the $(U,Pu)Me_3$ compounds have a very high resistance to dissolution in acids, which will cause undesired plutonium losses during reprocessing.
During neutron-induced fission of uranium and plutonium, according to

$$U(Pu) + n \rightarrow X_1 + X_2 + \nu n + \text{energy}$$

the fission products X_1 and X_2 are formed in concentrations which depend on:
a. the concentrations of uranium and plutonium in the fuel,
b. the neutron energy spectrum (thermal or fast).
The symbol ν stands for the number of neutrons, which is about 2.5, depending on the neutron energy spectrum.

When the yield of the fission products is plotted against mass number a graph is obtained with two peaks (fig. 1.1.). For plutonium-239 in a fast reactor the peak on the left is composed mainly of the elements strontium, yttrium, zirconium, molybdenum and technetium, having the mass numbers 88-100, and the light platinum metals (Ru, Rh and Pd) with mass numbers 101-108. The peak on the right consists of the elements xenon, cesium and barium (mass numbers 131-138), and the rare earth metals (La, Ce, Pr, Nd, Pm, Sm) with mass numbers 139-152 [2,3]. The yield of fission products has been given in fig. 1.1. for plutonium-

239. For fission of uranium-235 in a fast neutron flux, and also of Pu-239 and U-235 in a thermal neutron flux, the yield of light platinum metals will be lower compared with the fission of Pu-239 in fast neutrons (fig. 1.2. and fig. 1.3.) [4].

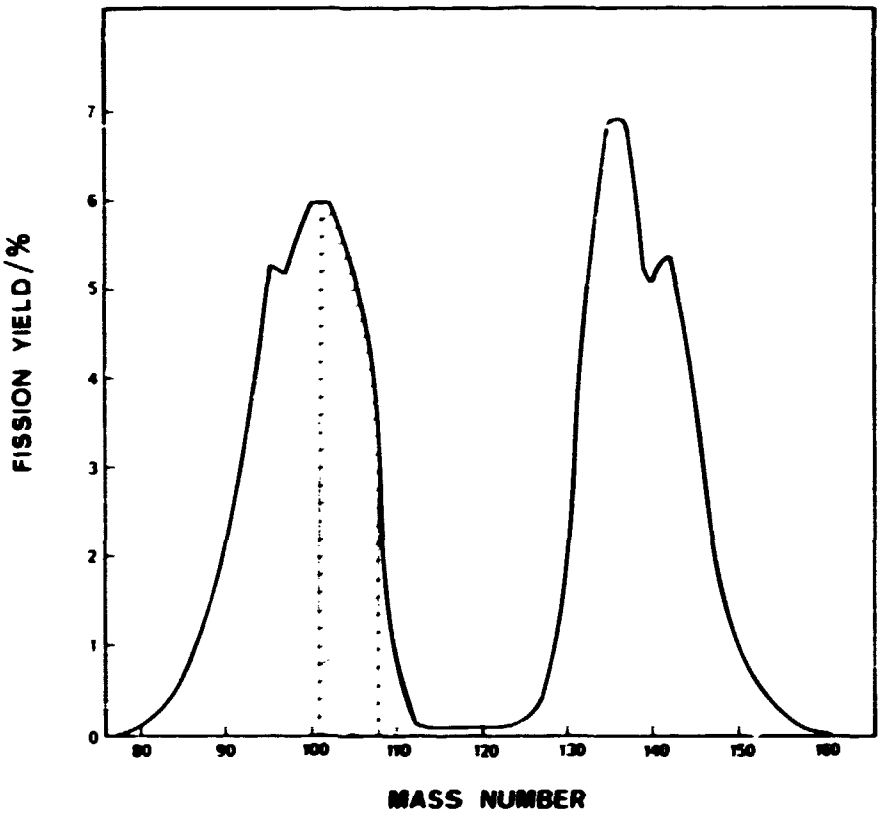

Fig. 1.1. Yield-mass curve for fast-neutron fission of Pu^{239} [2].

The fission products described above may react with each other and with the matrix and form very stable compounds.
Kleykamp [5], on the basis of post-irradiation studies, has classified the types of compounds formed into three groups:

a. fission product - fuel component phases,

b. fission product - fission product phases, and

c. fission product - cladding material inclusions.

Among the fission products the light platinum metals form a dominant group. In hypostoichiometric mixed-oxide fuel $[(U,Pu)O_{2-x})]$ at high temperatures the noble metals Rh and Pd form stable intermetallic

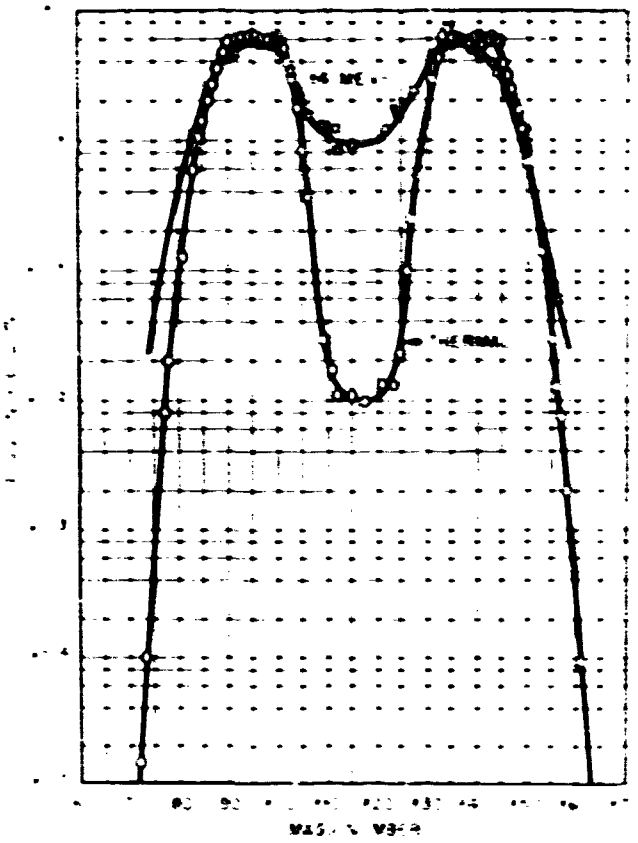

Fig. 1.2.
Yield-mass curve for fast and slow-neutron fission of U^{235} [4].

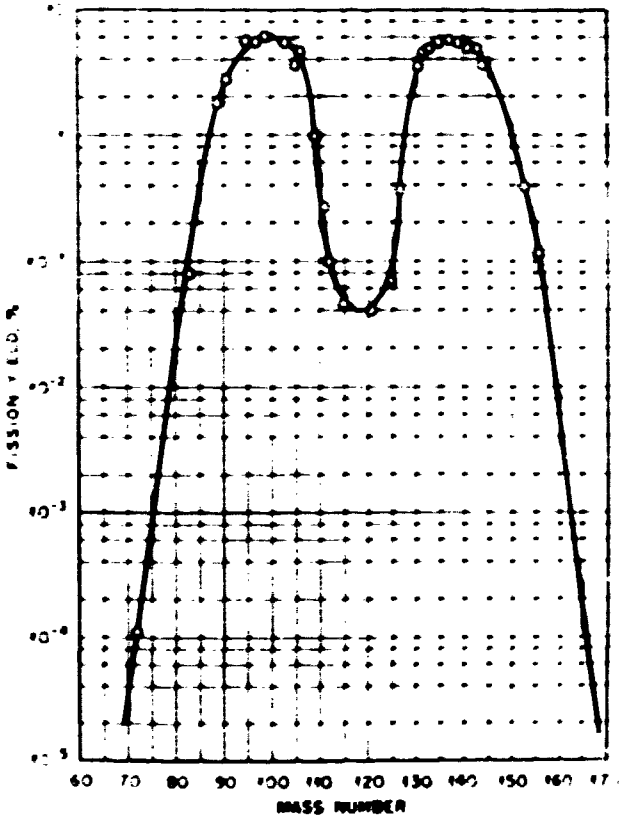

Fig. 1.3.
Yield-mass curve for slow-neutron fission of Pu^{239} [4].

compounds with the actinides of the type: $(U,Pu)(Rh,Pd)_3$ [2,6]. This suggests a very negative Gibbs energy of formation of the binary compounds. Palladium is a fission product which alloys in a variety of other fission products, fuel components and cladding materials. Besides the formation of $(U,Pu)(Rh,Pd)_3$, precipitation of (Mo,Tc,Ru,Rh,Pd) solid solutions occurs [5]. Actinide containing compounds $(U,Pu)(Pd,In,Sn,Te)_{3+x}$ with high Pd contents and high Pu/U ratios have been observed also in the fuel-cladding interface [6]. The $(U,Pu)Me_3$ phase (Me = Ru, Rh and Pd) has been detected in oxide as well as in carbide fuel [7].

In carbide fuels, the type of compound formed also depends on the stoichiometry. The reactions between hypostoichiometric (UC_{1-x}) and hyperstoichiometric (UC_{1+x}) fuel and various fission products have been investigated in detail [8]. In UC_{1-x} the following noble metal containing phases were identified: $U_2(Ru,Rh)C_2$, $(U,R.E.)_a(Ru,Rh)_b$ in which R.E. are rare earth metals, and $(U,R.E.)_c(Ru,Rh,Pd)_d$ [9]. In hyperstoichiometric fuel the phases identified were $U_2(Ru,Rh)C_2$, and $(U,Zr)\ Pd_{3-4}$ [10].

I.2. PHASE DIAGRAMS OF THE U-Me SYSTEMS

The extreme stability of the UMe_3 phases is illustrated by the phase diagrams (Me = Ru, Rh and Pd). It will be seen that the UMe_3 intermetallic phases have the highest melting points.

The uranium-ruthenium system

In the phase diagram of the uranium-ruthenium system in fig. 1.4. [11] the compound URu_3 is formed peritectically and melts incongruently at

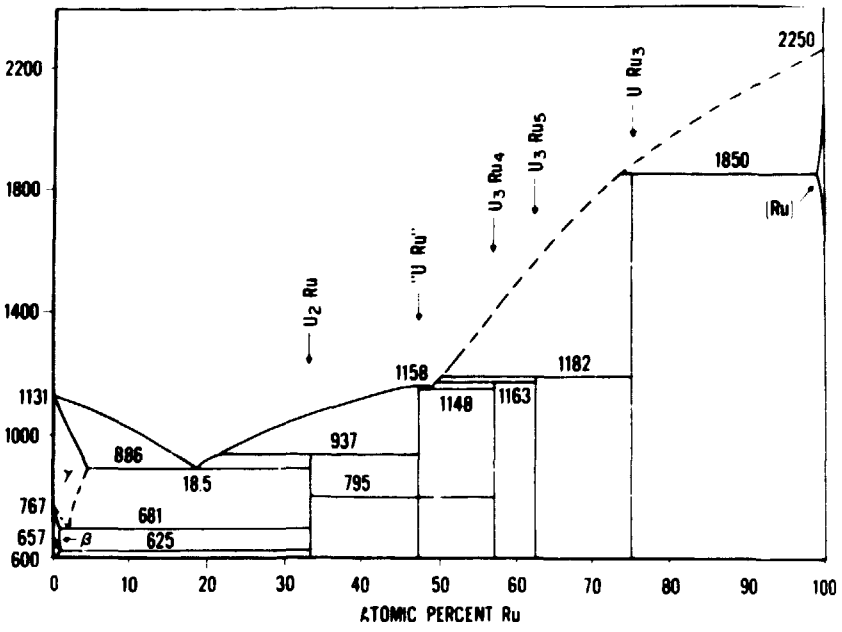

Fig. 1.4. U-Ru phase diagram [11].

about 1850 °C. URu_3 is cubic, $AuCu_3$ type, with a = 3.980 Å and a calculated density of 14.24 g cm^{-3} [12].

The uranium-rhodium system

Park [13] established the main features of the phase diagram of the uranium-rhodium system, as given in fig. 1.5. The compound URh_3 melts congruently at 1700 °C. It has been found recently that the melting point of URh_3 is in fact somewhat higher; 1750 ± 5 °C [14].

The compound URh_3 is cubic, $AuCu_3$ type, with a = 3.991 Å [15].

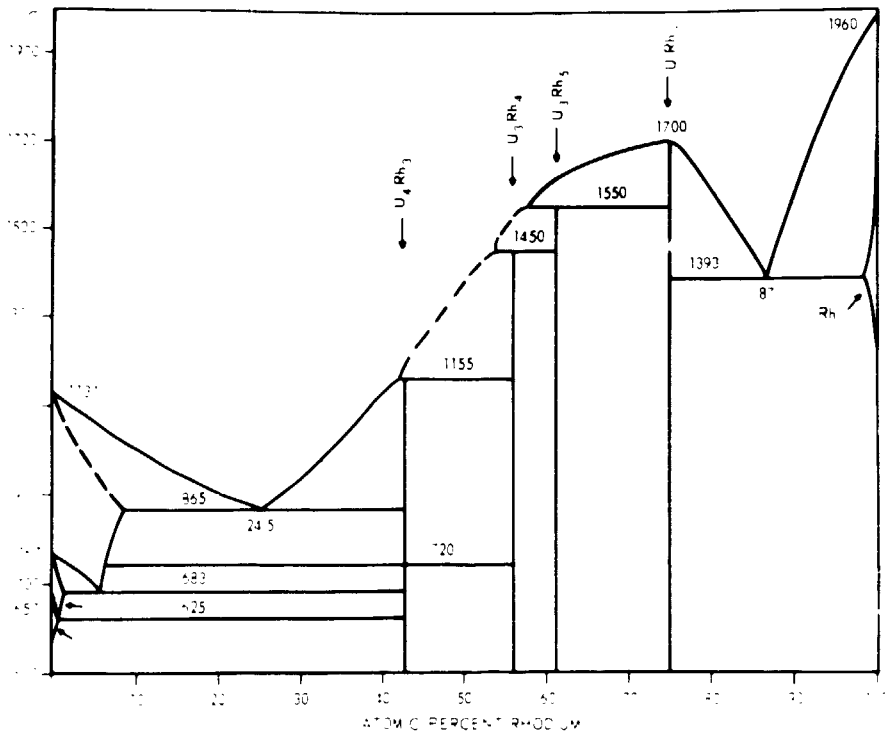

Fig.1.5. U-Rh phase diagram [13,23].

The uranium-palladium system

The phase diagram of the uranium-palladium system is given in fig. 1.6. The uranium-rich part of the phase diagram, up to 75 atom % palladium was established by Catterall et al. [16]. The compound UPd_3 melts congruently at about 1650 °C.

It has been found recently that the melting point of UPd_3 is somewhat higher; 1700 ± 10 °C [14]. The palladium-rich part of the U-Pd phase diagram has been studied by several authors [16,17,18], and has been found to be very complex. The results of the various authors do not agree very well. The compound UPd_3 is hexagonal, with a = 5.769 Å, c = 9.640 Å and calculated density of 13.39 g cm^{-3} [12]. The compound UPd_4 is cubic, $AuCu_3$ type, with a = 4.063 Å; and has a variation in its lattice parameters with composition [17].

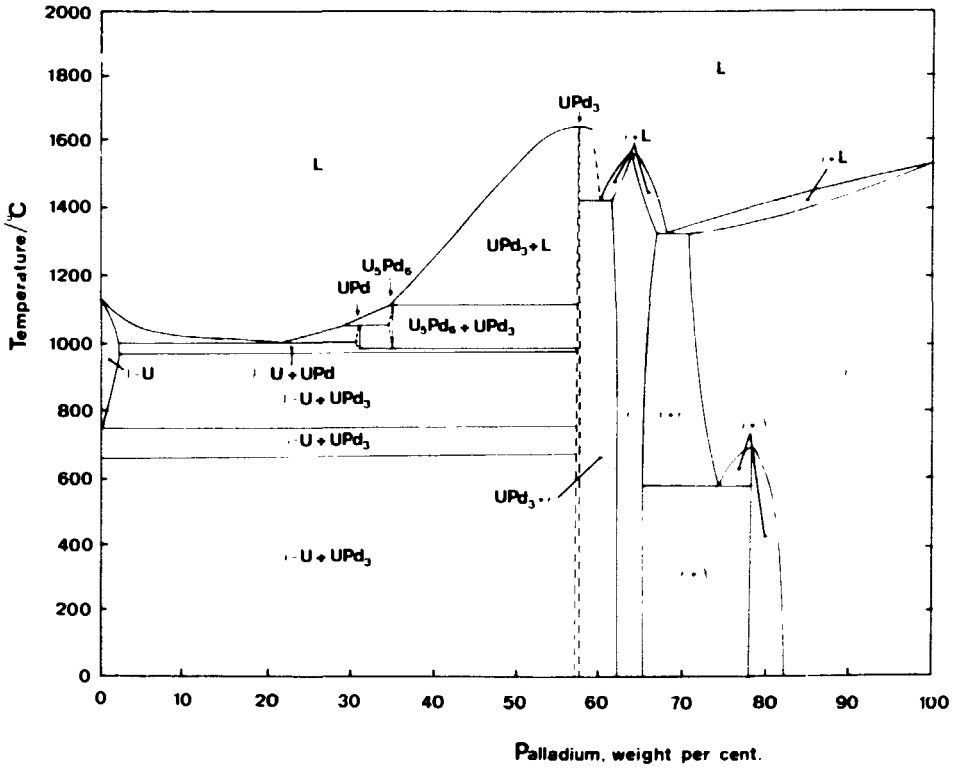

Fig. 1.6. U-Pd phase diagram [16,17,18].

I.3. PLUTONIUM ENRICHMENT IN $(U,Pu)Me_3$ INCLUSIONS

The compounds URu_3, URh_3, UPd_3, $PuRu_2$, $PuRh_3$ and $PuPd_3$ have such a high thermodynamic stability that the reaction:

$$(U,Pu)O_{2-x} + 3\ Me \rightarrow (U,Pu)Me_3 + (1-0.5x)O_2$$

takes place in the fuel [1,5]. It can thus be concluded that

$$\Delta G^o\{(U,Pu)Me_3\} < \Delta G^o\{(U,Pu)O_{2-x}\} - (1-0.5x)\overline{\Delta G}_{O_2} \qquad (1\text{-}1)$$

in which $\overline{\Delta G}_{O_2} = RT\ln p_{O_2}$ is the oxygen potential for the U-Pu oxide fuel, which is a function of temperature, U/Pu ratio and O/(U+Pu) ratio. PuO_2 and UO_2 form an ideal solid solution, and the ΔG^o of the solid solution is given by

$$\Delta G^o\{(U,Pu)O_2\} = n_1\ \overline{\Delta G}_{UO_2} + n_2\ \overline{\Delta G}_{PuO_2} + RT\{n_1\ \ln n_1 + n_2\ \ln n_2\} \qquad (1\text{-}2)$$

in which n_1 and n_2 are the mole fractions of UO_2 and PuO_2, respectively. One of the most crucial parameters for (U,Pu) oxide fuel is the oxygen potential $\overline{\Delta G}_{O_2}$. For a given O/M ratio (M = U+Pu) and for a given plutonium concentration, the U-Pu oxide has a higher oxygen equilibrium pressure or more positive oxygen potential than pure UO_2. Depending on temperature and composition, the oxygen pressure may be many orders of magnitude higher than in the case of uranium oxide of the same oxygen concentration, as can be seen in fig. 1.7. [19-22].
A quantitative analysis of particular metallic inclusions in mixed-oxide fuel, $(U_{0.8}\ Pu_{0.2})O_2$ adjacent to the central void, gave 18 at % U, 8 at % Pu, 1 at % Ru, 15 at % Rh and 59 at % Pd, which shows a significant Pu enrichment in these inclusions [1,5]. Composition and structure (fcc, $a_o = 4.127 \pm 0.002$ Å) are in agreement with the solid solution $(U,Pu)Me_3$.
A range of standard Gibbs energies of formation of $(U,Pu)Me_3$ phases can be calculated from relations (1-1) and (1-2) at a given temperature as a function of $\overline{\Delta G}_{O_2}$. A prediction can be made of the maximum Pu/U ratio in $(U,Pu)Me_3$ as a function of $\overline{\Delta G}_{O_2}$ at constant T, using the experimental values for $\Delta G^o(UMe_3)$, estimates for $\Delta G^o(PuMe_3)$ and an analysis of

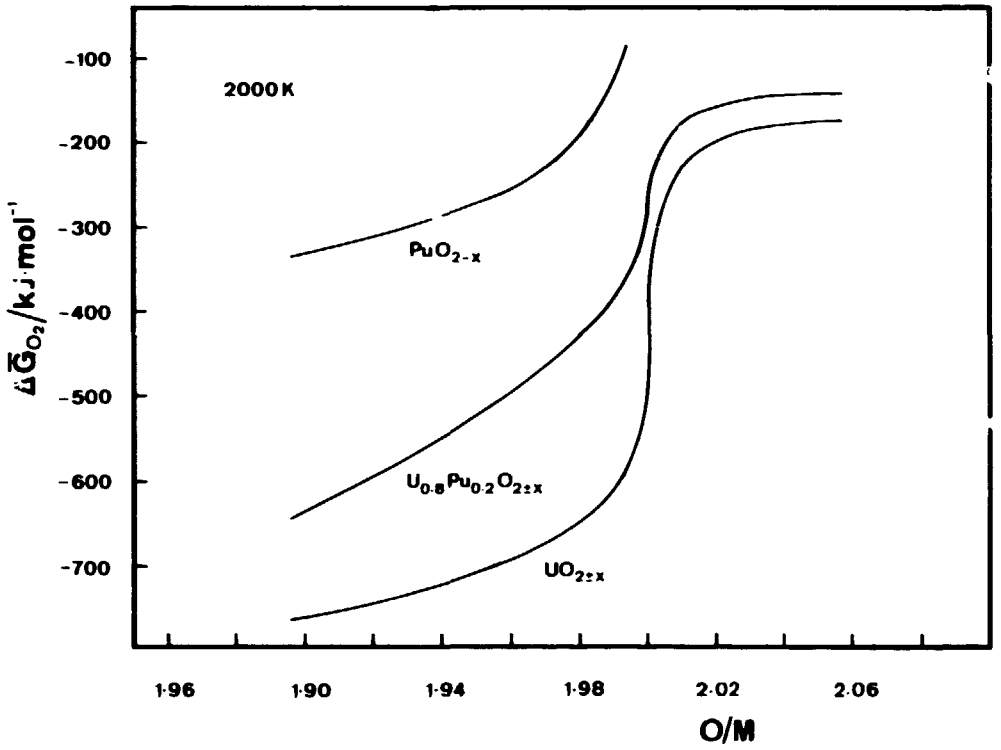

Fig. 1.7. Oxygen potentials at 2000 K for $UO_{2\pm x}$, PuO_{2-x} and $U_{0.8}Pu_{0.2}O_{2\pm x}$.

solid solutions, as given above [5].

The principal investigations described in this thesis with respect to the formation of $(U,Pu)Me_3$ phases in mixed-oxide fuel are the following.

Preparation methods of the UMe_3 compounds are given in chapter II. The enthalpy of formation of UPd_3 by fluorine bomb calorimetry and the Gibbs energies of formation of URh_3 and URu_3 by solid state EMF techniques are determined in chapters III and IV. Estimation procedures for estimating the enthalpies of formation of $PuMe_3$ compounds are discussed in chapter V. In chapter VI low and high-temperature heat capacity measurements of the UMe_3 compounds are given, and their thermodynamic functions are presented. Using these data a model was set up to describe plutonium enrichment in $(U,Pu)Me_3$ inclusions as a function of the O/(U + Pu) ratio in oxide fuel.

REFERENCES

[1] Bramman, J.I.; Sharpe, R.M.; Thom, D.; Yates, G. J. Nucl. Mater. 25 (1968) 201.

[2] Holleck, H.; Kleykamp, H. KFK-report 1181 (1970).

[3] Kleykamp, H. Mikrosondenuntersuchungen an bestrahlten Carbid-Brennstäben, Reaktortagung, Düsseldorf (1976).

[4] Reactor Handbook 2nd edition. Vol. III part A: physics. H. Soodak (ed.) Interscience Publishers, New York (1962) p. 10-11.

[5] Kleykamp, H. In: Behaviour and Chemical State of Irradiated Ceramic Fuels. IAEA, Vienna (1974) p. 157-166.

[6] Kleykamp, H.; Gottschalg, H.D.; Fritzen, R.; Laumer, W.; Späte, H. PSP-Bericht 636, October 1978.

[7] Holleck, H.; Kleykamp, H. KFK-report 1271-1 (1971).

[8] Smailos, E. KFK-report 1953 (1974).

[9] Holleck, H.; Smailos, E. KFK-report 1272/1 (1972).

[10] Holleck, H.; Smailos, E. KFK-report 1272/3 (1972).

[11] Park, J.J. J. Res. NBS. 72A (1968) 1.

[12] Heal, T.J.; Williams, G.I. Acta Crystallogr. 8 (1955) 494.

[13] Park, J.J. J. Res. NBS. 72A (1968) 11.

[14] Cordfunke, E.H.P. Personal communication.

[15] Dwight, A.E.; Downey, J.W.: Conner, R.A. Jr. Acta Crystallogr. 14 (1961) 75.

[16] Catterall, J.A.; Grogan, J.D.; Pleasance, R.J. J. Inst. Metals 85 (1956-57) 63.

[17] Pells, G.P. J. Inst. Metals 92 (1963-64) 416.

[18] Terekhov, G.I.; Sinyakova, S.I.; Vedernikov, M.V.; Ivanov, O.S. In: Physical Chemistry of Alloys an High melting Compounds of Thorium and Uranium. Academy of Science of the USSR. Institute for Metallurgy, Verlag Nauka, Moskau (1968) p. 103.

[19] Schmitz, F. J. Nucl. Mater. 58 (1975) 357.

[20] Tetenbaum, M.; Hunt, P.D. J. Chem. Phys. 49 (1968) 4739.

[21] Johnson, C.E.; Johnson, I.; Blackburn, P.E.; Crouthamel, C.E. Reactor Technology 15 (1972) 303.

[22] Cordfunke, E.H.P. Personal communication.

[23] Naraine, M.G.; Bell, H.B. J. Nucl. Mater. 50 (1974) 83.

CHAPTER II

THE CHEMISTRY OF THE UMe_3 COMPOUNDS

II.1. PREPARATION OF THE COMPOUNDS

II.1.1. Introduction

In this chapter the preparation of the binary compounds URu_3, URh_3 and UPd_3 will be described. Two different methods are given in the literature: (a) the reaction of the elements, and (b) the reaction of UN with the light platinum metals. Both reactions take place at temperatures above 1000 °C.

Since the starting materials, especially uranium, are very sensitive to moisture and oxygen, all compounds have to be handled in a glove box in order to avoid any contact with oxygen. Purified argon circulates through the glove box.

The reaction mixtures can be heated:

1. below 1000 °C in a quartz tube which is heated by means of a resistance furnace. The sample is placed in a TaC crucible, which was chosen because it does not react with the UMe_3 compounds. The quartz tube is assembled in the glove box and then placed in the furnace. The tube is connected with the gas purification system (BTS, molecular sieves and a column with powdered uranium) and then flushed with the purified gas. The temperature of the sample is measured with a Pt - Pt/10% Rh thermocouple placed in the furnace near the sample.
2. above 1000 °C using a high-frequency furnace. The equipment consists of a pyrex tube and a water-cooled copper concentrator containing a TaC crucible placed on an alundum support bar. The sample is placed in the TaC crucible. After the pyrex tube has been assembled the equipment is taken out of the glove box, placed within the induction coil and connected with the gas purification system. The system is flushed sufficiently with purified gas and the TaC crucible is heated by the induction coil. The temperature is measured with an optical pyrometer, the temperature readings being taken on the black-body hole of the TaC crucible. The accuracy of the readings is about 5 °C at 1000 - 1500 °C. The pyrometer used for this equipment was

calibrated at the Van Swinden Laboratory, The Hague.

The phases present in the reaction products have been determined by X-ray analysis on Guinier films.

II.1.2. Preparation of starting materials

Starting materials for the preparation of the intermetallic compounds, palladium, rhodium and ruthenium, were available as powders of 99.99% purity (Johnson & Matthey Chemicals Ltd.). These were heated at 500 °C in vacuum to remove any adsorbed moisture. Palladium powder was not heated above 400 °C to avoid sintering.
The X-ray patterns of the platinum metals were in agreement with those found in the literature: ruthenium has a hexagonal structure with lattice parameters a = 2.7057 Å; b = 4.2812 Å [1], while rhodium and palladium have fcc structures with a = 3.796(1) Å [2,3] and a = 3.882(2) Å, respectively [4,5].

Uranium powder was obtained by hydriding metallic uranium at 300 °C, followed by dehydriding at 450 °C:

$$U + 1\tfrac{1}{2}\ H_2 \underset{\downarrow}{\overset{\lesssim 300\ °C}{\rightleftarrows}} UH_3 \qquad \text{(argon/}H_2\text{)}$$

$$UH_3 \underset{\downarrow}{\overset{\sim 450\ °C}{\rightleftarrows}} U\ \text{(porous)} + 1\tfrac{1}{2}\ H_2 \qquad \text{(argon)}$$

This process was repeated several times to obtain a finely divided uranium powder. The final dehydriding step was carried out in pure argon. The X-ray diffraction results showed the uranium to be α, orthorhombic with lattice parameters a = 2.854 Å, b = 5.869 Å and c = 4.955 Å [6]. Below its melting point, uranium has the γ-modification (774.8 °C - 1132.2 °C (m.p.)) with the bcc structure with a = 3.53 Å at 800 °C [7].

Uranium nitride, UN, was prepared by the reaction of finely divided uranium powder with nitrogen. At 700 °C uranium sesquinitride, U_2N_{3+x}, is formed: it is decomposed in vacuum or inert atmosphere to UN at 1400 °C:

$$2\ U + \tfrac{1}{2}(3+x)\ N_2 \overset{700\ ^\circ C}{\rightleftharpoons} U_2N_{3+x} \qquad (N_2)$$

followed by:

$$U_2N_{3+x} \overset{1400\ ^\circ C}{\rightleftharpoons} 2\ UN + \tfrac{1}{2}(1+x)\ N_2 \qquad (\text{argon})$$

The X-ray pattern of UN is in agreement with that described in the literature (fcc NaCl-type, a = 4.890 Å [8]). The results of the chemical analyses of uranium and UN are given in table 2.1.

Table 2.1. Analytical results for U and UN: mass fraction w and molar mass M.

compound	$\frac{M}{mol}$	10^2 w (U) found	10^2 w (U) calculated	10^2 w (N) found	10^2 w (N) calculated	10^2 w (O)	10^2 w (C)
U	238.029	-	100.00	-	-	0.165	0.043
UN-34	252.036	94.42	94.44	5.45	5.557	0.046	≈ 30 ppm
UN-35	252.036	94.38	94.44	4.41	5.557	0.128	70 ppm
UN-37	252.036	94.23	94.44	5.49	5.557	0.155	130 ppm
UN-40	252.036	94.50	94.44	5.48	5.557	-	-

Uranium tetrafluoride, UF_4 (Merck), is a green, hygroscopic compound (m.p. 1036 °C). Two methods can be used to remove moisture:

a. heating a mixture of NH_4HF_2 and UF_4 in an inert atmosphere at 500 °C. By this method partial reduction may occur:

$$6\ UF_4 + 2\ NH_3 \rightarrow 6\ UF_3 + 6\ HF\uparrow + N_2\uparrow$$

b. heating UF_4 in hydrogen fluoride. Special equipment with PTFE (Teflon) and copper connections, had to be used for these experiments because of the reaction between HF and the glass. The UF_4 was loaded into a platinum crucible and placed in a nickel furnace tube. The tube was flushed with argon, and connected with the gas purification

system. The sample was heated in a HF/argon mixture for several hours at 600 °C, followed by 16 hours in argon at 600 °C. The X-ray pattern of UF_4 was in agreement with the literature data for the monoclinic crystal [9]: a = 12.73 Å, b = 10.75 Å, c = 8.43 Å and β = 126°20', below 833 °C.

In order to prepare calorimetric UF_4 samples, other preparation methods are recommended [15]:

c. the reaction of hydrogen fluoride with UH_3(s) at 850 K, and
d. the reaction of hydrogen fluoride with UCl_4(s). Uranium tetrafluoride was prepared by slowly passing (0.5 HF + 0.5 Ar) in a nickel tube at about 850 K over solid UCl_4 for several hours.

Uranium trifluoride, UF_3, has a dark violet colour (m.p. 1425 °C); it is less hygroscopic than UF_4. For the preparation of UF_3, a mixture of finely divided uranium powder and UF_4 was heated in argon at 1050 °C for about 3 hours. The X-ray diffraction results showed it to be hexagonal with lattice parameters a = 7.179 Å and c = 7.345 Å [10].

A calorimetric uranium trifluoride sample was prepared [15] by the reaction of uranium tetrafluoride with a stoichiometric amount of uranium hydride in a slow stream of argon at temperatures which were slowly increased from 700 to 900 K during 5 hours.

Nickel fluoride, NiF_2 (Cerac), was purified and crystallized in the same way as UF_4, by heating in a HF/argon mixture (nickel tube, platinum crucible) for 4 hours at 700 °C. To improve the crystallinity, a second heating in argon for 15 hours at 700 °C was required. The X-ray diffraction pattern showed only tetragonal NiF_2 with lattice parameters a = 4.6505 Å, c = 3.0837 Å [11]. The results of the chemical analyses of UF_4, UF_3 and NiF_2 and the calorimetric samples UF_4-18 and UF_3-6 are given in table 2.2.

II.1.3. Preparation of the UMe_3 compounds

II.1.3.1. UPd_3

For the preparation of UPd_3 the following reactions were used:

a. $U + 3\ Pd \rightarrow UPd_3$

b. $UN + 3\ Pd \rightarrow UPd_3 + \frac{1}{2}\ N_2\uparrow$

Table 2.2. Analytical results for UF_4, UF_3 and NiF_2: mass fraction, w and molar mass, M.

compound	M / mol	10^2 w(U) found	10^2 w(U) calc.	10^2 w(Ni) found	10^2 w(Ni) calc.	10^2 w(F) found	10^2 w(F) calc.	10^2 w(O)
UF_4-7	314.023	75.7	75.8	-	-	22.5	24.2	0.203
UF_3-1	295.024	80.5	80.7	-	-	19.1	19.3	0.156
NiF_2-4	96.707	-	-	60.7	60.7	37.9	39.3	1.016
UF_4-18	314.023	75.61	75.80			24.35	24.20	0.014
UF_3-6	295.024	80.54	80.68			19.33	19.32	0.074

Palladium powder and uranium nitride (or uranium powder) were mixed in the molar ratio Pd/U = 3.00. The components were carefully weighed and ground in the glove box; pellets of these mixtures were also made in the box. After the first heatings at about 1050 °C, the X-ray patterns showed poorly crystalline products and incomplete reaction. In order to get pure and crystalline UPd_3, grinding and heating at about 1080 °C was repeated several times. After each heating, the progress of the reaction was followed by X-ray diffraction. After a second heating, the X-ray pattern of one of the samples was almost similar to that calculated for a cubic fcc structure with a_o = 4.05 Å. This is probably UPd_4 which has a fcc structure (Cu_3Au-type) with a = 4.063 Å [12]. The X-ray patterns of the final preparations showed predominantly UPd_3 which has a hexagonal symmetry with a = 5.769 Å and c = 9.640 Å [13].

In some experiments uranium was used as a starting material. However, this method was rejected because U reacts with the TaC crucible. Some samples were heated by electron bombardment.

Other workers have prepared UPd_3 by heating in an electron beam. Our experience has shown that pellets of UN + Pd disintegrate rapidly when heated in this way. The X-ray pattern of one pellet showed the outside layer to be more rich in UPd_3(hex) than the inner layers. We conclude that pure UPd_3 cannot be prepared by this technique.

As a starting material UN is superior to U for the following reasons: UN does not melt, it is less oxygen sensitive, and does not react with TaC at high temperatures.

Finally, about 50 grams of pure, crystalline UPd_3 were prepared by the reaction of UN and palladium as described above. This sample was used for the investigations on the stoichiometry, for measurements of enthalpy increments (H_T-H_{298}), and for low-temperature heat-capacity measurements. A complete analysis of this sample is given in table 2.3.

II.1.3.2. URh_3

For the preparation of URh_3, uranium nitride and rhodium powder were mixed in the molar ratio Rh/U = 3.00. The components were weighed and ground in a glove box. After heating and grinding the mixtures several times, pure and crystalline URh_3 was obtained.

The mixtures were heated in a high-frequency furnace at approximately 1100 °C. TaC was used as the container material. To remove UO_2, the sample was washed with HNO_3/H_2O = 1 and dried in argon at 500 °C. The X-ray patterns of the final URh_3-preparations showed the presence of only face-centered cubic URh_3 (Cu_3Au-type). This is in agreement with the structure found in the literature [14] with a = 3.991 Å.

The results of back reflection measurements on $URh_{3.000}$ and $URh_{3.037}$ did not show any difference in the lattice parameters of the samples. It can be concluded that there is no solubility of Rh in URh_3. The X-ray diffraction results of the UMe_3 compounds are given in table 2.4. About 30 grams of URh_3 were prepared for the thermodynamic measurements.

II.1.3.3. URu_3

URu_3 can be prepared by the reaction of UN and ruthenium powder:

$$UN + 3\ Ru \rightarrow URu_3 + \tfrac{1}{2}\ N_2$$

Mixtures in the molar ratio Ru/U = 3.00 were prepared. The components were handled as described above, and heated at about 1300 °C. The X-ray patterns of the URu_3-samples showed the presence of only crystalline URu_3 with the face-centered cubic structure (Cu_3Au-type). After the final heating the samples were washed in HNO_3/H_2O = 1 to remove UO_2, and dried in argon at 500 °C. For the low-temperature heat-capacity measurements, about 30 grams of URu_3 were prepared.

Table 2.3. Analytical results for UPd_3, URh_3 and URu_3; molar mass M, mass fraction w.

com-pound	M mol	10^2 w(U) found	calc.	10^2 w(Pd,Rh,Ru) found	calc.	10^2 w(O)	10^2 w(N)	10^2 w(C)
UPd_3	557.229	42.48	42.72	57.27	57.28	0.066	0.014	0.021
URh_3	546.746	- *	43.54	-	56.46	0.062		0.030
URu_3	541.239	- *	43.98	-	56.02	-		-

* URh_3 and URu_3 are insoluble in acidic solutions, such as HCl, HNO_3 and H_2SO_4.

Table 2.4. X-ray diffraction results of the UMe_3 compounds.

compound	crystal structure	lattice parameters (measured)	lattice parameters from literature [ref.]
$UPd_{3.099}$	hexagonal	a = 5.773 ± 0.001 Å	a = 5.769 Å [13]
		c = 9.627 ± 0.002 Å	c = 9.640 Å [13]
$URh_{3.000}$	fcc	a_o = 3.9915± 0.0005 Å	a_o = 3.991 Å [14]
"$URh_{3.037}$"	fcc	a_o = 3.9911± 0.0005 Å	a_o = 3.991 Å [14]
$URu_{3.000}$	fcc	a_o = 3.979 ± 0.002 Å	a_o = 3.980 Å [13]

II.2. CHEMICAL REACTIVITY OF THE UMe_3 COMPOUNDS

II.2.1. Introduction

As pointed out before (chapter I.1.), an actual problem in nuclear industry is the recovery of uranium and especially of plutonium from spent $(U,Pu)O_2$ power reactor fuel. Within the scope of this, knowledge of the chemical reactivity of the intermetallic UMe_3 compounds is of technological importance. The removal of fission products of the type $(U,Pu)Me_3$ from irradiated fuel, and the separation of plutonium and uranium from the platinum metals, constitute principal problems in fuel reprocessing.

Apart from the conventional commercial reprocessing methods, in which spent fuel is dissolved in acids, pilot plant studies have been undertaken using fluidized-bed fluoride volatility processes [16,17]. Advantages of these type of processes, in which most powerful reactions take place, are: decontamination of uranium and plutonium from fission product elements; formation of the uranium product in the form (UF_6) desired for isotopic separation, formation of the plutonium products in a form (PuF_6) suitable for conversion to the metal or oxide, and radioactive waste products in a solid form which is desirable for long-term storage.

An excursion into the chemical reactivity of URu_3, URh_3 and UPd_3 in a variety of chemical environment has been made; the results are given below.

II.2.2. Reactions of UMe_3 with non-metallic elements

a. Reaction of UMe_3 with pure oxygen and air.
   UPd_3 powder reacts with air and oxygen at elevated temperatures to form U_3O_8 and palladium metal. URu_3 and URh_3 powders react very slowly with oxygen at elevated temperatures; only some surface attack has been observed.

b. Reaction of UMe_3 with fluorine.
   The UMe_3 compounds do react with fluorine. UPd_3 forms with fluorine a mixture of UF_6, $Pd(PdF_6)$ and palladium metal, as described in chapter III.4. The conversion of the uranium in UPd_3 is complete at elevated temperatures and pressures, using an auxiliary material.

The reactions of URu_3 and URh_3 in fluorine have not been studied experimentally; however, it can be calculated that URu_3 and URh_3 will react with fluorine to form UF_6, RuF_5 and RhF_3, respectively.

II.2.3. Reactions of UMe_3 with aqueous acidic solutions

The solubility of the UMe_3 compounds in solutions of HCl, HNO_3 and H_2SO_4 and combinations of these acids have been given in table 2.5. as a function of time, temperature and concentration. About 0.5 grams of UMe_3 were weighed into 100 ml acidic solution. The results in table 2.5. show that URu_3 and URh_3 do not dissolve in aqueous HCl, HNO_3 or H_2SO_4, even not in concentrated solutions. Only UPd_3 dissolves readily in concentrated and 6N HNO_3 and in aqua regia.
It is interesting to compare for instance, the solution behaviour of pure rhodium metal and URh_3 in a mixture of hydrochloric acid and sulfuric acid (HCl/H_2SO_2 = 2). Pure rhodium metal dissolves in this mixture, while URh_3 is only slightly soluble in HCl/H_2SO_4 = 2 and insoluble in concentrated H_2SO_4. This is an indication for the negative ΔG^o of URh_3 compared to rhodium in these acids.

II.2.4. Miscellaneous reactions

The reaction

$$3\ UF_4 + URu_3 \rightarrow 4\ UF_3 + 3\ Ru$$

should take place, as can be calculated from the enthalpies of formation of the compounds in the reaction.
A pressed pellet of URu_3, mixed with UF_4 was heated in argon in a high-frequency induction furnace at 1150 °C. After the heating two layers were visible in the pellet: the upper layer of the pellet had a grey colour and contained a large amount of ruthenium, some URu_3 and a little UF_3; the lower layer was black and contained almost entirely UF_3. The natural separation process, taking place in this reaction, is an interesting phenomenon.

Table 2.5. Solubility of UMe_3 compounds in acidic solutions

Solution	URu_3 [a]			URh_3 [b]				UPd_3 [c]			
	time/hours			time/hours				time/hours			
	01	06	02	01	06	24	02	01	06	24	02
	temperature/ °C			temperature/ °C				temperature/ °C			
	25	25	80	25	25	25	80	25	25	25	80
2N HCl	-	-	-	-	-	0	0[1])	-	-	0	0[2])
HCl/H_2O = 1	-	-	-	-	-	0	0[1])	-	-	0	0[2])
HCl(conc.)	-	-	-	-	0	0	0[1])	-	-	0	0[2])
2N HNO_3	-	-	-	-	-	-	-	-	0	0	+[3])
6N HNO_3	-	-	-	-	-	-	-	+	+	+	+[3])
HNO_3(conc.)	-	-	-	-	-	-	-	+	+	+	+[3])
2N H_2SO_4	-	-	-	-	-	-	-	-	0	0	0[4])
H_2SO_4/H_2O = 1	-	-	-	-	-	-	..	-	-	-	-
H_2SO_4(conc.)	-	-	-	-	-	-	-	-	-	-	0[4])
HCl/HNO_3 = 2	-	-	-	-	-	-	-	+	+	+	+[3])
HCl/H_2SO_4 = 2	-	-	-	-	-	-	-	-	-	-	-

- : no solubility; 0 : slightly soluble; + : soluble

colours of the solutions: [1]) rose, [2]) yellow, [3]) red-brown, [4]) yellow

[a]) Ruthenium metal : insoluble in aqua regia, soluble in fused alkali [19].

[b]) Rhodium metal : soluble in H_2SO_4 + HCl and concentrated H_2SO_4, slightly soluble in acids and aqua regia [19].

[c]) Palladium metal : soluble in aqua regia, hot HNO_3 and hot H_2SO_4, slightly soluble in HCl [19].

II.3. THE STOICHIOMETRY OF UPd_3

II.3.1. Introduction

From studies of the X-ray diffraction patterns of URh_3 and URu_3, after heating mixtures of Rh+URh_3 and Ru+URu_3 at about 1000 °C, it has been concluded that there is not solid solubility of Ru in URu_3 and of Rh in URh_3 (chapter IV.2.). Therefore EMF techniques have been applied to study the integral Gibbs energies of formation of URh_3 and URu_3, using the combinations: Rh, URh_3 and Ru, URu_3 in the electrodes of the EMF cells.

As can be concluded from the phase diagram of the U-Pd system, there will be solid solubility of palladium in UPd_3 at temperatures below 1100 °C; this has been confirmed by preliminaty experiments. In this part of chapter II the influence of the solubility of UN and Pd on the stoichiometry of UPd_3 will be studied.

II.3.2. Experimental

As starting materials for the solubility experiments were used UPd_3, palladium and UN. The UPd_3 samples were taken from the same batch as the sample used for the fluorine bomb calorimetry and the high and low-temperature heat-capacity studies.

The X-ray diffraction results showed hexagonal UPd_3 with a = 5.773 Å and c = 9.627 Å. This result is in good agreement with the lattice parameters for UPd_3 published by Heal and Williams [13]: a = 5.769 Å and c = 9.640 Å.

The calculation of the exact stoichiometry of the UPd_3 samples used in our investigations is quite complex, because of the variety of impurities in the samples. A small amount of UO_2 was visible in our UPd_3 sample. The sample was carefully analyzed for uranium, palladium, oxygen, carbon, nitrogen, hydrogen, and metallic impurities such as tantalum (the sample was prepared in a TaC crucible).

Since O, C and N are most probably combined with uranium to form UO_2, UC and UN, there will be less uranium available to react with palladium. The results of this particular UPd_3 preparation are presented in chapter II.4., in table 3.15. It was calculated that total palladium as UPd_3 is 57.2550 mass per cent and total uranium as UPd_3 is 41.3278 mass

percent. Based on the analytical results, the purity of the UPd_3 sample is 98.6 mass per cent and the calculated stoichiometry of the sample is $UPd_{3.099}$.
For the preparations of the UPd_x phases the following reactions were used:

a. $UPd_{3.099} + y\ UN \rightleftarrows UPd_x + \frac{1}{2}\ y\ N_2$

b. $UPd_{3.099} + z\ Pd \rightleftarrows UPd_x$

$UPd_{3.099}$ powder and uranium nitride (or palladium powder) were mixed in the desired molar ratio Pd/U = x. The components were carefully weighed and ground, and pellets were pressed in the glove box. After the first heatings at 1080 °C during 2 - 3 hours, the X-ray patterns still showed small amounts of UN and Pd, which had not yet dissolved in the UPd_x lattice. Especially the dissolution of UN proceeds slowly. In order to obtain UPd_x with constant lattice parameters, grinding, pelletizing and heating at about 1100 °C was repeated several times. After three or more heatings, when UN or Pd were not visible anymore on the X-ray patterns, a small amount of sample was mixed with α-SiO_2 as an internal standard to calculate the lattice parameters of UPd_x from the X-ray patterns.

II.3.3. Results

The results of the lattice parameters of the hexagonal UPd_x, from samples going from $UPd_{2.8}$ through $UPd_{3.5}$, have been presented in table 2.6. In some preparations up to nine heatings were required to obtain constant lattice parameters for the UPd_x-phases. We have made the assumption that loss of Pd due to evaporation is not significant at 1100 °C. The final results are plotted in fig. 2.1., from which it can be seen that the a-axis of the hexagonal UPd_x cell remains constant to within 0.1 percent of the average (a_o = 5.772 Å) going from $UPd_{2.8}$ through $UPd_{3.4}$. The c-axis of the UPd_x cell shows a contraction of more than 1 percent of the value for $UPd_{3.099}$ (c_o = 9.627 Å) going from $UPd_{3.1}$ through $UPd_{3.5}$. When x > 3.3 other reflections were noticed in hexagonal UPd_x, probably due to the presence of cubic UPd_4 [18].

The crystallinity of the hexagonal phase becomes also poorer.

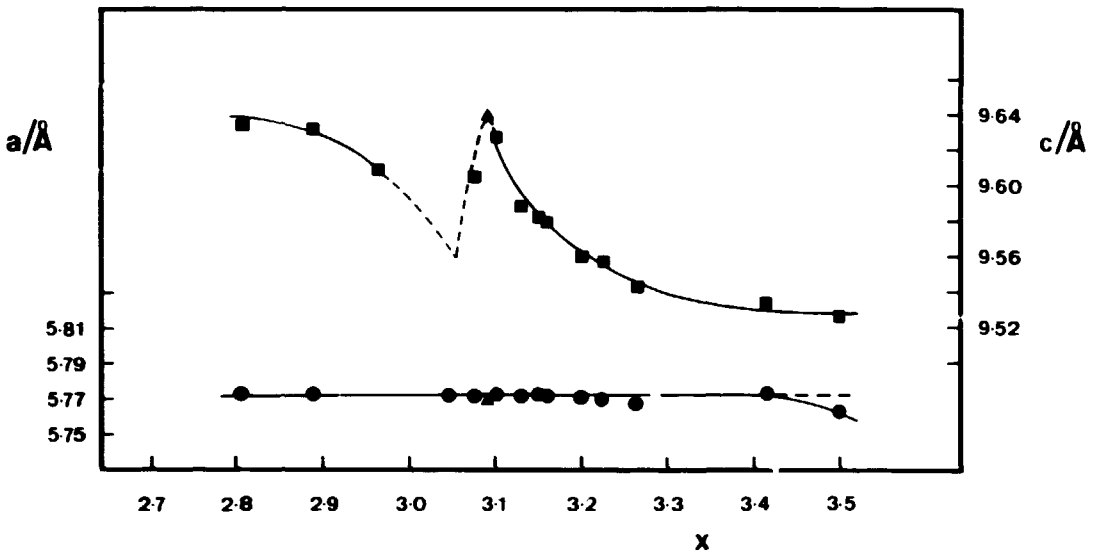

Fig. 2.1. Lattice parameters of hexagonal UPd_x as a function of x.
■●: our results.
▲ : Heal and Williams.

Going from $UPd_{3.0}$ to $UPd_{2.8}$ there is again a contraction of the c-axis (about 0.3 per cent of c_o= 9.635 Å).

II.3.4. Discussion

The behaviour of the c-axis in UPd_x in the range $UPd_{3.0}$ - $UPd_{3.1}$ is not quite understood. There is a maximum in the c-axis between x = 3.08 and x = 3.10, possible corresponding with the composition "UPd_3". The intermetallic compound of composition $UPd_{3.099}$ gave sharp powder spectra, comparable with the results of Heal and Williams [13]. These authors have published their X-ray data on a sample of composition $UPd_{3.008}$. However, they did not make any corrections for impurities in uranium, such as oxygen, carbon and nitrogen.
Since the X-ray data of our $UPd_{3.099}$ sample agree to within 0.1 percent with the data of Heal and Williams, we applied our impurity corrections for "UPd_3" (table 3.15.) on their sample. The recalculated stoichiometry will be $UPd_{3.09}$. This result has been shown in fig. 2.1.
The theoretical value for the axial ratio c/a of hexagonal closest-packed structures is $2\sqrt{2}/\sqrt{3}$ = 1.633, which makes the twelve smallest

interatomic distances equal. The value for $UPd_{3.099}$ of c/a = 1.668 is somewhat larger compared to the theoretical value, but lies within 2.5 percent of this value. The metallic radii of palladium and uranium are very close together: 1.37 Å and 1.38 Å, respectively.
Where the c-axis in UPd_x is the longest (c/a = 1.668), repulsion between U-Pd is the smallest.
In contrast to the Laves phases UX_2, where there are U-U and X-X contacts only, in UPd_3 there are U-Pd contacts only [13]. This could explain that adding Pd to "UPd_3" will cause more attraction between U and Pd and consequently a contraction of the c-axis, until another structure appears.

Table 2.6. Solubility of palladium in UPd_3

UPd_x x	Number of heatings at 1100 °C ; and lattice parameters of hexagonal UPd_x(A)						
	3	4	5	6	7	8	9
2.806	-	-	-	-	-	a = 5.773(1) c = 9.629(2)	a = 5.773(1) c = 9.635(3)
2.884	-	-	-	-	-	a = 5.774(1) c = 9.635(4)	a = 5.774(1) c = 9.633(3)
2.967	-	a = 5.774(1) c = 9.626(2)	a = 5.773(1) c = 9.624(1)	a = 5.776(2) c = 9.619(4)	a = 5.775(1) c = 9.615(3)	a = 5.775(1) c = 9.610(3)	-
3.077	a = 5.772(2) c = 9.611(4)	a = 5.772(1) c = 9.608(2)	a = 5.772(1) c = 9.603(3)	a = 5.772(1) c = 9.605(2)	-	-	-
3.099	-	-	-	a = 5.773(1) c = 9.627(2)	-	-	-
3.130	a = 5.771(2) c = 9.604(5)	a = 5.772(1) c = 9.597(3)	a = 5.772(1) c = 9.592(3)	a = 5.774(2) c = 9.589(3)	a = 5.773(1) c = 9.591(2)	a = 5.771(1) c = 9.587(2)	-
3.150	a = 5.771(1) c = 9.592(2)	a = 5.772(2) c = 9.588(4)	a = 5.772(1) c = 9.593(1)	-	a = 5.773(1) c = 9.583(1)	-	-
3.161	a = 5.771(1) c = 9.595(2)	a = 5.769(2) c = 9.599(4)	a = 5.771(2) c = 9.586(5)	a = 5.774(1) c = 9.588(2)	a = 5.771(1) c = 9.581(2)	a = 5.771(1) c = 9.582(1)	-
3.203	a = 5.772(1) c = 9.574(2)	a = 5.771(1) c = 9.572(3)	a = 5.771(1) c = 9.567(2)	-	a = 5.770(1) c = 9.560(2)	-	-
3.225	-	a = 5.770(1) c = 9.569(2)	a = 5.771(1) c = 9.562(2)	a = 5.771(1) c = 9.563(1)	a = 5.770(1) c = 9.562(1)	a = 5.769(1) c = 9.557(1)	-
3.263	-	a = 5.771(2) c = 9.551(4)	a = 5.769(1) c = 9.552(1)	a = 5.770(1) c = 9.547(2)	a = 5.768(1) c = 9.545(1)	a = 5.767(1) c = 9.543(1)	-
3.416	a = 5.766(1) c = 9.538(2)	a = 5.766(1) c = 9.544(3)	a = 5.773(2) c = 9.536(4)	-	-	-	-
3.499	-	a = 5.763(1) c = 9.526(3)	-	-	-	-	-

REFERENCES

[1] Hellawell, A.; Hume-Rothery, W. Phil. Mag. 45 (1954) 797.

[2] Owen, E.A.; Yates, E.L. Phil. Mag. 16 (1933) 606.

[3] Goldschmidt, H.J.; Land, T. J. Iron Steel Inst. 155 (1947) 221.

[4] Michel, A.; Bénard, J.; Chaudron, G. Bull. Soc. Chim. France. 12 (1945) 336.

[5] Hume-Rothery, W. The Structure of Metals and Alloys. The Institute of Metals. London (1956) p. 94.

[6] Sturcken, E.F. Acta Crystallogr. 13 (1960) 852.

[7] Klepper, H.H.; Chiotti, P. ISC-report 893 (1957).

[8] Rundle, R.E.; Baenziger, N.C.; Wilson, A.S.; McDonald, R.A. J. Amer. Chem. Soc. 70 (1948) 99.

[9] Larson, A.C.; Roof, R.B. Jr.; Cromer, D.T. Acta Crystallogr. 17 (1964) 555.

[10] Staritzky, E.; Douglass, R.M. Anal. Chem. 28 (1956) 1056.

[11] Haendler, H.M.; Patterson, W.L. Jr.; Bernard, W.J. J. Amer. Chem. Soc. 74 (1952) 3167.

[12] Holleck, H.; Kleykamp, H. J. Nucl. Mater. 35 (1970) 158.

[13] Heal, T.J.; Williams, G.I. Acta Crystallogr. 8 (1955) 494.

[14] Dwight, A.E.; Downey, J.W.; Conner, R.A. Jr. Acta Crystallogr. 14 (1961) 75.

[15] Cordfunke, E.H.P.; Ouweltjes, W. J. Chem. Thermodynamics 13 (1981) 193.

[16] Anastasia, L.J.; Alfredson, P.G.; Steindler, M.J. Nuclear Applications 4 (1968) 320.

[17] Anastasia, L.J.; Alfredson, P.G.; Steindler, M.J. Nuclear Applications 7 (1969) 433.

[18] Pells, G.P. J. Inst. Metals 92 (1963-64) 416.

[19] Weast, R.C.: editor, Handbook of Chemistry and Physics, CRC, Boca Raton, Florida (1979 - 1980).

CHAPTER III

FLUORINE BOMB CALORIMETRY

III.1. THE CALORIMETRIC SYSTEM

III.1.1. Introduction

Bomb calorimetry is a well known technique used in thermochemistry. In the past century the first oxygen bomb calorimeter was introduced by Berthelot [1] to determine heats of combustion of organic and inorganic substances in an excess of oxygen, usually up to pressures of 30 atm. Until 1957 combustions in halogens were carried out in calorimeters of the constant-pressure flow-type. The use of halogens in calorimetry was extended to the constant-volume type, using glass reaction vessels, by Gross et al. [2].

Fluorine bomb calorimetry was extended to high-pressure (up to 15 atm of fluorine) metal combustion bombs by Hubbard et al. at the Argonne National Laboratory (ANL) in the United States in 1961 [3].

This technique has been developed over the past twenty years, and is now in precision and accuracy comparable to other types of calorimetry. Fluorine calorimetry was developed primarily to take advantage of the extreme reactivity of fluorine [4]. It is often possible to get complete reaction of substances with fluorine to form products of singular oxidation states.

Three basic directions in the development of fluorine bomb calorimetry have been:

a. the development of techniques for safe operation, since fluorine is recognized as a dangerous material[4];
b. the development of a low-temperature still in order to obtain fluorine of very high purity (99.99%) and to prevent undesirable side reactions [5]; and
c. to design an apparatus for handling fluorine, such as reaction vessels and handling manifolds, using appropriate construction materials.

The construction of the calorimeter and reaction vessel, and the calorimetric procedures will be discussed below.

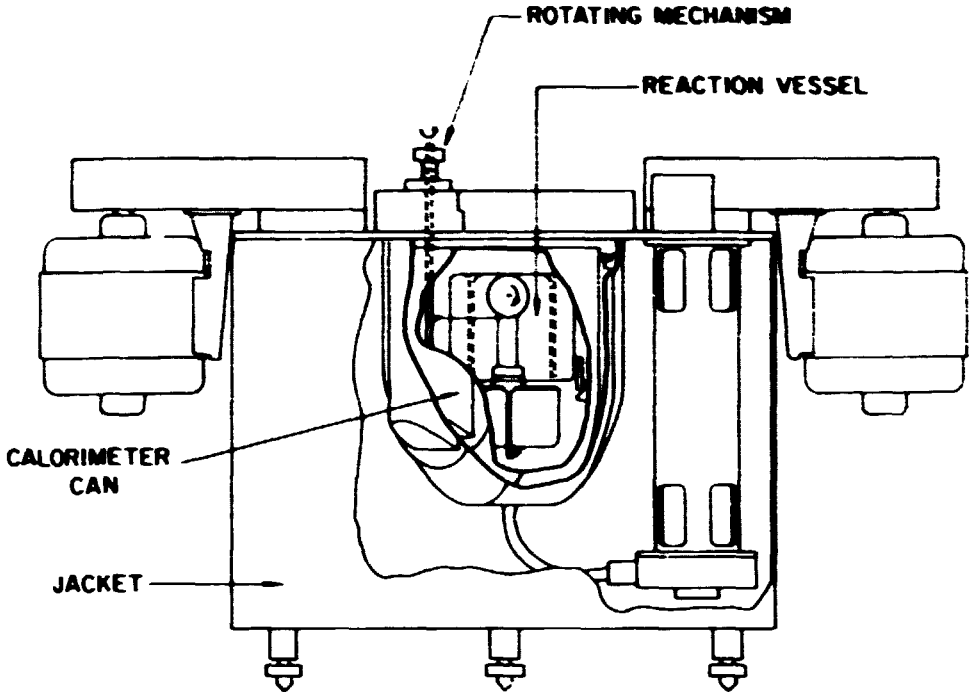

a. sectional view

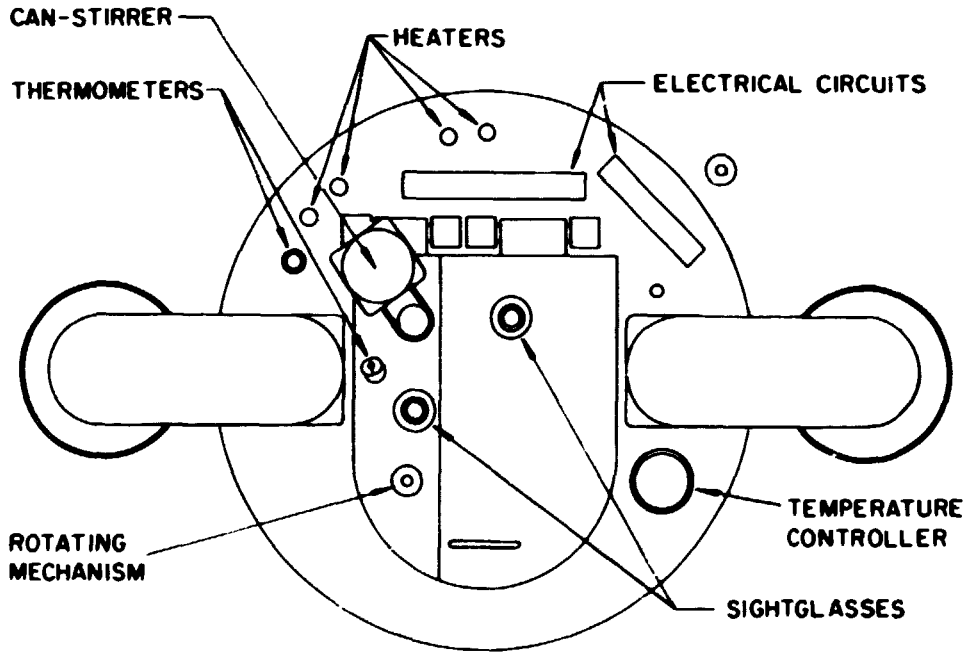

b. top view

Fig. 3.1. Calorimetric system.

III.1.2. The calorimetric equipment

A sectional view and a top view of the calorimetric system are given in fig. 3.1. More detailed isometric views of the calorimeter can and the reaction vessel are given in figs. 3.2 and 3.3.
The calorimeter can is suspended in the jacket well with three pins which rest in plastic V-grooves. There is a 1 cm air gap between the can and the walls of the jacket to minimize convection effects.
The shape of the can is rather unusual in order to keep its volume as small as possible. The following items are shown in fig. 3.2.: a stirrer for circulating water in the can; a rotating shaft with hook for opening the valve of the reaction vessel; oil seals through which the shafts pass; a heater; a thermometer port, and supports for the reaction vessel.
The two-compartment nickel reaction vessel (fig. 3.1. and 3.2.) is supported by two bearings mounted on yokes on the calorimeter can

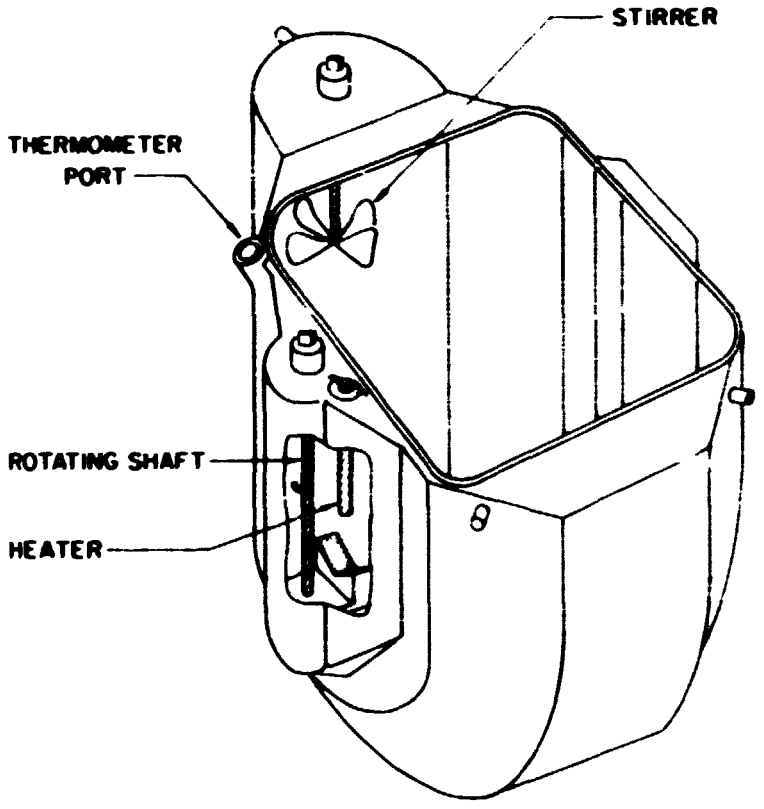

Fig. 3.2. Calorimeter can.

walls. A spring clip (not visible) on the bottom of the can, that serves as an electrical lead, is also used for positioning the reaction vessel. Electrical energy has to be used for the ignition of substances in the reaction vessel. The **rotating mechanism** in the can works as follows: a steel wire, wound on a pulley connected to the tank valve, is hooked to a rotating shaft. The tank valve can be opened from outside the calorimeter, by turning the shaft. The constant temperature jacket and the jacket lid (fig. 3.1b.) are interconnected and filled with water. The external parts of the jacket are made of nickel-plated brass, the inner surface of the jacket (the walls and top of the well) and the calorimeter can are chromium-plated copper sheet of 1 mm thickness. All the surfaces are polished to minimize heat transfer by radiation. The water in the jacket is circulated by stirrers. A centrifugal pump at the base of one of the stirrers pumps water through a hollow hinge into the double-walled jacket lid which consists of two parts, and then back into the jacket. The water level in the lid can be checked through **sightglasses**. Excess of water overflows through a tube. The water in the jacket is maintained at a constant temperature (25 °C) to within ± 0.001 °C. A flat nickel wire wound resistance bulb (Hallikainen Instr. model 1080), connected with a thermotrol (model 1053 A) was used to control the temperature. When the jacket temperature is too low, intermittent heat imput is supplied by a 100-watt tubular **heater**. When the jacket temperature has to be raised by several degrees a 500-watt **heater** is used. Excess heat flows to the surroundings which are thermostatted at about 20 °C.

A synchronous motor drives the calorimeter can stirrer. Fig. 3.1b. also shows ports for the calorimeter can **thermometer** (Hewlett Packard, model 2801), jacket **thermometer** and jacket **temperature controller**, respectively. The calorimeter heater terminals, jacket heater terminals, and terminals for the electrical ignition circuit are combined in **electrical circuits**.

The calorimetric system described above has been described earlier for a rotating reaction vessel by Hubbard et al. [6]. The reaction vessel used in our investigations is shown in fig. 3.3. A two-compartment combustion bomb is required, for instance, when substances are studied that react spontaneously.

With this type of reaction vessel, the reacting gas can be isolated

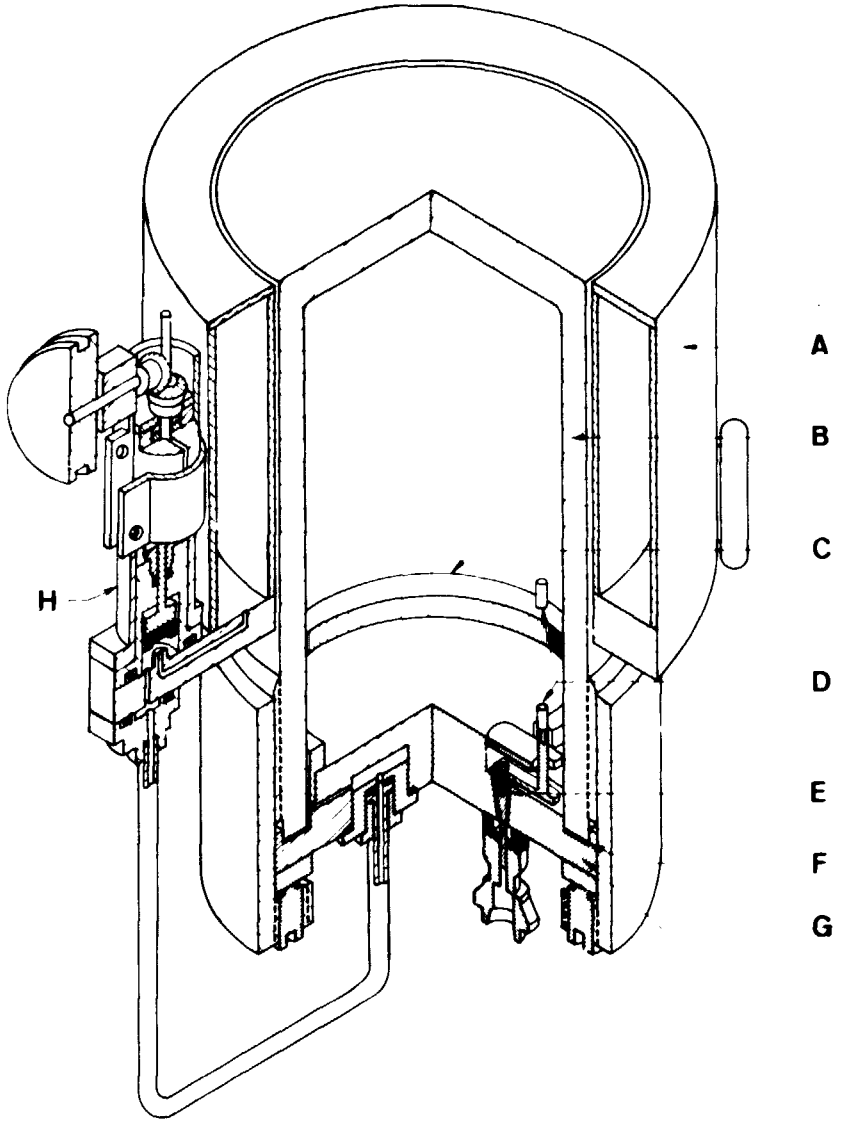

Fig. 3.3. Reaction vessel.

from the calorimetric sample until it is desired to start the reaction. Nuttall et al. described the two-compartment combustion bomb [7]; the tank valve (H) has been improved since.

Compounds of which the heat of combustion in fluorine has to be determined are accurately weighed in nickel crucibles in a glove box and placed on the nickel bomb head (G) within the retaining ring (C). The bomb head has been pressed tightly against the nickel wall (d = 0.5 cm) of the bomb body (B) by means of a special constructed joint. A very effective seal was obtained with a gold gasket inserted in a PTFE

gasket (F). The nickel fluorine tank (A) has been charged with purified fluorine (99.99%) up to pressures of 18-24 atm. In the glove box the tank, which fits concentrically around the bomb body, has been connected with the bomb head. All metal parts which come in contact with fluorine (fittings, tube and valves) are made of nickel. Gaskets, insulation and the valve button are made of PTFE.
After assembling and taking out of the glove box the system can be evacuated by means of a valve in the bomb head (not visible in fig. 3.3). The two electrodes (D) are used if samples have to be electrically ignited. One of the electrodes has been isolated with PTFE (E).

III.1.3. Experimental procedures and calibration of the calorimeter

When it has been decided which type of reaction vessel has to be used in the combustion experiments, a series of calibrations can be performed. In all our combustion experiments a two-compartment high-pressure nickel reaction vessel had to be used. The calibration was performed by measuring the temperature rise after burning of benzoic acid in oxygen in order to determine the energy equivalent of the calorimetric system (ε (calor)) under experimental conditions. Benzoic acid (National Bureau of Standards; sample 39i; certified energy of combustion under prescribed conditions: $-(26.434 \pm 0.003)$kJ g^{-1}) was pressed in a series of pellets of approximately 1 gram each. A benzoic acid pellet and a piece of cotton thread were accurately weighed in a deep (3 cm) platinum crucible of about 3.5 grams. Two platinum electrodes were connected with the nickel electrodes in the bomb. The platinum electrode in contact with the bomb was bent concentrically as a support for the platinum crucible containing the sample. The electrodes were interconnected with a very thin (d = 0.005 cm) platinum ignition wire. The cotton thread was tied to the middle of the Pt-wire and the other end was placed underneath the benzoic acid pellet. A combustion is started by discharging a capacitor (charged to 100 V) through the ignition wire, which will cause the cotton to burn and ignite the benzoic acid pellet. A small platinum crucible with 1 ml of water was placed on the bomb head. After the bomb has been assembled and the evacuated tank has been connected with it, the bomb will be flushed with oxygen three times and then charged to 30 atm. with oxygen.
Water is added to the can. The calorimeter can (including the water)

and the can lid are placed on a balance, and the amount of water in the can is adjusted against a tare weight to ± 0.03 g. Total weight of water and can is about 4 kg. The lid is then placed on top of the can, in order to avoid vaporization of the water, and the can is placed in the jacket well. The wires of the can heater and the ignition wires of the can are connected with the electrical circuit of the jacket. The lid is taken off the can, and the charged bomb is carefully lowered into the calorimeter can, placed on two yokes and positioned by a clip. (In an experiment where the tank valve has to be opened, the steel wire connected with the valve has to be hooked on the rotating shaft). The calorimeter can lid is pressed into its place after a standard time of two minutes and one half of the jacket lid is lowered over the well. The calorimeter can thermometer is placed into position, the can stirrer is connected with the motor, and the rotating shaft with a pulley (which will not be used during calibrations). After lowering the second half of the jacket lid, the calorimeter can is heated to a temperature about 0.06 °C lower than the temperature at which observations of the initial period are to be started. The temperature of the calorimeter is allowed to drift 0.06 °C in about 10 minutes.

During the experiment the temperature is printed every 10 seconds. A typical temperature-time curve of an isoperibol bomb calorimetric experiment (the combustion of one gram of benzoic acid in oxygen) is given in fig. 3.4. This curve gives the information by which the heat of combustion is evaluated. The measurement of the heat of combustion starts when the sample is ignited electrically or by opening the tank valve and bringing the reactive gas into contact with the sample.

The evaluation of the results is as follows.

In practice the calorimeter is not perfectly isolated and a correction has to be made for the heat transport from the inner vessel (calorimeter) to the surroundings (jacket). According to Newton's law the temperature of the calorimeter approaches that of the jacket asymptotically.

The rate of change of temperature is given by:

$$\frac{\delta\Theta}{\delta t} = \alpha(\Theta_o - \Theta) \qquad (3\text{-}1)$$

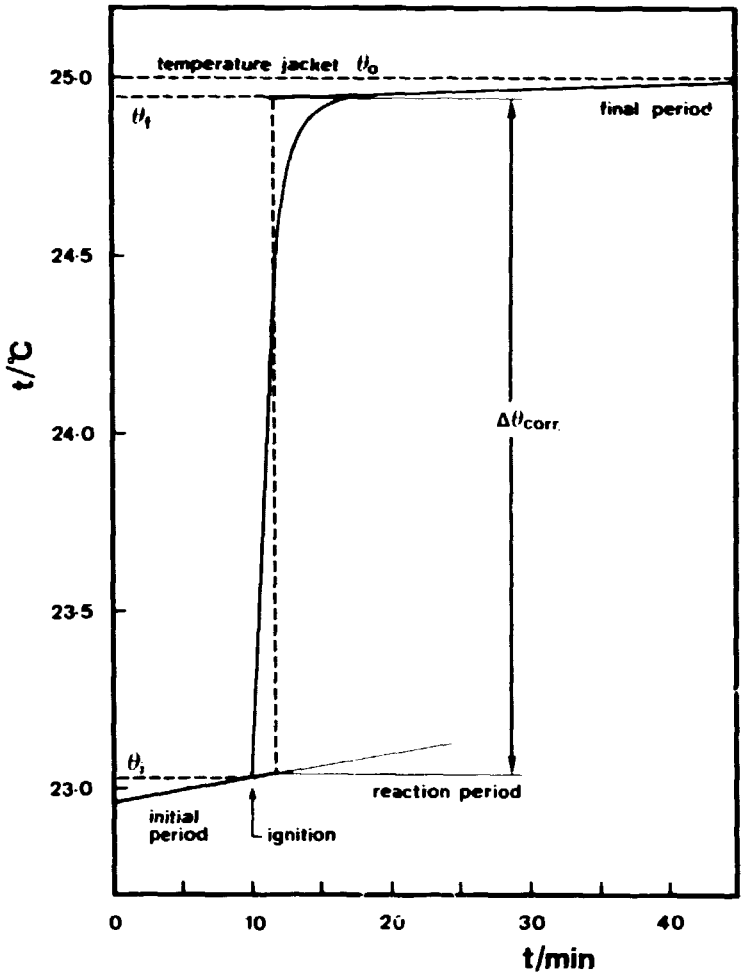

Fig. 3.4. Temperature - time curve of an isoperibol bomb calorimetric experiment.

where Θ = temperature of the calorimeter.
Θ_o = temperature of the jacket.
α = constant.

A graphical method [8], based on linear extrapolation of initial and final period, is often used to correct for the exchange of heat (see for example fig. 3.4).

The convergence temperature Θ_c can be calculated from the relation:

$$\left(\frac{\delta\Theta}{\delta t}\right)_{final} = \alpha(\Theta_c - \Theta_{m,f}) \qquad (3\text{-}2)$$

where $(\frac{\delta\theta}{\delta t})_{final}$ = the rate of change of temperature in the final period.

θ_c = convergence temperature.

$\theta_{m,f}$ = temperature in the middle of the final rating period.

The corrected temperature rise $\Delta\theta_{corr}$ is given by:

$$\Delta\theta_{corr} = (\theta_f - \theta_i) - \int_{t_i}^{t_f} \alpha'(\theta_c - \theta)dt \qquad (3\text{-}3)$$

where t_i = time at beginning of reaction.

t_f = time at completion of reaction.

θ_i = temperature at t_i.

θ_f = temperature at t_f.

$\Delta\theta_{corr}$ has been derived as follows:

All calorimetric temperatures were measured to 0.1 mK with a quartz-crystal thermometer [9] (Hewlett-Packard Model 2801 A), which averaged temperature readings over a constant time interval. The temperature readings were transferred via a coupler (Hewlett-Packard Model 2540) to a teletypewriter (Teletype Corporation Model ASR-33), which simultaneously give a printed record and a punched paper tape. The corrected temperature rise of the experiment was machine-computed from the punched tape.

III.1.4. The determination of reaction mechanism and analysis of calorimetric samples

The uncertainties associated with the fluorine combustion calorimetry of most inorganic substances are due to uncertainties in the analyses to define the sample, the reaction mechanism, or the state of combination of impurities, rather than uncertainties in the calorimetric method itself.

In any reaction calorimetry, but especially in fluorine calorimetry, the following determinations are very important:

a. the main reaction, the amount of reaction, and possible side reactions,

b. the exact stoichiometry of the sample, and

c. the impurities in the sample in ppm quantities.

Determination of the amount of reaction is usually by weight of sample introduced into the bomb and determination of the amount of unreacted sample (residue).
Solid combustion products have to be examined by X-ray diffraction and if necessary by chemical analysis.
For instance, in the combustions in fluorine of the palladium in UPd_3:

$$UPd_3 + F_2(g) \rightarrow UF_6(g) + Pd(PdF_6) + PdF_2 + Pd$$

the amount of reaction was about 80-85 mass percent formation of $Pd(PdF_6)(c)$; the main reaction was the formation of $Pd(PdF_6)$ but as a side reaction about 5 mass percent PdF_2 was formed, which was determined by X-ray diffraction. About 10-15 mass percent of the palladium did not react with fluorine.
Gaseous reaction products can be trapped in steel cylinders with liquid nitrogen, fluorine can be pumped off and the remaining gas examined by mass-spectrometry, gas chromatography or other techniques. For example, in the UPd_3-experiments carbon was used as an auxiliary material:

$$C + 2\ F_2(g) \rightarrow CF_4(g)$$

After the combustions the CF_4 gas was analyzed by gas chromatography and about 0.03 mol percent C_2F_6 and C_3F_8 gas was detected.
Analytical methods have been used to determine total uranium, fluorine and palladium in the calorimetric samples, as well as traces of oxygen, nitrogen, hydrogen, carbon and metal impurities.
In order to set up an analytical method for traces of impurities in calorimetric samples, the following aspects are important:

a. all impurities in the starting materials have to be known, because the heat of combustion of the impurities in fluorine can differ considerably from the heat of combustion of the calorimetric samples in fluorine (see below, tables 3.3., 3.4. and 3.5.),
b. the preparation methods, including gasses used during preparation, container materials and cleaning agents (such as SiC to remove UO_2 from metallic uranium) have to be studied.

Short summaries of the analytical methods used will be given below.

Determination of uranium

Uranium contents in samples were determined at The Netherlands Energy Research Foundation (ECN) by a computer-controlled potentiometric titration method described by Slanina et al. [10].

The method involves: control of burette, imput of titration parameters (concentration of titrant and temperature), continuous measurement of the potential, and, finally, determination of the end-point of the titration.

For the redox titrimetric determination of uranium, the method of Davies and Gray [11] has been used. Uranium is reduced to U(IV) in a solution containing H_3PO_4 by an excess of $FeSO_4$. All remaining Fe(II) is oxidized to Fe(III) by a mixture of HNO_3, $(NH_4)_2\ MoO_4$ (ammonium molybdate) and NH_2SO_3H (sulphamic acid), and the resulting U(IV) solution is titrated with 0.05 N $K_2Cr_2O_7$. The end-point is determined by means of a platinum electrode. This method has a very high accuracy; better than 0.05%. In our investigatio.s the method has been used to determine uranium in UF_4, UF_3, UPd_3 and UN.

At Argonne National Laboratory (ANL) a standard method for colorimetric determination of uranium in aqueous solutions (ASTM designation: E318-69; reapproved 1974) has been used. The method is based upon the measurement of the absorbance of the uranium -di- benzoylmethane complex at 415 nm [12].

Uranium in the measured volume of sample is first oxidized to U(VI) by potassium permanganate.

With this method as little as 0.5 μgU/ml can be detected. The method has been used mainly to determine small amounts of unreacted uranium left in the combustion bomb after the combustions of UPd_3 in fluorine. The UPd_3 combustion residues were dissolved in 100 ml sample solution (HCl and H_2SO_4/HNO_3). The experimental values were ranging between 0.25 μgU/ml and 2.68 μgU/ml.

Large amounts of uranium in, for instance, UF_4 or UF_3 can also be determined colorimetrically. The results for the uranium content in UF_4-14 using both the ANL-method and the ECN-method are in good agreement (table 3.1.).

Determination of fluorine

At ECN the same computer-controlled potentiometric titration set-up, as

Table 3.1. Analytical results

Sample	Uranium content (mass percent)		
	ANL	ECN	Theoretical
UF_4-14	75.57 ± 0.15 75.53 ± 0.15	75.62 ± 0.05	75.80

described for uranium [10], has been used for determination of fluorine. A sample changer and sample-diluter were added to the apparatus, and F^- has been determined by means of an ion-selective electrode. Using this method the amount of fluorine in UF_4, UF_3 and NiF_2 has been determined.

At ANL fluorine was determined in different samples containing small amounts dissolved in 0.6 N HCl. An aliquot of the solutions was pyrohydrolysed at 900 °C in a H_2O-saturated oxygen atmosphere, using U_3O_8 as an accelerator. Next an aliquot of the distillate was titrated by a standard additions technique (NaF-titrant) using a fluoride ion sensitive electrode. The method was used to determine small amounts of F^- (3.7 - 10.8 μg F^-/ml) in the post combustion residues of UPd_3 and $Pd(PdF_6)$.

Determination of palladium in UPd_3

A sample of UPd_3 was dissolved in $HCl-HNO_3$. After dissolution H_2SO_4 was added and $HCl-HNO_3$ was fumed off. After dilution the solution was filtered and the palladium in the solution formed a deposit on a platinum kathode, by passing a current through the solution (current 0.1 amp. during 1.5 hours).

Palladium can also be determined colorimetrically using 2-nitroso-1-naphthol. This method is based upon the measurement of the absorbance of the purple palladium 2-nitroso-1-naphtholate complex in toluene at 370 nm [13]. The procedure is accurate to within 1 mass percent Pd. This method was used to determine palladium in some $Pd(PdF_6)$ preparations.

Determination of oxygen at Los Alamos Scientific Laboratory

The determination of oxygen in ppm quantities in metals and inorganic materials was performed at Los Alamos Scientific Laboratory (LASL), Los Alamos, New Mexico in the United States, by a capillary trap method, without high vacuum [14,15]. The sample is dropped into molten platinum in a graphite crucible. Oxygen in the sample reacts to form carbon monoxide, which is swept out by a stream of argon at atmospheric pressure, oxidized to carbon dioxide, which is then condensed in a capillary trap and measured with a capillary manometer. The apparatus is sensitive to 3 ppm of oxygen. The method was modified by adding a MgO trap to remove fluoride in UF_3 and UF_4 [16].

Determination of hydrogen at Los Alamos Scientific Laboratory

One method used was inert gas fusion in a LECO RH-1 Hydrogen Determinator. The sample was contained in a Ni capsule to prevent sublimation and sodium thiosulfate was added to the absorption train to trap fluoride. This analyzer and method are described in literature from the LECO Company.

In another method used, the sample is heated to 950 °C in argon and the evolved gases are swept through heated CuO into a moisture monitor (CEC or similar). The water (H_2) is measured by integrating the moisture monitor signal [17].

Determination of HF in UF_4 at ECN

Traces of HF in UF_4 can be determined as follows:

The UF_4 sample was heated in an argon flow at 800 °C, and HF was swept out and trapped in a liquid-nitrogen cooled trap. Next the HF was transferred into NaOH and F^- was determined.

Determination of nitrogen at ECN

Both mass spectrometric and chemical procedures can be used to determine nitrogen in uranium dioxides as well as in UN and UPd_3.

The chemical determination of nitrogen used at ECN was based on the classical Kjeldahl procedure [18]. The samples were first dissolved in a sulphuric-phosphoric acid mixture, any nitrogen present being converted to ammonia in the process.

The ammonia was separated by distillation, in the presence of Devarda's

alloy, from an alkaline solution (NaOH) of the dissolved sample. The ammonia in the distillate was determined by spectrophotometry using the phenol hypochlorite (Nessler's) reagent procedure.

Determination of carbon at ECN

Small amounts of carbon (ppm quantities) in uranium, UN and UPd_3 were determined by combustion of the samples in oxygen and detection of the amount of CO_2 swept out in a high-frequency analyzer. For the determination of carbon in URh_3, about 500 mg URh_3-sample was mixed with 1 gram of small pieces of iron and melted. The carbon content of this mixture was determined as described above. This procedure was followed because of the poor reactivity of pure URh_3 with oxygen.

Determination of metallic impurities at ECN

Two different methods have been used to determine metallic impurities in ppm quantities in U, UN, UPd_3 and URh_3.

a. the atomic absorption technique. With this method Ta has been determined in UPd_3 (85 ± 5 ppm) and in URh_3 (130 ± 20 ppm). This technique is also suitable to detect Al, Cr, Fe, Ni and other elements which are commonly found in uranium metal. Si cannot be detected in ppm quantities with atomic absorption;
b. the emission spectrographic technique. Emission spectrographic analysis for an uranium sample are given in table 3.2.

III.1.5. Impurity and stoichiometry corrections for UF_4 and UF_3

A considerable problem in the combustion experiments of UF_4 and UF_3 was the impurity correction and stoichiometry correction for the samples. The main reason is that the heats of reaction in F_2 of UF_4 and UF_3 to form UF_6(g) are not very large, whereas, the heats of reaction in fluorine of many possible impurities, such as UO_2, UN, UC, C and H to form UF_6, CF_4 and HF, are very large.

One of the UF_4-samples contained a total of 0.66 mass percent impurities which implied a heat correction of about 3.0 percent of the total heat involved in the experiments. The UF_3-sample contained 1.3 mass percent impurities with a heat correction of about 1.9 percent of the total heat, and the UPd_3-sample contained 3.1 mass percent impurities with a heat correction of 3.4 percent of the total heat involved in the

Table 3.2. Emission spectrographic analysis of "α-zaal" uranium

metallic impurities in "α-zaal" uranium			
impurity	mass percent	impurity	mass percent
Al	0.0011	Mo	0.0001
Cu	0.0002	Si	0.0020
Fe	0.0045	Sn	0.0001
Mn	0.0004	Ni	0.0025

experiments (see chapter III section III.2 and III.4.). The state of combination of impurities in the samples has to be studied also; this is a special problem in samples containing uranium.
An oxygen analyses in UF_4 or UF_3 does not answer the question whether the oxygen is present as oxygen in solution or as UO_2. The solid solubility of the elements O, C, N and H in inorganic uranium compounds such as UF_4, UF_3 and UPd_3 is expected not to be more than 30 ppm [19]. The remainder of the impurities O, C, N and H will be present as UO_2, UC, UN and HF which also implies a change in stoichiometry of the compound under consideration.
Three different ways to apply the impurity correction for UF_4-14 will be illustrated in tables 3.3., 3.4. and 3.5. In table 3.3. all traces of impurities are neglected in making the calculations for ΔH_f^o (UF_4, c, 298.15 K).
If we make the assumption that all traces of impurities are present in solid solution in the calorimetric sample, we will obtain a more negative value for ΔH_f^o (UF_4, c, 298.15 K), as illustrated in table 3.4.
Another approach will be that the impurities O,C, and N will be present as UO_2, UC and UN in the calorimetric sample (UH_3 is not stable at the preparation temperature of the sample); and Fe, Ni and Al will be present as fluorides. The results are presented in table 3.5.

We conclude that, if we take into account the impurities and the state of combination of these impurities in UF_4-14, we will obtain a more negative value for ΔH_f^o(UF_4, c, 298.15 K). This value for the enthalpy

of formation of UF_4 will be about 9 kJ mol^{-1} more negative compared to the value obtained when impurities in UF_4-14 are neglected.

Table 3.3. Analysis and impurity corrections for UF_6-14

element	total mass percent	impurity	mass percent	heat of combustion (Jg^{-1})	total U as UF_6	total F as UF_6
		impurities present in UF_6-14				
U	75.62				75.62	
F	24.36					24.36
		none	none	none		
	99.98 +		0.00	0.00	75.62	24.36 +
	± 0.04				75.62	24.14 (UF_6)
		excess F	0.22			0.22 −
		total	0.22	0.00 +		

mass and impurity correction for UF_6-14

$$(1 - 0.0022)\ g\ UF_6 = -(907.8 - 0.0)\ J\ g^{-1}$$

$$\Delta U_c^o/M(UF_6) = -\ 909.8\ J\ g^{-1}$$

$$\Delta U_c^o\ (UF_6) = -\ 285.7\ kJ\ mol^{-1}$$

$$\Delta H_c^o\ (UF_6) = -\ 288.2\ kJ\ mol^{-1}$$

and $\Delta H_f^o(UF_6, c, 298\ K) = -\ 1909.0\ kJ\ mol^{-1}$

Table 3.4. Analysis and impurity correction for UF_4-14

element	total mass percent	impurity	impurities present in UF_4-14: mass percent	heat of combustion ($J\ g^{-1}$)	total U as UF_4	total F as UF_4
U	75.62				75.62	
F	24.36					24.36
O	0.0363	O(sol)	0.0363	-		
C	0.0043	C(sol)	0.0043	3.33		
N	0.0020	N(sol)	0.0020	-		
H	0.0028	H(sol)	0.0028	7.59		
Fe	0.0083	Fe(sol)	0.0083	1.46		
Ni	0.0019	Ni(sol)	0.0019	0.21		
Si	0.0030	Si(sol)	0.0030	1.72		
Al	0.0015	Al(sol)	0.0015	0.84		
	100.0401 +		0.0601	15.15	75.62	24.36 +
	± 0.04				75.62	24.14
						$-(UF_4)$
		excess F	0.2200			0.22
		total	0.2801	15.15 +		

mass and impurity correction for UF_4-14

$(1 - 0.002801)$ g UF_4 = $-(907.8 - 15.2)$ J g^{-1}

$\Delta U_c^o/M(UF_4)$ = - 895.1 J g^{-1}

$\Delta U_c^o\ (UF_4)$ = - 281.1 kJ mol^{-1}

$\Delta H_c^o\ (UF_4)$ = - 283.6 kJ mol^{-1}

and $\Delta H_f^o(UF_4, c, 298\ K)$ = - 1913.6 kJ mol^{-1}

Table 3.5. Analysis and impurity corrections for UF_4-14

element	total mass percent	impurities present in UF_4-14 impurity	mass percent	heat of combustion ($J\ g^{-1}$)	total U as UF_4	total F as UF_4	
U	75.62				75.62		
F	24.36					24.36	
O	0.0363	UO_2	0.3063	12.56	-0.2700		
C	0.0043	UC	0.0625	7.55	-0.0595		
N	0.0020	UN	0.0360	2.72	-0.0340		
H	0.0028	H(sol)	0.0025	6.78			
		HF *	0.0059	-		-0.0056	
Fe	0.0083	FeF_2	0.0139	-		-0.0056	
Ni	0.0019	NiF_2	0.0031	-		-0.0012	
Si	0.0030	SiC**	0.0043	2.72			
Al	0.0015	AlF_3	0.0047	-		-0.0032	
	100.0401 ± 0.04		0.4392	32.33	75.2565 75.2565	24.3444 24.0265	+
		excess F	0.3179			0.3179	-
		total	0.7571	32.33	+		

* measured amount of HF

** SiC due to cleaning of uranium metal surface

mass and impurity correction for UF_4-14

$$(1 - 0.007571)\ g\ UF_4 = -(907.8 - 32.3)\ J\ g^{-1}$$

$$\Delta U_c^o / M(UF_4) = -882.2\ J\ g^{-1}$$

$$\Delta U_c^o\ (UF_4) = -277.0\ kJ\ mol^{-1}$$

$$\Delta H_c^o\ (UF_4) = -279.5\ kJ\ mol^{-1}$$

and $\Delta H_f^o(UF_4, c, 298.15\ K) = -1917.7\ kJ\ mol^{-1}$

REFERENCES

[1] Berthelot, M. Ann. chim. phys. (5), 23 (1881) 160.

[2] Gross, P.; Hayman, C.; Levi, D.L. Trans Faraday Soc. 51 (1955) 626.

[3] Greenberg, E.; Settle, J.L.; Feder, H.M.; Hubbard, W.N. J. Phys. Chem. 65 (1961) 1168.

[4] Hubbard, W.N.; Johnson, G.K.; Leonidov, V.Ya. In Experimental Chemical Thermodynamics, Combustion Calorimetry, Vol. 1, Chap. 12. S. Sunner, M. Månsson: editors, Pergamon Press: Oxford (1979).

[5] Stein, L.; Rudzitis, E. and Settle, J.L. Purification of Fluorine by Distillation, ANL-6364. Argonne National Laboratory. June (1961).

[6] Hubbard, W.N.; Katz, C.; Waddington, G. J. Phys. Chem. 58 (1954) 142.

[7] Nuttall, R.L.; Wise, S.; Hubbard, W.N. Rev. Sci. Instrum. 32 (1961) 1402.

[8] Kubaschewski, O.; Alcock, C.B. Metallurgical Thermochemistry, Pergamon Press (1979).

[9] Johnson, G.K.; Van Deventer, E.H.; Kruger, O.L. and Hubbard, W.N. J. Chem. Thermodynamics 1 (1969) 89.

[10] Slanina, J; Bakker, F.; Lautenbag, C.; Lingerak, W.A. and Sier, T. Mikrochim. Acta 1 (1978) 519.

[11] Davies, W. and Gray, W. Talanta 11 (1964) 1203.

[12] Maeck, W.J.; Booman, G.L.; Elliot, M.C.; Rein, J.E. Anal. Chem. 31 (1959) 1130.

[13] Cheng, K.L. Anal. Chem. 26 (1954) 1894.

[14] Smiley, W.G. Anal. Chem. 27 (1955) 1098.

[15] Rodden, C.J. Ed., "Analysis of Essential Nuclear Reactor Materials", Division of Technical Information, U.S. Atomic Energy Commission, U.S. Government Printing Office, Washington, D.C. (1964) pp. 240-246.

[16] Greenfield, D.F.; Hyde, K.R. UKAEA Research Group Report, AERE HL-67-1684. March (1967).

[17] Vance, D.E.; Smith, M.E.; Waterbury, G.R. Los Alamos Scientific Laboratory, report LA-4681 (1971).

[18] Sinclair, V.M.; Davies, W.; Melhuish, K.R. Talanta 12 (1965) 841.

[19] Wilkinson, W.D. Uranium Metallurgy. Vol. I.: Uranium Process Metallurgy and Vol. II.: Uranium Corrosion and Alloys. Interscience Publishers. New York (1962).

III.2. THE ENTHALPIES OF FORMATION OF URANIUM TETRAFLUORIDE AND URANIUM TRIFLUORIDE [a]

III.2.1. Introduction

In a previous paper the enthalpies of formation of UF_3 and UF_4 were determined by Cordfunke and Ouweltjes [1]. Based on solution calorimetric measurements, they found that both ΔH_f^o (UF_4, c, 298.15 K) and ΔH_f^o (UF_3, c, 298.15 K), were more negative than previous literature values [2-4]. Therefore, it was decided to obtain independent measurements of the enthalpies of formation of UF_4 and UF_3 using fluorine bomb calorimetry. In this chapter, the results of that determination are detached.

III.2.2. Experimental

III.2.2.1. Principle of the calorimetric reactions

The reactions of UF_4 and UF_3 with fluorine according to:

$$UF_4(c) + F_2(g) \rightarrow UF_6(c), \qquad (3\text{-}4)$$

and,

$$UF_3(c) + 3/2\ F_2(g) \rightarrow UF_6(c), \qquad (3\text{-}5)$$

were chosen because these reactions can be forced to go nearly to completion by using an auxiliary combustion aid.

The auxiliary reaction:

$$U(c) + 3\ F_2(g) \rightarrow UF_6(c), \qquad (3\text{-}6)$$

required to derive the enthalpies of formation of UF_4 and UF_3, was previously studied at Argonne National Laboratory [5].

III.2.2.2. Calorimetric system

The calorimetric system consisted of a nickel combustion bomb similar

---

[a] Work performed under the auspices of the U.S. Department of Energy.

to that described previously [6] and a bomb calorimeter, laboratory designation ANL-R-2, similar to that described by Hubbard et al. [7]. The calorimetric temperatures were measured by quartz-crystal thermometry [8]. The system was calibrated by the combustion in oxygen of benzoic acid (National Bureau of Standards sample 39i) whose certified energy of combustion under prescribed conditions is -(26.434 + 0.003) kJ g^{-1}. A series of calibration experiments, some before, some in between and some following the UF_4 and UF_3 combustions, were performed. The energy equivalent of the calorimetric system, ε(calor) was determined to be (13851.6 $\pm$ 2.2) J K^{-1} for the first six UF_4 (sample 14) combustions, and (13844.4 $\pm$ 4.2) J K^{-1} for the last UF_4 (sample 18) and UF_3 combustions.

III.2.2.3. Materials

The preparation methods of the compounds UF_4 and UF_3 have been described in detail previously [1].

The uranium tetrafluoride samples were prepared by the reaction of hydrogen fluoride with UH_3 at about 850 K [1]. Two different UF_4 samples were used for the calorimetric measurements.

Uranium trifluoride was prepared by the reaction of UF_4 at about 1150K with a stoichiometric amount of UH_3 [1]. The complete chemical analyses of the calorimetric samples are given in tables 3.6., 3.7. and 3.8. Uranium rods from the same batch as used by Johnson [5] to determine the enthalpy of formation of UF_6, were used to prepare the samples UF_4-18 and UF_3-6.

Analytical methods applied were : automatic potentiometric titration, ion specific electrode technique, inert gas fusion and atomic absorption.

The amount of U^{6+} in the UF_4-14 samples was determined to be less than 0.05 mass per cent. The UF_3-6 sample contained (0.55 $\pm$ 0.05) mass per cent UF_4 as was detected on the X-ray diagram [1] by comparison with reference diagrams having known amounts of UF_4. Tungsten foil (thickness 0.025 mm) was purchased from Schwarzkopf Development Corporation for use as an auxiliary combustion aid. Five combustion experiments with this foil were performed and the standard energy of combustion in fluorine of this sample was found to be (- 9382.79 $\pm$ 1.26)J g^{-1}.

The standard energy of combustion of rhombic sulfur (used for ignition)

was found to be -37917.08 J g^{-1} [9]. Purified fluorine (99.99 moles per cent) was prepared by distillation of commercial fluorine (99.98 moles per cent) in a low temperature still [10].

III.2.2.4. Combustion technique and procedures

Preliminary experiments established that the uranium fluoride samples underwent some surface attack when exposed to high pressure fluorine, necessitating the use of a two-chambered bomb. However, the samples did not sustain combustion. Thus it was necessary to use an auxiliary combustion aid to promote reaction. It was found that the combustion of several pieces of tungsten foil under the samples supplied sufficient energy to drive the reaction to or nearly to completion. In approximately 1/3 of the experiments the reaction was complete and in the rest a small amount of partially fluorinated residue, U_4F_{17}, remained. The tungsten foils in addition to supplying energy, also tended to prevent the samples from coming into contact with the nickel support crucible. Such contact would bring about premature cooling of the samples and increase the amount of residue.

The calorimetric procedure was as follows. The combustion bomb was taken into the glovebox and opened. The nickel support crucible (≈28 grams) was weighed and two or three weighed, corrugated tungsten foils were placed on the bottom of the crucible. A saucer-shaped tungsten foil was weighed and the uranium fluoride sample plus a small amount of sulfur used to ignite the sample, were accurately weighed into this saucer. The saucer was placed on the top of the crucible with the lip of the saucer resting on the top edge of the crucible. The bomb was assembled, connected with the fluorine tank, which had been charged to 1827 kPa with fluorine, and taken out of the glovebox. The bomb and connecting tube were evacuated and the system was placed in the calorimeter. After the forerating period, the sample was ignited by opening the tank valve. Following the combustion the bomb was removed from the calorimeter, dried, evacuated, returned to the glovebox, and opened. A small amount of a black residue, obtained from incomplete fluorination of the UF_4 and UF_3 was often found in the nickel crucible. The mass of this residue was determined by weighing the crucible plus residue, carefully removing the residue, and reweighing the crucible. The residue was identified by X-ray analysis as U_4F_{17}.

The mass of the combustion residue varied between 0 - 9 mg for UF_4 and 0 - 1 mg for UF_3. The crucible itself underwent in most cases a small increase in mass which was assumed to be due to the formation of NiF_2.

III.2.3. Results

The results of six combustions of uranium tetrafluoride (sample 14) in fluorine according to reaction (3-4) are presented in table 3.9., and the results of the six combustions of uranium tetrafluoride (sample 18) are presented in table 3.10.

The results of five combustions of uranium trifluoride (sample 6) according to reaction (3-5) are presented in table 3.11. The corrections to standard states were applied as described by Hubbard [11].

In the tables, masses are denoted by m; $\Delta\Theta_c$ is the corrected temperature increase of the calorimeter; ε(calor) is the energy equivalent of the calorimetric system; $\Delta U(WF_6)$ and $\Delta U(SF_6)$ are the corrections for the combustion of tungsten and sulfur; ΔU(condense) is the correction for the hypothetical condensation of gaseous UF_6 product; ΔU(blank) is the correction for the expansion of fluorine from the tank into the empty bomb; ΔU(Ni) is the correction for the formation of NiF_2 coating on the nickel crucible; and $\Delta U(U_4F_{17})$ is the correction for the hypothetical conversion of U_4F_{17} to UF_6(c).

For the calculation of ΔU(contents), the following c_p values ($JK^{-1}g^{-1}$) were used: UF_4, 0.369 [12]; UF_3, 0.322 [12,13]; Ni, 0.4439 [14]; W, 0.1318 [14]; S, 0.7071 [15] and UF_6(c), 0.474 [16]. Similarly, the following C_v values, ($JK^{-1}mol^{-1}$) were used: F_2, 22.97 [17]; WF_6, 110.7 [14] SF_6, 88.89 [15] and UF_6, 121.3 [18].

For the calculation of ΔU(gas), μ in the equation of state $pV = nRT(1-\mu p)$ and $(\delta U/\delta p)_T$ were estimated by the method of Hirschfelder et al. [19] from the intermolecular-force constants for UF_6 [20], WF_6 [20], SF_6 [21] and F_2 [22]. The following values were used for the densities ($g\ cm^{-3}$) of the different substances in the bomb; UF_3, 8.97 [23]; UF_4, 6.72 [23]; W, 19.3 [24]; Ni, 8.9 [24]; and crystalline UF_6, 4.68 [24]. The volume of the empty bomb was 0.3131 dm^3, and the volume of the fluorine tank was 0.2361 dm^3. In order to calculate ΔU(condense), the energy of sublimation of UF_6 was taken to be 47.10 kJ mol^{-1} based on $\Delta H_{sub} = 49.58 \pm 0.42$ kJ mol^{-1} [16]. The vapour pressure

of UF_6(c) at 298.15 K was taken to be 14.91 kPa [25]. The energy of combustion of Ni to form NiF_2, $\Delta U(Ni)$ was taken as -11158.3 J g^{-1} [26]. The energy of combustion of U_4F_{17} was taken to be -721.5 J g^{-1}.

The impurity corrections in tables 3.6., 3.7. and 3.8. are based on the following assumptions. There will be a relatively small solid solubility of the elements O, C, N and H in the calorimetric samples in the order of 10 - 35 ppm. No exact data are known, but comparison was made with uranium metal.

The solid solubility of C in α-uranium is less than 20 ppm [30]; of O in uranium at the melting point is 34 ppm [31], and of N in uranium at the melting point is about 10 ppm [32].

The amount of H detected in the samples was the H in solution [33]; the amount of HF was determined separately in one of the UF_4-samples. The remainder of the impurities will be combined as UO_2, UN, UC and HF, respectively, and during combustion of the calorimetric samples in fluorine, O_2(g), N_2(g), CF_4(g) and HF(g), respectively, are formed. The metal impurities in solution in uranium metal, were assumed to have been originally present as fluorides in UF_4 and not to undergo any further reaction during combustion in fluorine. An exception is silicon which was detected in the samples in 30 ppm quantities. This amount is more likely due to the cleaning of uranium metal with sandpaper before preparation of the calorimetric samples.

The excess of fluorine in the UF_4-samples will be present mainly in solution and not in the form of higher uranium fluorides, since the amount of U^{6+} found in the samples was below the detection limit.

A thermal correction was applied to the UF_3-6 sample for the presence of 0.55 mass per cent UF_4. The excess of fluorine in an UF_x-sample was calculated in the tables 3.6., 3.7. and 3.8. in mass per cent:

$$\text{excess F} = \{\text{F(analyzed)} - \text{F(impurities)}\} - \left\{\frac{\text{U(analyzed)} - \text{U(impurities)}}{\text{M(U)}}\right\} \times \text{M(F)} \qquad (3\text{-}7)$$

The uncertainty in the impurity corrections is large. One reason is that oxygen is segregated in the uranium fluoride samples. The uncertainties in the amounts of UO_2, UC, UN and H(sol) were estimated to be 40, 40, 50 en 20 per cent, respectively.

The derived results for UF_4 and UF_3 are presented in table 3.12. The enthalpy of formation of UF_6(c), which was needed to derive the enthalpies of formation of UF_4 and UF_3, was taken to be -(2197.2 ± 1.8) kJ mol^{-1}. This value is 0.5 kJ mol^{-1} more positive than that reported previously [5]. This revision is discussed below.

The entropies, S° (298.15 K), of U, F_2, UF_3 and UF_4 were taken to be 50.21, 202.67, 123.43 and 151.67 J K^{-1} mol^{-1}, respectively. The uncertainties given in the table are uncertainty intervals as defined by Rossini [34], equal to twice the final overall standard deviation.

The recent redetermination of the enthalpy of formation of UF_6(c) reported by Johnson [5] included thermal corrections for the energies of combustion of the small amounts of UF_3 and UF_4 which is formed along with UF_6 during the combustion of uranium in fluorine. The values measured in this work for the energies of combustion of UF_3 and UF_4 differ by 47.9 and 58.3 J g^{-1}, respectively, from those used by Johnson. When these corrections are recalculated, based on the present measurements, the enthalpy of formation of UF_6(c) becomes 0.5 kJ mol^{-1} more positive, i.e., ΔH_f^o (UF_6, c, 298.15 K) = -(2197.2 ± 1.8) kJ mol^{-1}. Similarily ΔH_f^o(UF_6, g, 298.15 K) becomes -(2147.6 ± 1.8) kJ mol^{-1}.

III.2.4. Discussion

For comparison, the published values for the enthalpies of formation of UF_3(c) and UF_4(c) are tabulated in table 3.13. Hayman [2,35] derived his values from measurements of the enthalpies of fluorination of UF_3(c) and UF_4(c) to UF_6(g) at 315 K by means of fluorine flow calorimetry which were combined with the enthalpy of fluorination of U(c) to UF_6(g) at 298 K, measured in the same way. However, it turned out that the latter value is in error by about 11 kJ mol^{-1}, as has been found in a recent redetermination by Johnson [5]. Moreover, Hayman's value for the enthalpy of fluorination of UF_4, -(237.7 ± 0.7) kJ mol^{-1}, is too negative, because no corrections were made for the metal impurities in his sample. When these corrections are applied, Hayman's recalculated enthalpy of fluorination of UF_4 becomes -(234.6 ± 3.0) kJ mol^{-1}. When this value is combined with Johnson's value for the enthalpy of formation of UF_6, ΔH_f^o(g, 298.15 K) = -(2147.6 ± 1.8) kJ mol^{-1}, the recalculated value for the enthalpy of formation of UF_4 becomes -(1913.0 ±

3.5) kJ mol^{-1}, which should be seen as a tentative value, because some corrections cannot be checked properly.

For instance, there is confusion about the right amount of Si in Hayman's UF_4 sample. If 500 ppm Si [2] was detected instead of 50 ppm Si [35], the recalculated value for the enthalpy of formation of UF_4 becomes -(1921.1 ± 3.5) kJ mol^{-1}.

Hayman's value for the enthalpy of fluorination of UF_3, -(641.8 ± 1.9) kJ mol^{-1} has to be corrected also for impurities in the sample. However, since no metal impurities have been given, such a correction cannot be made, and it is evident that the value given will become more negative. A combination with Johnson's value for ΔH_f^o (UF_6, g) therefore, can only result in a tentative value for UF_3, ΔH_f^o (c, 298.15 K) = -(1505.8 ± 4.6) kJ mol^{-1}.

We assume here that only Hayman's energy of combustion of uranium to UF_6 is in error, and that his energies of combustion of UF_3 and UF_4 have, apart from impurity corrections, the correct value.

The combustion of fluorides in fluorine is less complicated than the combustion of low-melting metals. This justifies that only the uranium combusion might be in error. However, a disadvantage of the use of the fluorine calorimetric method, to determine the enthalpies of formation of uranium fluorides, is that all impurities in the samples have to be known exactly, as well as the state in which the impurities are present (which is not always possible), in order to apply the proper corrections on the heats of combustion of the samples.

Khanaev, and Khanaev and Kripin [3,4] measured the enthalpies of solution of UF_4(c) and UF_3(c), respectively, in a $[HCl + H_3BO_3 + FeCl_3]_{solution}$ at 323 K from which they derive for the enthalpies of formation the values -(1898.4 ± 0.9) kJ mol^{-1} and -(1494 ± 5) kJ mol^{-1}. A recalculation of their results, using revised values for the auxiliary data, such as for H_2O [36], $FeCl_2$, $FeCl_3$ and HCl [36], yields for UF_4(c) and UF_3(c) an average value [obtained from two different cycles] of ΔH_f^o (298.15 K) = -(1897.4 ± 1.2) kJ mol^{-1} and -(1482 ± 5) kJ mol^{-1}, respectively.

When we compare the data in table 3.13., obtained from different studies, it appears that for UF_4 there is an excellent agreement between the various results; only Khanaev's values seem to be too positive. It is noted that comparison of the published results for ΔH_f^o (NdF_3, c,

298.15 K) [28] also shows that Khanaev's results [29] are too positive by about 20 kJ mol^{-1}.

For UF_4(c) we suggest an average enthalpy of formation of -(1918.2 ± 3.5) kJ mol^{-1}. For UF_3(c) the situation is equally good, because we know, as stated above, that Hayman's value is too positive in this case. For this reason we take the average of the two independent measurements, described in this paper, and in the previous one in this series. The value $\Delta H_f^o(UF_3, c, 298.15\ K) = -(1505.5 \pm 6.0)$ kJ mol^{-1} has been obtained.

The authors wish to thank: W. Ouweltjes and F.G.M. Kleverlaan for preparing UF_3 and UF_4; F. Bakker, P. van Vlaanderen, K.J. Jensen, R.J. Meyer and G. Waterbury (Los Alamos Scientific Laboratory) for analytical services; P.A.G. O'Hare and W.N. Hubbard for many helpful discussions.

Table 3.6. Analysis and impurity corrections for UF_4-14

element	total mass percent	impurities present in UF_4-14					error in heat of comb. (J g^{-1})
		impurity	mass percent	heat of combustion (J g^{-1})	total U as UF_4	total F as UF_4	
U	75.62				75.62		
F	24.36					24.36	
O	0.0363	O(sol)	0.0035	-			
		UO_2	0.2768	11.35	-.2440		± 4.5
C	0.0043	C(sol)	0.0015	1.16			
		UC	0.0312	3.77	-.0297		± 1.5
N	0.0020	N(sol)	0.0010	-			
		UN	0.0180	1.36	-.0170		± 0.7
H	0.0028	H(sol)	0.0025	6.78			± 1.4
		HF	0.0059	-		-0.0056	
Fe	0.0083	FeF_2	0.0139	-		-0.0056	
Ni	0.0019	NiF_2	0.0031	-		-0.0012	
Si	0.0030	SiC	0.0043	2.72			
Al	0.0015	AlF_3	0.0047	-		-0.0032	± 0.3
	100.0401		0.3664	27.14	75.3293	24.3444	
	(± 0.04)				75.3293	24.0498 (UF_4)	
		excess F	0.2946			0.2946	
		total	0.6610	27.14			

mass and impurity correction for UF_4-14 : $(1 - 0.006610)\ g\ UF_4 = -(907.8 - 27.1)\ J\ g^{-1}$

$$\Delta U_c^o/M(UF_4) = -(886.6 \pm 10.4)\ J\ g^{-1}$$

Table 3.7. Analysis and impurity corrections for UF_4-18

element	total mass percent	impurities present in UF_4-18: impurity	mass percent	heat of combustion ($J\ g^{-1}$)	total U as UF_4	total F as UF_4	error in heat of comb. $J\ g^{-1}$
U	75.61				75.61		
F	24.35					24.35	
O	0.0140	O(sol)	0.0035	-			
		UO_2	0.0886	3.63	-0.0781		± 1.5
C	0.0039	C(sol)	0.0015	1.16			
		UC	0.0250	3.02	-0.0238		± 1.2
N	0.0012	N(sol)	0.0010	-			
		UN	0.0036	0.27	-0.0034		± 0.7
H	0.0033	H(sol)	0.0030	8.13			± 1.6
		HF	0.0059	-		-0.0056	
Fe	0.0011	FeF_2	0.0018	-		-0.0007	
Al	0.0008	AlF_3	0.0025	-		-0.0017	
Ca	0.0005	CaF_2	0.0010	-		-0.0005	
Si	0.0028	SiC	0.0040	2.46			± 0.3
	99.9873		0.1414	18.67	75.5047	24.3415	
	(± 0.02)				75.5047	24.1058 (UF_4)	
		excess F	0.2357			0.2357	
		total	0.3771	18.67			

Mass and impurity correction for UF_4-18 : $(1 - 0.003771)$ g UF_4 = $-(902.4 - 18.7)$ J g^{-1}

$$\Delta U_c^o/M(UF_4) = -(887.0 \pm 6.1)\ J\ g^{-1}$$

Table 3.8. Analysis and impurity corrections for UF_3-6

element	total mass per cent	impurities present in UF_3-6					error in heat of comb. J g^{-1}
		impurity	mass percent	heat of combustion (J g^{-1})	total U as UF_3	total F as UF_3	
U	80.54				80.54		
F	19.33					19.33	
O	0.0743	O(sol)	0.0035	-			
		UO_2	0.5975	24.50	-0.5267		± 9.8
C	0.0041	C(sol)	0.0015	1.16			
		UC	0.0271	3.28	-0.0258		± 1.3
N	0.0013	N(sol)	0.0010	-			
		UN	0.0054	0.41	-0.0051		± 0.7
H	0.0033	H(sol)	0.0030	8.13			± 1.6
		HF	0.0060	-		-0.0057	
Fe	0.0012	FeF_2	0.0020	-		-0.0008	
Al	0.0009	AlF_3	0.0028	-		-0.0019	
Ca	0.0005	CaF_2	0.0010	-		-0.0005	
Si	0.0030	SiC	0.0043	2.72			± 0.3
		UF_4	0.5500	4.91	-0.4169	-0.1331	± 0.5
	99.9583 (± 0.04)		1.2051	45.11	79.5655	19.1880	
					79.5655	19.0517 (UF_3)	
		excess F	0.1363			0.1363	
		total	1.3414	45.11			

mass and impurity correction for UF_3-6 : (1 - 0.013414) g UF_3 = -(2356.2 - 45.1) J g^{-1}

$$\Delta U_c^o/M(UF_4) = -(2342.5 \pm 20.6) \text{ J } g^{-1}$$

Table 3.9. Results of uranium tetrafluoride (UF_4-14) combustion experiments at 298.15 K

Experiment No.	1	2	3	4	5	6
$m(UF_4)/g$	2.56354	2.56684	2.56017	2.58929	2.56827	1.54231
$m(W)/g$	1.54147	1.54539	1.51645	1.57883	1.62110	1.54671
$m(S)/g$	0.00364	0.01670	0.00967	0.01510	0.01813	0.01327
$m(U_4F_{17})/g$	0.00627	0.00000	0.00108	0.00000	0.00000	0.00039
$\Delta\theta_c/K$	1.21298	1.25339	1.21411	1.27271	1.30768	1.17732
$\varepsilon(calor)(-\Delta\theta_c)/J$	-16801.7	-17361.5	-16817.4	-17629.1	-18113.5	-16307.8
$\Delta U(contents)/J$	-23.5	-24.3	-23.5	-24.7	-25.4	-22.4
$\Delta U(gas)/J$	1.0	1.0	1.0	1.0	1.0	1.4
$\Delta U(WF_6)/J$	14462.5	14499.3	14227.8	14813.0	15209.6	14511.7
$\Delta U(SF_6)/J$	138.0	633.2	366.7	572.5	687.4	503.2
$\Delta U(blank)/J$	-2.0	-2.0	-2.0	-2.0	-2.0	-2.0
$\Delta U(condense)/J$	-87.6	-87.6	-87.6	-87.6	-87.6	-87.7
$\Delta U(Ni)/J$	3.3	3.3	2.1	3.3	5.5	5.2
$\Delta U(U_4F_{17})/J$	-4.5	0.0	-0.8	0.0	0.0	-0.3
$\{\Delta U_c^o/M(sample)\}/J\ g^{-1}$	-902.9	-911.1	-911.5	-909.0	-905.3	-906.9

$\{\Delta U_c^o/M(sample)\} = -(907.8 \pm 1.4)\ J\ g^{-1}$ [a]

mass and impurity correction : $(1 - 0.006610)\ g\ UF_4 = -(907.8 - 27.1)\ J\ g^{-1}$ [c]

$\Delta U_c^o/M(UF_4) = -(886.6 \pm 10.4)\ J\ g^{-1}$ [b]

[a] $\pm$ the standard deviation of the mean ; [b] $\pm$ uncertainty interval ; [c] see table 3.6.

Table 3.10. Results of uranium tetrafluoride (UF_4-18) combustion experiments at 298.15 K

Experiment No.	1	2	3	4	5	6
$m(UF_4)/g$	1.80759	1.82607	1.83507	1.81313	1.84265	1.82192
$m(W)/g$	1.67079	1.69914	1.70630	1.68972	1.70164	1.65297
$m(S)/g$	0.02019	0.02761	0.02592	0.02938	0.02018	0.01733
$m(U_4F_{17})/g$	0.00913	0.00022	0.00049	0.00000	0.00026	0.00000
$\Delta\Theta_c/K$	1.29655	1.33812	1.33794	1.33546	1.32065	1.27774
$\varepsilon(calor)(-\Delta\Theta_c)/J$	-17950.0	-18525.5	-18523.0	-18488.6	-18283.6	-17689.5
$\Delta U(contents)/J$	-24.8	-25.6	-25.6	-25.5	-25.3	-24.4
$\Delta U(gas)/J$	1.4	1.4	1.4	1.4	1.4	1.4
$\Delta U(WF_6)/J$	15675.8	15941.8	16009.0	15853.4	15965.3	15508.6
$\Delta U(SF_6)/J$	765.5	1046.9	982.8	1114.0	765.2	657.1
$\Delta U(blank)/J$	-6.9	-6.9	-6.9	-6.9	-6.9	-6.9
$\Delta U(condense)/J$	-87.6	-87.6	-87.6	-87.6	-87.6	-87.6
$\Delta U(Ni)/J$	6.4	0.0	2.1	2.4	0.0	2.9
$\Delta U(U_4F_{17})/J$	-6.6	-0.2	-0.4	0.0	-0.2	0.0
$\{\Delta U_c^o/M(sample)\}/J\ g^{-1}$	-900.0	-906.7	-898.2	-903.1	-907.2	-899.3

$\{\Delta U_c^o/M(sample)\} = -(902.4 \pm 1.6)\ J\ g^{-1}$ [a]

mass and impurity correction : $(1 - 0.003771)\ g\ UF_4 = -(902.4 - 18.7)\ J\ g^{-1}$ [c]

$\Delta U_c^o/M(UF_4) = -(887.0 \pm 6.1)\ J\ g^{-1}$ [b]

[a] $\pm$ the standard deviation of the mean ; [b] $\pm$ uncertainty interval ; [c] see table 3.7.

Table 3.11. Results of uranium trifluoride combustion experiments at 298.15 K

Experiment No.	1	2	3	4	5
$m(UF_3)/g$	1.00178	1.00569	1.00199	1.00128	1.00242
$m(W)/g$	2.18080	2.22054	2.19529	2.20141	2.13686
$m(S)/g$	0.01250	0.02180	0.02109	0.02020	0.01674
$m(U_4F_{17})/g$	0.00032	0.00037	0.00029	0.00051	0.00107
$\Delta\theta_c/K$	1.67472	1.72756	1.70745	1.70887	1.65625
$\varepsilon(calor)(-\Delta\theta_c)/J$	-23185.5	-23917.0	-23638.6	-23658.3	-22929.8
$\Delta U(contents)/J$	-31.6	-32.6	-32.2	-32.2	-31.2
$\Delta U(gas)/J$	1.9	1.9	1.9	1.9	1.8
$\Delta U(WF_6)/J$	20460.9	20833.8	20596.8	20654.3	20048.6
$\Delta U(SF_6)/J$	474.0	826.6	799.7	765.0	634.7
$\Delta U(blank)/J$	-5.7	-5.7	-5.7	-5.7	-5.7
$\Delta U(condense)/J$	-87.7	-87.7	-87.7	-87.7	-87.7
$\Delta U(Ni)/J$	5.5	13.4	10.2	3.6	8.3
$\Delta U(U_4F_{17})/J$	-0.2	-0.3	-0.2	-0.4	-0.8
$\{\Delta U_c^o/M(sample)\}/J\ g^{-1}$	-2364.2	-2354.2	-2351.1	-2355.6	-2356.1

$\{\Delta U_c^o/M(sample)\} = -(2356.2 \pm 2.1)\ J\ g^{-1}$ [a]

mass and impurity correction : $(1 - 0.013414)\ g\ UF_3 = -(2356.2 - 45.1)\ J\ g^{-1}$ [c]

$\Delta U_c^o/M(UF_3) = -(2342.5 \pm 20.6)\ J\ g^{-1}$ [b]

[a] $\pm$ the standard deviation of the mean ; [b] $\pm$ uncertainty interval ; [c] see table 3.8.

Table 3.12. Derived results for UF_4 and UF_3 at 298.15 K

	UF_4-14 [a]	UF_4-18 [a]	UF_3-6 [b]
$\{\Delta U_c/M\}$/J g^{-1}	- 886.6 ± 10.4	- 887.0 ± 6.1	-?342.5 ± 20.6
ΔU_c^o/kJ mol^{-1}	- 278.4 ± 3.3	- 278.5 ± 1.9	- 691.1 ± 6.1
ΔH_c^o/kJ mol^{-1}	- 280.9 ± 3.3	- 281.0 ± 1.9	- 694.8 ± 6.1
ΔH_f^o/kJ mol^{-1}	-1916.3 ± 3.8	-1916.2 ± 2.6	-1502.4 ± 6.4

[a] The molar mass of UF_4 was taken to be 314.023 g mol^{-1}

[b] The molar mass of UF_3 was taken to be 295.024 g mol^{-1}

Table 3.13. Published values of the enthalpies of formation of $UF_3(c)$ and $UF_4(c)$ at 298.15 K

Investigator and method		$\Delta H_f^\circ(UF_3)$/kJ mol^{-1}		$\Delta H_f^\circ(UF_4)$/kJ mol^{-1}	
		original	corrected	original	corrected
Hayman (1967)[2,35]	Fluorine flow calorimetry	- (1494.1 ± 3.3)	- (1505.8 ± 4.6)	- (1898.3 ± 2.9)	- (1913.0 ± 3.5)
Khanaev (1968)[3]	Solution calorimetry	-----		- (1898.4 ± 0.9)	- (1897.4 ± 1.2)
Khanaev and Kripin (1970)[4]	Solution calorimetry	- (1494.5 ± 5)	- (1482 ± 5)	-----	
Cordfunke and Ouweltjes[1]	Solution calorimetry	- (1508.5 ± 5.5)		- (1920.0 ± 3.7)	
This work	Fluorine bomb calorimetry	- (1502.4 ± 6.4)		- (1916.3 ± 3.2)	

REFERENCES

[1] Cordfunke, E.H.P.; Ouweltjes, W. J. Chem. Thermodynamics, 13 (1981) 193.

[2] Hayman, C. In Thermodynamik - Symposium. Schäfer, Kl.: editor. Heidelberg: Germany, September (1967).

[3] Khanaev, E.I. Izv. Sib. Otd. Akad. Nauk SSSR, Ser. Khim. Nauk. 9 (1968) 123.

[4] Kanaev, E.I.; Kripin, L.A. Soviet Radiochem. 12 (1970) 158.

[5] Johnson, G.K. J. Chem. Thermodynamics 11 (1979) 483.

[6] Nuttall, R.L.; Wise, S.; Hubbard, W.N. Rev.Sci. Instr. 32 (1961) 1402.

[7] Hubbard, W.N.; Katz, C.; Waddington, G. J. Phys. Chem. 58 (1954) 142.

[8] Johnson, G.K.; Van Deventer, E.H.; Kruger, O.L.; Hubbard, W.N. J. Chem. Thermodynamics 1 (1969) 89.

[9] O'Hare, P.A.G.; Settle, J.L.; Hubbard, W.N. Trans. Faraday Soc. 62 (1966) 558.

[10] Stein, L.; Rudzitis, E.; Settle, J.L. Purification of Fluorine by Distillation. USAEC Report No. ANL-6364. June (1961).

[11] Hubbard, W.N. In Experimental Thermochemistry, Vol. II, Chap. 6; Skinner, H.A.: editor, Interscience: New York; (1962).

[12] Cordfunke, E.H.P.; Prins, G.; Muis, R.P. J. Chem. Thermodynamics, to be published.

[13] Westrum, E.F. University of Michigan, Ann Arbor, Personal communication.

[14] Wagman, D.D.; Evans, W.H.; Parker, V.B.; Halow, I.; Bailey, S.M.; Schumm, R.H. Nat. Bur. Stand. U.S. Tech. Note 270-4; (1969).

[15] JANAF Thermochemical Tables, Second Edition, Nat. Bur. Stand. U.S. Techn. NSRDS - NBS37, June; (1971).

[16] Parker, V.B. National Bureau of Standards, Washington, D.C., Private Communication.

[17] Wagman, D.D.; Evans, W.H.; Parker, V.B.; Halow, I.; Bailey, S.M.; Schumm, R.H. Nat. Bur. Stand. U.S. Tech. Note 270-3; (1968).

[18] Gaunt, J. Trans. Faraday Soc. 49 (1953) 1122.

[19] Hirschfelder, J.O.; Curtiss, C.F.; Bird, R.B. Molecular Theory of Gases and Liquids. Wiley, New York; (1964).

[20] Morizot, P.; Ostorero, J.; Plurien, P. J. Chem. Phys. 70 (1973) 1582.

[21] Ueda, K.; Kigoshi, K. J. Inorg. Nucl. Chem. 36 (1974) 989.

[22] White, D.; Hu, J.H.; Johnston, H.L. J. Chem. Phys. 21 (1953) 1149.

[23] Cordfunke, E.H.P. The Chemistry of Uranium, Elsevier: Amsterdam (1969).

[24] Handbook of Chemistry and Physics, 56th edition, Weast, R.C.: editor. C.R.C. Press, Inc.: Cleveland. (1975-1976).

[25] Oliver, C.D.; Milton, H.T.; Grisard, J.W. J. Am. Chem. Soc. 75 (1953) 2827.

[26] Rudzitis, E.; Van Deventer, E.H.: Hubbard, W.N. J. Chem. Eng. Data 12 (1967) 133.

[27] Codata, Tentative set of key values for thermodynamics, part V (1975).

[28] Kim, Y.-C.; Oishi, J. J. Chem. Thermodynamics, 12 (1980) 407.

[29] Khanaev, E.I.; Kotov, M.G.; Afanas'ev, Yu.A.; Il'ina, L.D. Radiokhimiya 19 (1977) 265.

[30] Wilkinson, W.D. Uranium Metallurgy, Vol. I.: Uranium Process Metallurgy and Vol. II.: Uranium Corrosion and Alloys. Interscience Publishers. New York (1962).

[31] Katz, J.J.; Rabinowitch, E. The Chemistry of Uranium, McGrawHill Book Company, Inc. New York (1951), p. 246.

[32] Bugl, J.; Bauer, A.A. J. Am. Ceram. Soc. 47 (1964) 425.

[33] Waterbury, G. Personal Communication.

[34] Rossini, F.D. In Experimental Thermochemistry chap. 14. Rossini, F.D.: editor. Interscience: New York (1956).

[35] Hayman, C.; Stuart, M.A.; Stuart, M.C. Report on Thermodynamic Measurements on Uranium Compounds, Contract No. CON/HAR/EMR/1349, Fulmer Research Institute Limited, R.165/14/ November 1965.

[36] Codata Bulletin 10, December (1973); J. Chem. Thermodynamics 7 (1975) 1.

III.3. THE ENTHALPY OF FORMATION OF PALLADIUM (II) HEXAFLUOROPALLADATE (IV), $Pd(PdF_6)$, BY PF_3 REDUCTION CALORIMETRY [a,b]

III.3.1. Introduction

There has been interest in the binary fluorides of the platinum metals for many years. In spite of numerous experimental and theoretical studies on the subject [1], almost no reliable thermochemical data, such as enthalpies of formation, are available for these fluorides. The enthalpy of formation of RuF_5 has been measured previously [2].
Three binary fluorides of palladium have been identified by X-ray diffraction analysis: PdF_2 [3-5], which is the only established difluoride of the platinum metals; PdF_4 [6], and "PdF_3" [7] which has been shown to be the mixed-valence compound $Pd(II)\{Pd(IV)F_6\}$ [8,9]. Predicted values for the enthalpy of formation of PdF_2 and PdF_3, -469 and -510 kJ mol^{-1}, respectively, were published by Brewer et al. [10]. This paper describes a determination of the enthalpy of formation of $Pd(PdF_6)$ using a bomb-calorimetric method.

III.3.2. Experimental

III.3.2.1. Principle of the calorimetric reactions

The reaction of $Pd(PdF_6)$ with gaseous PF_3, according to

$$Pd(PdF_6)(c) + 3PF_3(g) = 3PF_5(g) + 2Pd(c), \qquad (3\text{-}8)$$

was chosen because it takes place spontaneously. The enthalpy of the reaction required to derive the standard enthalpy of formation of $Pd(PdF_6)$:

$$PF_3(g) + F_2(g) = PF_5(g), \qquad (3\text{-}9)$$

has been previously reported [11,12].

---

[a] Work performed under the auspices of the U.S. Department of Energy.
[b] This chapter has been published as an article with the same title in The Journal of Chemical Thermodynamics, 13 (1981) 471, by G. Wijbenga and G.K. Johnson.

III.3.2.2. Calorimetric system

The bomb calorimeter employed in this study (Laboratory designation ANL-R-2) was similar to that described previously [13]. A two-compartment nickel bomb (Laboratory designation Ni-3) similar to that described previously [14] was used for the experiments. The calorimetric temperatures were measured by means of a quartz-crystal thermometer [15]. The system was calibrated by the combustion in oxygen of benzoic acid (National Bureau of Standards sample 39i), whose certified specific energy of combustion under prescribed conditions is $-(26.434 \pm 0.003)$ kJ g^{-1}. A series of calibration experiments was performed following the $Pd(PdF_6)$ reductions. The average value and standard deviation of the mean for ε(calor), the energy equivalent of the calorimetric system, was determined to be (13844.4 ± 2.1) J K^{-1}.

III.3.2.3. Materials

A $Pd(PdF_6)$ sample was generously provided by Dr. Alain Tressaud (Université de Bordeaux I, France). It was prepared by passing high purity fluorine over palladium sponge, 99.99 mass per cent pure (supplied by Comptoir-Lyon-Alemand Louyot). The fluoride product was treated four times for eight hours each at 823 K with flowing purified fluorine to minimize PdF_2 contamination. Each fluorination was followed by grinding the product in a dry box, then checking it by X-ray diffraction analysis [8,16]. In the pure form, $Pd(PdF_6)$ is a black solid at room temperature. The compound reacts immediately with moisture to form HF, palladium, palladium oxides, and palladium hydroxides. The sample was examined by X-ray diffraction and lines due only to PdF_2 and $Pd(PdF_6)$ were found. The mass percentage of PdF_2 present in the sample, (2.5 ± 0.5), was determined by comparing the intensities of the PdF_2 lines with those of standard samples containing known mass percentages of PdF_2. The sample was shipped under helium to Argonne National Laboratory where it was stored in a helium-atmosphere glovebox.

Phosphorous trifluoride was obtained from Ozark Mahoning Co. As received, the gas contained about 0.2 volume percent of O_2, about 6 volume percent of N_2, and traces of PF_5 and POF_3. The oxygen and nitrogen were removed by condensing the PF_3 in a steel trap with liquid nitrogen and pumping on the solid. This procedure was repeated several times. Gas-chromatographic analysis of the resultant PF_3 showed oxygen and

nitrogen levels of mass fraction 5 x 10^{-6} and 10 x 10^{-6}, respectively.

III.3.2.4. Procedures

Preliminary experiments showed that the palladium fluoride when exposed to PF_3 reacted spontaneously to give Pd. A two-chambered combustion bomb was thus required. The calorimetric procedure was as follows. The combustion bomb was taken into the glovebox and opened. The $Pd(PdF_6)$ sample was accurately weighed into a pre-weighed 4 g nickel support crucible, which was then placed on the bomb head. The bomb was assembled, connected with the tank which had been charged to 1830 kPa with PF_3, and taken out of the glovebox. The bomb and connecting tube were evacuated, and the system was placed in the calorimeter.

After the forerating period, the reduction of $Pd(PdF_6)$ was started by opening the tank valve, as described elsewhere [17]. After the reduction, the bomb was removed from the calorimeter, dried, evacuated, returned to the glovebox, and opened.

The solid reaction product was identified by X-ray analysis to be pure palladium metal. The mass of the residue was determined by weighing the nickel crucible plus residue, removing the residue, and reweighing the crucible. In all the experiments the mass of the residue was about 10 mg less than the previously calculated mass of palladium in the $Pd(PdF_6)$. This mass loss may be due to the formation of a gaseous complex of PF_3 with palladium metal [18] or entrainment of the fine powder in the swirling gases in the bomb. The presence of small amounts of unreacted $Pd(PdF_6)$ in the residue was also possible. To determine the amount of unreacted $Pd(PdF_6)$, the residue was washed with 0.6 mol kg^{-1} HCl for 30 minutes at room temperature; the solution was then filtered to remove palladium and analyzed for fluorine by use of an ion-specific electrode.

The nickel support crucible did not change in mass during the experiments.

III.3.3. Results

The results of four reductions of palladium(II) hexafluoropalladate(IV) with PF_3 according to reaction (3-8) are presented in table 3.14. The corrections to standard states were applied as described by Hubbard [19]. The correction for the expansion of PF_3 from the tank into the

Table 3.14. Results of $Pd(PdF_6)$ reduction experiments at 298.15 K

Experiment No.	1	2	3	4
$m^i\{Pd(PdF_6)\}/g$	0.74185	0.64942	0.63698	0.53393
$m^f\{Pd(PdF_6)\}/g$	0.00266	0.00309	0.00244	0.00244
$m\{Pd(PdF_6),reacted\}/g$	0.73919	0.64633	0.63454	0.53169
$\Delta\Theta_c/K$	0.14570	0.12719	0.12369	0.10334
$\varepsilon(calor)(-\Delta\Theta_c)/J$	-2017.1	-1760.9	-1712.4	-1430.7
$\Delta U(contents)/J$	-6.5	-5.5	-5.8	-4.5
$\Delta U(gas)/J$	0.2	0.2	0.2	0.1
$\Delta U(blank)/J$	-72.6	-72.6	-72.6	-72.6
$\{\Delta U_c^o/M(sample)\}/J\ g^{-1}$	-2835.5	-2845.0	-2821.9	-2835.7

$\{\Delta U_c^o/M(sample)\}$	$= -(2834.5 \pm 4.8)\ J\ g^{-1}$ [a]
Impurity correction	$= -(43.0 \pm 5.6)\ J\ g^{-1}$ [a]
$\Delta U_c^o/M\{Pd(PdF_6)\}$	$= -(2877.5 \pm 22.1)\ J\ g^{-1}$ [b]
$\Delta U_c^o = \Delta H_c^o$	$= -(940.3 \pm 7.2)\ kJ\ mol^{-1}$ [b,c]
$\Delta H_f^o\{Pd(PdF_6)\}$	$= -(967.4 \pm 7.3)\ kJ\ mol^{-1}$ [b,c]

[a] Standard deviation of the mean.

[b] $\pm$, Uncertainty interval equal to twice the final overall standard deviation [23].

[c] The molar mass of $Pd(PdF_6)$ was taken to be 326.79 g mol^{-1}.

empty bomb, which is designated by ΔU(blank), was obtained by interspersing four blank experiments among the $Pd(PdF_6)$ reductions. These experiments gave an average value and standard deviation of the mean of $-(72.6 \pm 5.1)$J for this correction. The other entries in the table have the usual significance.

For the calculation of ΔU(contents), the following values of c_p/J $K^{-1}g^{-1}$ were used: Pd, 0.243 [20] and Ni, 0.4439 [20]. The following values of C_v/J $K^{-1}mol^{-1}$ were used: $PF_3(g)$, 50.38 [21] and $PF_5(g)$, 74.85 [21]. The following values for the densities, ρ/g cm^{-3}, of the different substances in the bomb were used: Pd, 11.4; Ni, 8.9; and PdF_3, 5.06. For the calculation of ΔU(gas), μ in the equation of state $pV = nRT(1-\mu p)$, and $(\delta U/\delta p)_T$ were estimated by the method of Hirschfelder et al. [22] from the estimated intermolecular-force constants for PF_3 and PF_5. Typical values of μ and $(\delta U/\delta p)_T$ for the gaseous mixture in the bomb following combustion were 5.9×10^{-5} kPa^{-1} and 0.294 $Jmol^{-1}$ kPa^{-1}, respectively. The volume of the empty bomb was 0.3131 dm^3, and the volume of the tank was 0.2361 dm^3.

The impurity correction in table 3.14. is for the (2.5 ± 0.5) mass per cent PdF_2 in the sample. The value for $\Delta H_f^o(PdF_2, c, 298.15\ K)$ was taken to be $-(469 \pm 42)$ kJ mol^{-1} [10], and its enthalpy of reaction with PF_3 was derived to be $-(167 \pm 42)$ kJ mol^{-1}. The large uncertainty attached to the impurity correction reflects the uncertainty in the estimated value for $\Delta H_f^o(PdF_2, c, 298.15\ K)$ and the uncertainty in the amount of PdF_2 in the sample. No correction was made for any interaction between Pd and PF_3.

The standard enthalpy of formation of $Pd(PdF_6)$, $\Delta H_f^o(Pd(PdF_6), c, 298.15\ K)$, of $-(967.4 \pm 7.3)$ kJ mol^{-1} was derived by subtracting the measured enthalpy of reaction from three times the enthalpy of reaction (2): $-(635.9 \pm 0.3)$ kJ mol^{-1} [12]. The only previous value for the enthalpy of formation of $Pd(PdF_6)$ is an estimate of $-(1020 \pm 170)$ kJ mol^{-1} [10].

The authors wish to thank A. Tressaud for preparing the $Pd(PdF_6)$ sample; C.Chow, K.J. Jensen and B.S. Tani for analytical services; E.H.P. Cordfunke, W.N. Hubbard and P.A.G. O'Hare for many helpful discussions.

REFERENCES

[1] Weinstock, B. Chem. Eng. News 42, 38 (1964) 86.

[2] Porte, H.A.; Greenberg, E.; Hubbard, W.N. J. Phys. Chem. 69 (1965) 2308.

[3] Ruff. O.; Ascher, E. Z. Anorg. Chem. 183 (1929) 193.

[4] Bartlett, N.; Hepworth, M.A. Chem. and Ind. London (1956) 1425.

[5] Bartlett, N.; Maitland, R. Acta Crystallogr. 11 (1958) 747.

[6] Rao, P.R.; Tressaud, A; Bartlett, N. J. Inorg. Nucl. Chem. (Suppl) (1976) 23.

[7] Hepworth, M.A.; Jack, K.H.; Peacock, R.D.; Westland, G.J. Acta Crystallogr. 10 (1957) 63.

[8] Bartlett, N.; Rao, P.R. Proc. Chem. Soc. (1964) 393.

[9] Tressaud, A.; Wintenberger, M.; Bartlett, N.; Hagenmuller, P.C.R. Acad. Sci. Ser. C 282 (1976) 1069.

[10] Brewer, L.; Bromley, L.A.; Gilles, P.W.; Lofgren, N.L. In The Chemistry and Metallurgy of Miscellaneous Materials: Thermodynamics Chap. 6. Quill, L.L.; editor, McGraw-Hill: New York. (1950). pp. 76-192.

[11] Rudzitis, E.; Van Deventer, E.H.; Hubbard, W.N. J. Chem. Thermodynamics 2 (1970) 221.

[12] Johnson, G.K.; Malm, J.G.; Hubbard, W.N. J. Chem. Thermodynamics 4 (1972) 879.

[13] Hubbard, W.N.; Katz, C.; Waddington, G.J. Phys. Chem. 58 (1954) 142.

[14] Nuttall, R.L.; Wise, S.; Hubbard W.N. Rev. Sci. Instrum. 32 (1961) 1402.

[15] Johnson, G.K.; Van Deventer, E.H.; Kruger, O.L.; Hubbard, W.N. J. Chem. Thermodynamics 1 (1969) 89.

[16] Tressaud, A. Personal communication, (1980).

[17] Wijbenga, G. Thesis, Amsterdam, (1981).

[18] Cotton, F.A.; Wilkinson, G. Advanced Inorganic Chemistry, 2nd edition. Interscience: New York. (1966).

[19] Hubbard, W.N. In Experimental Thermochemistry. Vol. II, chap. 6. Skinner, H.A.: editor. Interscience: New York. (1962).

[20] Wagman, D.D.; Evans, W.H.; Parker, V.B.; Halow, I.; Bailey, S.M.; Schumm, R.H. Natl. Bur. Stand. U.S. Tech. Note 270-4. (1969).

[21] O'Hare, P.A.G. The Thermodynamic Properties of P_2, P_4, and Some Phosphorus Fluorides. ANL-7459. Angonne National Laboratory. (1968).

[22] Hirschfelder, J.O.; Curtiss, C.F.; Bird, R.B. Molecular Theory of Gases and Liquids. Wiley: New York. (1964).

[23] Rossini, F.D. In Experimental Thermochemistry. chap. 14. Rossini, F.D.: editor. Interscience: New York. (1956).

III.4. THE ENTHALPY OF FORMATION OF UPd_3, BY FLUORINE BOMB CALORIMETRY [a,b]

III.4.1. Introduction

The intermetallic compound UPd_3 is of immediate interest because of its formation during fission of nuclear fuel in a reactor. The $(U,Pu)Me_3$-phases, in which Me = Ru, Rh and Pd, were detected in carbide and even in oxide fuel [1]. In order to understand the formation of $(U,Pu)Pd_3$ phases in irradiated nuclear fuel, thermodynamic data of the binary UMe_3 compounds are very useful.

Very little is known about the thermochemical properties of UPd_3. Only one thermodynamic value has been reported, the standard Gibbs energy of formation $\Delta G_f^o(UPd_3, c, 1673K) = -259$ kJ mol^{-1}, which was obtained by mass spectrometric measurements [3]. In this paper the determination of the enthalpy of formation of UPd_3, using the fluorine bomb calorimetric method, will be described.

III.4.2. Experimental

III.4.2.1. Principle of the calorimetric reactions

The reaction of UPd_3 with fluorine according to:

$$2UPd_3 + (15-3x)F_2(g) \rightarrow 2UF_6(g) + (3-x)[Pd(PdF_6)(c)] + 2x\ Pd(c) \quad (3\text{-}10)$$

in which x is the mol fraction of Pd metal (= 0.5 ± 0.2), was chosen because almost the entire UPd_3-sample reacts with fluorine to form UF_6 and a mixture of $Pd(PdF_6)$ and palladium.
Since there are two unknowns in reaction (3-10), $\Delta H_f^o(UPd_3, c, 298.15K)$ and x, it is necessary to find a proper "analytical" method to accurately determine x in reaction (3-10). A second reaction:

$$(3-x)[Pd(PdF_6)(c)]+(9-3x)PF_3(g) \rightarrow (9-3x)PF_5(g)+(6-2x)Pd(c) \quad (3\text{-}11)$$

---

[a] Work performed under the auspices of the U.S. Department of Energy.
[b] This chapter has been submitted for publication as an article with the same title in The Journal of Chemical Thermodynamics, by G. Wijbenga.

was chosen because phosphorous trifluoride gas reduces the $Pd(PdF_6)$ in the $Pd(PdF_6)$-palladium mixture, left over after the first reaction, spontaneously. $\Delta H_f^o\{Pd(PdF_6), c, 298.15K\}$ and $\Delta H_r^o(298.15K)$ for the reaction $PF_3 + F_2 \rightarrow PF_5$, are known and the energy released in reaction (3-11) can be measured, thus x can be calculated from reaction (3-11). By using this result for x in reaction (3-10), the enthalpy of formation of UPd_3 can be derived. The auxiliary data are given in table 3.16.

III.4.2.2. Calorimetric system

The calorimetric system consisted of a nickel combustion bomb similar to that described previously [7] and a bomb calorimeter, laboratory designation ANL - R-2, similar to that described by Hubbard et al. [8] The calorimetric temperatures were measured by quartz-crystal thermometry [9]. The system was calibrated by the combustion in oxygen of National Bureau of Standards benzoic acid (sample 39i), which has a certified energy of combustion under prescribed conditions of $-(26.434 \pm 0.003)kJ\ g^{-1}$. A series of calibration experiments, some before, some in between and some following the UPd_3 combustions, were performed. The energy equivalent of the calorimetric system, $\varepsilon(calor)$, was determined to be $(13853.4 \pm 2.2)J\ K^{-1}$ for the first four UPd_3 combustions, and $(13844.4 \pm 4.2)J\ K^{-1}$ for the last two UPd_3 combustions.

III.4.2.3. Materials

The starting materials for the preparation of UPd_3 were palladium sponge of high purity (99.99%, Johnson & Matthey Chemicals Limited), and uranium nitride (UN). UN was prepared by the reaction of finely divided uranium powder with nitrogen. At 700 °C, uranium sesquinitride (U_2N_{3+x}) is formed; it is decomposed in vacuum or inert atmosphere to UN at 1400 °C.

Before use, the palladium sponge was dried in vacuum at 500 °C to remove any adsorbed moisture. UPd_3 was prepared by heating mixtures of UN with palladium in the stoichiometric composition at 1080 °C. A high-frequency induction furnace was used to heat the samples [2].

Tantalum carbide was used as the container material. The reaction products were ground in a dry box and reheated; this was done until the reaction was complete as indicated by X-ray diffraction analysis.

UPd_3 is a grey solid; it reacts with moisture when exposed to air, as can be concluded from a change in the lattice parameters.
The X-ray diffraction results of the UPd_3-sample, used for the combustion experiments, showed the presence of only hexagonal UPd_3 with a = 5.773 ± 0.001 Å and c = 9.627 ± 0.002 Å. This result is in good agreement with the X-ray diffraction results found in the literature [10]. A small amount of UO_2 was visible in the X-ray diffraction results of the UPd_3-sample. Chemical analyses of UPd_3 are given in table 3.15.
Graphite felt (sheets of thickness 5.23 mm, National Grade WDF) used as a combustion aid for the UPd_3 sample, was purchased from Union Carbide Corporation.
A series of combustion experiments with this graphite felt in fluorine was performed previously [11], and a value and standard deviation of the mean of $-(77769.3 \pm 18.4) J\ g^{-1}$ was obtained for the standard energy of combustion of the graphite sample, $\Delta U_c^o M$(sample). Hexagonal black selenium shot was taken from the same batch that was used for the determination of $\Delta H_f^o(SeF_6, g)$ [12]. Purified fluorine (99.99 moles per cent) was prepared by distillation of commercial fluorine in a low-temperature still [13]. The phosphorus trifluoride gas, used in the reduction experiments, was obtained from Ozark Mahoning Co. Removal of the small amounts of oxygen and nitrogen in the PF_3 gas was done by condensing the PF_3 in a steel trap with liquid nitrogen and pumping off the solid, as described previously [6].

III.4.2.4. Preliminary experiments
In order to establish the conditions under which UPd_3 could be completely fluorinated or oxidized, several preliminary combustion experiments were done. Combustion experiments with UPd_3 in oxygen showed incomplete combustion of UPd_3; under calorimetric conditions only about 15 per cent of the UPd_3 had reacted. It was found by X-ray analyses that Pd and U_3O_8 were formed on the outside of a molten residue. The heat released in the reaction:

$$3\ UPd_3 + 4\ O_2 \rightarrow U_3O_8 + 9\ Pd,$$

had evidently melted the palladium which in turn covered the UPd_3. The use of auxiliary combustion aids, such as graphite cloth on which

UPd_3-powder was spread, and magne[illegible] powder, mixed with UPd_3, did not improve the results of the combustions.

It was therefore decided to continue combustion experiments of UPd_3 in fluorine. If no auxiliary was used, combustion of UPd_3 in fluorine was incomplete, presumably because the palladium fluoride reaction product (PdF_2, "PdF_3" and Pd) melted and covered unreacted UPd_3, thereby quenching the reaction. Both thin and massive nickel containers were attacked by the reaction mixture, however, the latter much less. Thus contact between UPd_3 and the nickel container material had to be avoided. Different auxiliary combustion aids were tested, including tungsten foil, AlF_3-powder, graphite cloth and graphite felt. Graphite felt was selected because its high energy of combustion caused UPd_3 to burn nearly completely to UF_6 and a mixture of palladium metal, $Pd(PdF_6)$, and a small amount of PdF_2. Complete fluorination of UPd_3 could only be obtained by carefully spreading powdered UPd_3 on graphite felt, which provided about 85 per cent of the total energy evolved.

The felt could easily be cut into thin layers and weighed. To prevent spattering of the UPd_3 onto the bomb surfaces, the graphite felt was arranged so as to completely cover the UPd_3. This was done by carefully spreading the UPd_3 in between three graphite felt disks. Selenium shot was put on the top disk as an ignitor.

High fluorine pressures up to 2375 kPa were used. Under these conditions more than 60 mass per cent of the palladium fluoride reaction product which was found by X-ray diffraction to be pure $Pd(PdF_6)$, sublimed.

On the bottom of the nickel container several small metal drops were found, X-ray diffraction results showed the metal to be pure palladium (about 15 mass per cent of the total palladium involved in the experiments). The palladium fluoride reaction product in the nickel container was mainly $Pd(PdF_6)$; however, a small amount of PdF_2 was found, estimated between 2 and 8 mass per cent of the total $Pd(PdF_6)$. The best way to "analyse" the amount of palladium fluoride ($Pd(PdF_5)$) in the experiments was to reduce the $Pd(PdF_6)$, left over after the fluorination of UPd_3, with $PF_3(g)$ and to measure the heat of reduction. From this result the amount of fluorinated palladium can be calculated.

III.4.2.5. Procedures

A preliminary combustion of a piece of carbon in fluorine served to pre-fluorinate the combustion bomb, as well as the cylindrical thick-bottomed nickel container. During the calorimetric experiments, the bomb was opened only in a helium-atmosphere glove box, in order to minimize adsorption of moisture on the bomb walls and consequent reaction with fluorine. The calorimetric procedure was as follows.

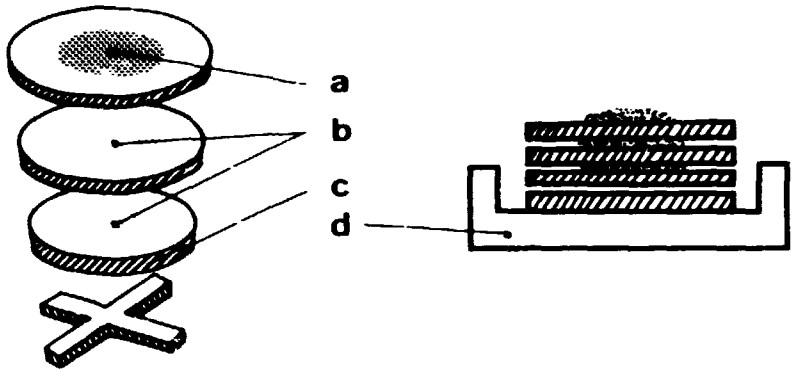

Fig. 3.5. Combustion technique of UPd_3 in fluorine.

a selenium c graphite disks

b UPd_3 d nickel container

The bomb was taken into the glove box and dismantled. The nickel support container (about 40 grams), four pieces of graphite felt, and the UPd_3 and selenium were accurately weighed (fig. 3.5.). The bottom piece of carbon was cut cross shaped, in order to avoid the formation of unreacted UF_4 on the bottom of the nickel container. The UPd_3 was carefully spread in between the remaining three cylindrical disks of graphite. A little selenium was put on the top piece. The nickel container with contents was placed on the bomb head, the bomb was assembled, connected with the tank, which had been charged to 2375 kPa with fluorine, and taken out of the glovebox. The bomb and connecting tube were evacuated, and the system was placed in the calorimeter.

After the forerating period, the combustion of the sample was started by opening the tank valve. After the combustion, the bomb was removed from the calorimeter, dried and the bomb gases were condensed into a liquid nitrogen-cooled trap and fluorine was pumped off the condensate.

Analyses of the residual gas for C_2F_6 and C_3F_8 by gas chromatography showed that the amount of C_2F_6 was less than 0.02 mole per cent of the CF_4, and the amount of C_3F_8 was less than 0.005 mole per cent of the total CF_4.

The evacuated bomb was returned to the glove box; the tank was disconnected, charged with PF_3 up to 1830 kPa, and again connected with the bomb. During this procedure the bomb was not dismantled. The system was taken out of the glovebox, evacuated and placed in the calorimeter. The heat of reduction of the unknown amount of $Pd(PdF_6)$, left in the bomb after the fluorination of UPd_3, was measured. After the reduction, the bomb gases were condensed into a liquid nitrogen-cooled trap. Analyses of the gas, a PF_3/PF_5 mixture, by mass spectrometrical method showed yields of PF_5 ranged between 1.86 vol. percent of the PF_3, depending on the amount of $Pd(PdF_6)$ involved in the experiments. The post reduction residue was identified by X-ray analysis as palladium metal. This residue was washed in 0.6 mol dm^{-3} HCl for about 30 minutes at room temperature, the solution was then filtered to remove palladium, and analysed for uranium and fluorine. Total uranium (ascribed to UF_4) was found to be 0.26 mg or less, and total fluorine (ascribed to UF_4 and $Pd(PdF_6)$) 0.61 mg or less.

The palladium residue was then dissolved in a mixture of concentrated H_2SO_4 and concentrated HNO_3. In order to dissolve all the palladium, the mixture was heated and some water was added. This solution was analysed for uranium. Total uranium (ascribed to unreacted UPd_3) was found to be 0.38 mg or less.

No black graphite fibers were found in the residues.

III.4. Results

The results of six combustions of UPd_3 in fluorine according to reaction (3-10), immediately followed by the reduction of the $Pd(PdF_6)(c)$ with PF_3 according to reaction (3-11) are presented in tables 3.17. and 3.18.

Since an amount of PdF_2 was found by X-ray analysis in some interrupted experiments (after the fluorination step), the estimate has been made that the $Pd(PdF_6)$-phase in the bomb contains (5 ± 3) mass per cent PdF_2. From the total energy (ΔU(total)) involved in the reduction

experiments the amounts of palladium fluorides, $m\{Pd(PdF_6)total\}$ and $m(PdF_2)$, can be calculated according to:

$$\Delta U(total)=(0.05x)\{\Delta U_c^o/M(PdF_2)\}+ [0.95x - m\{Pd(PdF_6)unreacted\}]\Delta U_c^o/M\{Pd(PdF_6)\} \quad (3\text{-}12)$$

where x is total mass of PdF_2 and $Pd(PdF_6)$. The item $m\{Pd(PdF_6)unreacted\}$ represents a small amount of unreduced $Pd(PdF_6)$ as was found by chemical analysis (table 3.18.). By combining the heats of reduction of the palladium fluorides, $\Delta U_c^o/M(PdF_2)= -1156.5\ Jg^{-1}$ and $\Delta U_c^o/M\{Pd(PdF_6)\}= -2877.5\ Jg^{-1}$, respectively (see table 3.16.), with $\Delta U(total)$, $m(PdF_2)$ and $m\{Pd(PdF_6)\}$ have been calculated (table 3.18.). The corrections to standard states were applied in the usual manner [14]. The auxiliary data used in the calculations are all given in table 3.16.

An additional explanation of some entries in tables (3.17.) and (3.18.) is as follows: For the calculations of $\Delta U(gas)$, μ, in the equation of state $pV = n\,RT(1 - \mu p)$ and $(\partial U/\partial P)_T$ were estimated by the method of Hirschfelder et al [24], from the intermolecular force constants for PF_3 and PF_5, and for UF_6 [25], CF_4 [24], SeF_6 [26], and F_2 [27]. The volume of the empty bomb was 0.3132 dm^3, and the volume of the tank was 0.2361 dm^3.

$\Delta U(PF_3,blank)$ is the correction for the expansion of PF_3 from the tank into the empty bomb. An average value and standard deviation of $\Delta U(PF_3,blank) = -(72.6 \pm 5.1)J$ was obtained. The term $\Delta U(F_2, blank)$ is a combined correction for the endothermic expansion of F_2 into the combustion bomb and the exothermic reaction of F_2 with surfaces in the bomb. An average value and standard deviation of $\Delta U(F_2,blank) = -(15.8 \pm 2.7)J$ was obtained. The expansion experiments were interspersed with the fluorination/reduction experiments of tables (3.17.) and (3.18.).

$\Delta U(C)$ and $\Delta U(Se)$ are the corrections for the combustion in fluorine of graphite and selenium, respectively.

The correction $\Delta U(C_2F_6 + C_3F_8)$ accounts for the formation of variable, small amounts of C_2F_6 and C_3F_8, which are itemized as $n(C_2F_6$ formed) and $n(C_3F_8$ formed); $\Delta U(C_2F_6 + C_3F_8)$ represents the additional energy that would have been evolved had C_2F_6 and C_3F_8 been completely

fluorinated to CF_4. The calculated energy of the reactions is based on auxiliary values of ΔH_f^o for CF_4, C_2F_6 and C_3F_8. $\Delta U(UF_4)$ accounts for the formation of a very small amount of UF_5; its energy of fluorination is based on the auxiliary value of $\Delta U_c^o/M$.
$\Delta U\{Pd(PdF_6)\}$ and $\Delta U(PdF_2)$ are the corrections for the combustion in fluorine of $Pd(PdF_6)$ and PdF_2, based on the auxiliary values of $\Delta U_c^o/M$ in table (3.16.). The masses of $Pd(PdF_6)$ and PdF_2 are calculated in table (3.18.). The chemical analyses of the calorimetric UPd_3-sample are given in table (3.15.). The impurity corrections in UPd_3 are based on the assumption that the solid solubility of the elements O, C, N, Si and Ta will be very small; less than 20 ppm. These elements will be present mainly as: UO_2, UC, UN, USi and $TaPd_3$, respectively. The impurity correction applied in table (3.17.) was calculated from the total amount of impurities (1.2817 mass per cent) with its total heat of combustion (97.6 J g^{-1}). The large uncertainty attached to the impurity correction reflects mainly the uncertainty in the estimated amount of PdF_2 in the experiments.
The excess Pd in the sample will be present in solution and has been calculated from the total uranium and palladium present as UPd_3.
The unreacted UPd_3, $m^f(UPd_3)$, found in the postreduction palladium residues, was substracted from the original UPd_3 weighings, $m^i(UPd_3)$, and itemized as $m(UPd_3$ reacted).
The average heat of combustion of $UPd_{3.099}$ in table 3.17., $\Delta U_c^o/M(UPd_{3.099}) = -(2828.5 \pm 54)Jg^{-1}$, has been determined for the reaction:

$$UPd_{3.099}(c) + 3\ F_2(g) \rightarrow UF_6(g) + 3.099\ Pd(c) \qquad (3\text{-}13)$$

From the average heat of combustion of $UPd_{3.099}$, the enthalpy of combustion (table 3.17.) has been calculated to give $\Delta H_c^o(UPd_{3.099}) = -(1610.9 \pm 30.7)kJ\ mol^{-1}$. By substracting the enthalpy of formation of $UF_6(g)$, $-(2147.6 \pm 1.8)kJ\ mol^{-1}$ (table 3.16.) the standard enthalpy of formation of $UPd_{3.099}$, $\Delta H_f^o\{UPd_{3.099}, c, 298.15K\} = -(536.7 \pm 30.8)$ $kJ\ mol^{-1}$, was derived.

The amount of fluorinated palladium in the reduction experiments according to reaction (3-11) has also been determined in a different way by analysing the amount of PF_3 converted to PF_5 after the reduction

experiments. The results of four determinations are given in table 3.19. PF_5 in PF_3 was measured mass-spectrometrically in volume per cent and recalculated to mole per cent. The tank was charged with 0.19651 mole PF_3 from which $n(PF_5)$ could be calculated. Since for the reaction: $PF_3(g) + F_2(g) \rightarrow PF_5(g)$, $n(PF_5) = n(F_2)$, the amount of fluorine which has been connected with palladium can be calculated ($m(F_2)$). The heat of the reaction $PF_3 + F_2 \rightarrow PF_5$ is known from table 3.16., $-16670.3\ Jg^{-1}$, and $\Delta U(F_2)$ can be calculated. From the total energy (ΔU (total)) involved in the reduction experiments and $\Delta U(F_2)$, $\Delta U\{Pd(PdF_6)\} + \Delta U(PdF_2)$ can be calculated:

$$\Delta U(\text{total}) + \Delta U(F_2) = [\Delta U\{Pd(PdF_6)\} + \Delta U(PdF_2)] \qquad (3\text{-}14)$$

These values for $[\Delta U\{Pd(PdF_6)\} + \Delta U(PdF_2)]$ were inserted in table 3.17. in order to calculate the values for $\Delta U_c^o/m$ (sample) in table 3.19. From the average heat of combustion of $UPd_{3.099}$ in table 3.19., $\Delta U_c^o/M(UPd_{3.099}) = -(2861 \pm 226)J\ g^{-1}$, the standard enthalpy of formation of $UPd_{3.099}$, $\Delta H_f^o\{UPd_{3.099}, c, 298.15K\} = -(519 \pm 128)kJ\ mol^{-1}$, has been derived, in the same way as for table 3.17. Although this result must be considered as a tentative value, due to the large uncertainty in the analysis of $PF_5(g)$, it supports the value derived above. An advantage of this method is that we do not need to know the enthalpies of formation of $Pd(PdF_6)$ and PdF_2, as well as their amounts in the mixture of palladium fluorides.

III.4.4. Discussion

The standard enthalpy of formation of $UPd_{3.099}$ (c), $\Delta H_f^o(UPd_{3.099}, c, 298.15K)$, has been determined to be $-(536.7 \pm 30.8)\ kJ\ mol^{-1}$. To calculate the enthalpy of formation of the stoichiometric compound we assume that excess of palladium is entirely in solid solution, as is justified by solid solubility measurements of Pd in UPd_3 [2]. We then find in good approximation $\frac{4.099}{4}\{\Delta H_f^o(UPd_{3.099})\} = \Delta H_f^o(UPd_3, c, 298.15\ K) = -(550 \pm 31)kJ\ mol^{-1}$.

The only previous value for the enthalpy of formation of UPd_3 is an estimate of $-251\ kJ\ mol^{-1}$ [31]. The enthalpy of formation of UPd_3 is comparable with the very negative enthalpies of formation of $ZrPt_3$: $-(517 \pm 33)kJ\ mol^{-1}$ [32], and $HfPt_3$: $-(552 \pm 48)kJ\ mol^{-1}$ [32], in

accordance with the predicitions of the Engel-Brewer theory [33].

The author gratefully acknowledges:
W. Ouweltjes for preparing PPd_3; G.K. Johnson for purifying F_2;
M. Bouchard, S. Bourne, C. Chow, A. Essling, I.M. Fox, M.I. Homa, W.A. Lingerak, F. Williams, K.J. Jensen, R.J. Meyer and G. Waterbury (Los Alamos Scientific Laboratory) for analytical services;
T. Engelkemeier for mass-spectroscopy on PF_3/PF_5 mixtures; B.S. Tani and P. van Vlaanderen for X-ray diffraction analyses; and Prof. L. Brewer, Prof. N. Bartlett, W.N. Hubbard and P.A.G. O'Hare for helpfull discussions.
The author especially wishes to thank Prof. E.H.P. Cordfunke and G.K. Johnson for studying the paper thoroughly and giving valuable comments.

Table 3.15. Analysis and impurity corrections of UPd_3

		impurities present in UPd_3				
element	total mass per cent	impurity	mass per cent	heat of combustion (Jg^{-1})	total uranium as UPd_3	total palladium as UPd_3
U	42.48				42.48	
Pd	57.27					57.27
O	0.0660	UO_2	0.5570	22.84	-0.4910	
C	0.0205	UC	0.4268	51.61	-0.4063	
N	0.0140	UN	0.2519	18.99	-0.2379	
H	< 0.0010	-	-	-		
Al	0.0005	Al(sol)	0.0005	0.28		
Si	0.0020	USi	0.0190	2.66	-0.0170	
Fe	0.0019	Fe(sol)	0.0019	0.33		
Ni	0.0011	Ni(sol)	0.0011	0.12		
Ta	0.0085	$TaPd_3$	0.0235	0.75		-0.0150
total	99.8655		1.2817	97.58	41.3278	57.2550

Table 3.16. Auxiliary data at 298.15K

C_p^o/J K^{-1}g^{-1}	UPd_3(c), 0.183 [28]; Ni(c), 0.4439 [15]; Se(c), 0.3213 [16]; C(graphite), 0.7100 [16]; Pd(c), 0.243 [15].
ρ/g cm^{-3}	Ni(c), 8.907 [17]; Se(c), 4.804 [18]; Pd(c), 11.4 [29]; PdF_3(c), 5.06 [29]; C(graphite), 2.27 [19]; UPd_3(c), 13.39 [10].
C_v^o/J K^{-1}mol^{-1}	F_2(g), 22.983 [15]; UF_6(g), 121.3 [20]; SeF_6(g), 102.17 [12]; CF_4(g), 52.76 [15]; PF_3(g), 50.38 [21]; PF_5(g), 74.85 [21].
$\{\Delta U_c^o/M\}$/Jg^{-1}	Se(c), -(14078.7 $\pm$ 2.5) [12]; C(graphite), -(77769.3 $\pm$ 18.4) [11]; U(c), -(9199.64 $\pm$ 7.7) [4]; UF_4(c), -(875.8 $\pm$ 8.4) [34]; Pd(PdF_6)(c), -(2937.7 $\pm$ 22) [6]; PdF_2(c), -(3230.7 $\pm$ 291) [35].
$\{\Delta U^o/M(F_2)\}$Jg^{-1}	PF_3 + F_2 reaction: -(16670.3 $\pm$ 7.5) [5].
ΔH_f^o/kJ mol^{-1}	UF_6(g), -(2147.6 $\pm$ 1.8) [4]; CF_4(g), -(933.20 $\pm$ 0.8) [22]; C_2F_6(g), -(1343.9 $\pm$ 5.0) [23]; C_3F_8(g), -(1754.8 $\pm$ 20.0) [23]; SeF_6(g), -(1116.92 $\pm$ 0.59) [12]; Pd(PdF_6)(c), -(967.4 $\pm$ 7.3) [6]; PdF_2(c), -(469 $\pm$ 42) [35].
ΔH_r^o/kJ mol^{-1}	PF_3 + F_2 reaction: -(635.9 $\pm$ 0.3) [5].
$\{\Delta U_c^o/M(PdF_2)\}$Jg^{-1}	PF_3 + PdF_2 reaction: -(1156.5) [5,6].
$[\Delta U_c^o/M\{Pd(PdF_6)\}]$Jg^{-1}	PF_3 + Pd(PdF_6) reaction: -(2877.5) [5,6].

Table 3.17. Results of UPd_3 combustion experiments [a]

Experiment No.	2	4	5	6	11	12
$m^i(UPd_3)/g$	0.51341	0.53204	0.55797	0.51332	0.54602	0.53160
$m^f(UPd_3)/g$	0.00070	0.00089	0.00035	0.00042	0.00089	0.00077
$m(UPd_3$ reacted)/g	0.51271	0.53115	0.55762	0.51290	0.54513	0.53083
m(C reacted)/g	0.28745	0.26561	0.28291	0.28619	0.27894	0.28647
m(Se reacted)/g	0.05846	0.05344	0.04704	0.07398	0.05366	0.04593
$n(C_2F_6$ formed)/μmol	4.41	4.41	5.37	4.08	5.71	2.47
$n(C_3F_8$ formed)/μmol	1.08	1.08	0.96	0.74	1.34	1.26
$m(UF_4$ formed)/g	0.00016	0.00016	0.00010	0.00011	0.00035	0.00016
Δθc/K	1.85987	1.73499	1.83704	1.86976	1.81672	1.84525
ε(calor)(-Δθc)/J	-25765.5	-24035.5	-25449.2	-25902.5	-25151.5	-25546.5
ΔU(contents)/J	-43.7	-40.8	-43.2	-43.9	-42.6	-43.3
ΔU(gas)/J	-1.1	-1.0	-1.1	-1.1	-1.0	-1.1
ΔU(C)/J	22354.8	20656.3	22001.7	22256.8	21693.0	22278.6
ΔU(Se)/J	823.0	752.4	662.3	1041.5	755.5	646.6
$\Delta U(F_2$,blank)/J	-15.8	-15.8	-15.8	-15.8	-15.8	-15.8
$\Delta U(C_2F_6 + C_3F_8)/J$	-3.4	-3.4	-3.8	-2.9	-4.4	-2.6
$\Delta U(UF_4)/J$	-0.1	-0.1	-0.1	-0.1	-0.3	-0.1
$\Delta U\{Pd(PdF_6)\}/J$ [b]	1123.7	1069.3	1175.5	1128.8	1119.7	1083.1
$\Delta U(PdF_2)/J$ [b]	65.0	61.9	68.0	65.3	64.8	62.7
$\{\Delta U_c^o/m(sample)\}/Jg^{-1}$	-2853.7	-2930.8	-2879.6	-2873.7	-2903.0	-2897.9

Table 3.17. (continued)

average $(\Delta U^{o}_{c}/m(\text{sample}) = -(2889.8 \pm 10.9)\,J\,g^{-1}$ [c]
mass correction (table 3.15.) = (0.012817 ± 0.001345)
Impurity correction (table 3.15.) = $(97.6 \pm 3.0)\,J\,g^{-1}$ [c]
mass and impurity correction for $UPd_{3.099}$:
$(1-0.012817)\,g\ UPd_{3.099} = -(2889.8 - 97.6)\,J\,g^{-1}$
$\Delta U^{o}_{c}/M(UPd_{3.099}) = -(2828.5 \pm 12.0)\,J\,g^{-1}$ [c]
other uncertainties (PdF_2-analysis) = $(\pm 24.6)\,J\,g^{-1}$ [c]
$\Delta U^{o}_{c}/M(UPd_{3.099}) = -(2828.5 \pm 54)\,J\,g^{-1}$ [d]
$\Delta U^{o}_{c} = -(1605.9 \pm 30.7)\,kJ\ mol^{-1}$ [d,e]
$\Delta H^{o}_{c} = -(1610.9 \pm 30.7)\,kJ\ mol^{-1}$ [d,e]
$\Delta H^{o}_{f}(UPd_{3.099}) = -(536.7 \pm 30.8)\,kJ\ mol^{-1}$ [d,e]

[a] For the reaction $UPd_{3.099}(c) + 3\ F_2(g) \rightarrow UF_6(g) + 3.099\ Pd(c)$.

[b] Masses of $Pd(PdF_6)$ and PdF_2 are given in table 3.18.

[c] Standard deviation of the mean.

[d] ±, Uncertainty interval equal to twice the final overall standard deviation [30]

[e] The molar mass of $UPd_{3.099}$ was taken to be 567.763 g mol^{-1}.

Table 3.18. Results of PF_3 reduction experiments

Experiment No.	2	4	5	6	11	12
$\Delta\theta_c$/K	0.07544	0.07154	0.07927	0.07582	0.07529	0.07253
ε(calor)$(-\Delta\theta_c)$/J	-1045.1	-991.1	-1098.2	-1050.4	-1042.3	-1004.1
ΔU(contents)/J	-2.1	-2.0	-2.2	-2.1	-2.1	-2.0
ΔU(gas)/J	0.1	0.1	0.1	0.1	0.1	0.1
$\Delta U(PF_3, \text{blank})$/J	-72.6	-72.6	-72.6	-72.6	-72.6	-72.6
ΔU(total)/J	-1119.7	-1065.6	-1172.9	-1125.0	-1116.9	-1078.6
$m\{Pd(PdF_6)\text{unreacted}\}$/g	0.00150	0.00138	0.00101	0.00143	0.00107	0.00166
$m\{rd(PdF_6)\text{total}\}/g^a$	0.38253	0.36400	0.40016	0.38427	0.38116	0.36870
$m(PdF_2)/g^a$	0.02013	0.01916	0.02106	0.02022	0.02006	0.01941

[a]From equation (3-12)

Table 3.19. Determinations of PF_5 in PF_3 after reduction experiments.

Experiment no.	4	5	6	11
PF_5 in PF_3 (volume per cent)	1.68	1.72	1.83	1.86
PF_5 in PF_3 [a] (mole per cent)	1.743	1.785	1.899	1.930
$n(PF_5)$/mol [b]	0.003425	0.003508	0.003732	0.003793
$m(F_2)$/g	0.13104	0.13329	0.14180	0.14412
$\Delta U(F_2)$/J	2184.5	2222.0	2363.8	2402.5
ΔU(total)/J [c]	-1065.6	-1172.9	-1125.0	-1116.9
$\Delta U\{Pd(PdF_6)\}$/J + $\Delta U(PdF_2)$/J [d]	1118.9	1049.1	1238.8	1285.6
$\{\Delta U_c^o/m(\text{sample})\}/Jg^{-1}$	-2954	-3228	-2787	-2718

Average $\{\Delta U_c^o/m(\text{sample})\} = -(2922 \pm 113)Jg^{-1}$ [e]

mass and impurity correction for $UPd_{3.099}$ (table 3.17.).

$\Delta U_c^o/M(UPd_{3.099}) = -(2861 \pm 226)Jg^{-1}$ [f]

$\Delta U_c^o = -(1624 \pm 128)kJ\ mol^{-1}$ [f]

$\Delta H_c^o = -(1629 \pm 128)kJ\ mol^{-1}$ [f]

$\Delta H_f^o(UPd_{3.099}) = -(519 \pm 128)kJ\ mol^{-1}$ [f]

[a] The densities of PF_3 and PF_5 were taken to be 3.907 g/l and 5.805 g/l, respectively.

[b] Total amount of PF_3 in reaction vessel: 0.19651 mole.

[c] From table 3.18.

[d] Inserted in table 3.17. to recalculate $\{\Delta U_c^o/m(\text{sample})\}$.

[e] Standard deviation of the mean.

[f] ±, Uncertainty interval equal to twice the final overall standard deviation [30].

REFERENCES

[1] Holleck, H.; Kleykamp, H. KFK-report 1271-1, Karlsruhe (1971).

[2] Wijbenga. G. Thesis Amsterdam, to be published.

[3] Lorenzelli, N.; Marcon, J.P. J. Nucl. Mat. 44 (1972) 57.

[4] Johnson, G.K. J. Chem. Thermodynamics 11 (1979) 483.

[5] Johnson, G.K.; Malm, J.G.; Hubbard, W.N. J. Chem. Thermodynamics 4 (1972) 879.

[6] Wijbenga, G.; Johnson, G.K. J. Chem. Thermodynamics 13 (1981) 471.

[7] Nuttall, R.L.; Wise. S.; Hubbard, W.N. Rev. Sci. Instrum. 32 (1961) 1402.

[8] Hubbard, W.N.; Katz, C.; Waddington, G. J. Phys. Chem. 58 (1954) 142.

[9] Johnson, G.K.; Van Deventer, E.H.; Kruger, O.L.; Hubbard, W.N. J. Chem. Thermodynamics 1 (1969) 89.

[10] Heal, T.J.; Williams, G.I. Acta Crystallogr. 8 (1955) 494.

[11] Ader, M. J. Chem. Thermodynamics 6 (1974) 587.

[12] O'Hare, P.A.G.; Settle, J.L.; Hubbard, W.N. Trans Faraday Soc. 62 (1966) 558.

[13] Stein, L.; Rudzitis, E.; Settle, J.L. Purification of Fluorine by Distillation, USAEC Report ANL-6364. Argonne National Laboratory. June (1961).

[14] Hubbard, W.N. In Experimental Thermochemistry, Vol. II, Chap. 6. Skinner, H.A.: editor, Interscience: New York. (1962).

[15] Wagman, D.D.; Evans, W.H.; Parker, V.B.; Halow, I.; Bailey, S.M.; Schumm, R.H. Nat. Bur. Stand. U.S. Tech. N 270-4. (1969).

[16] Wagman. D.D.; Evans, W.H.; Parker, V.B.; Halow, I.; Bailey, S.M.; Schumm, R.H. Nat. Bur. Stand. U.S. Tech. Note 270-3. (1968).

[17] Swanson, H.E.; Tatge, E. Standard X-ray Diffraction Powder Patterns, Nat. Bur. Stand. (U.S.) Circ. 539, Vol. I. (1953).

[18] Swanson, H.E.; Gilfrich, N.T.; Ugrinic, G.M. Standard X-ray Diffraction Powder Patterns, Nat. Bur. Stand. (U.S.) Circ. 539, Vol. V. (1955).

[19] Crystal Data, Determinative Tables, ACA Monograph Number 5. American Crystallographic Association. (1963).

[20] Gaunt, J. Trans. Faraday Soc. 49 (1953) 1122.

[21] O'Hare, P.A.G. The Thermodynamic Properties of P_2, P_4 and Some Phosphorus Fluorides. ANL-7459. Argonne National Laboratory. (1968).

[22] Greenberg, E.; Hubbard, W.N. J. Phys. Chem. 72 (1968) 222.

[23] JANAF Thermochemical Tables. The Dow Chemical Co.: Midland, Michigan. June (1969).

[24] Hirschfelder, J.O.; Curtiss, C.F.; Bird, R.B. Molecular Theory of Gases and Liquids. Wiley: New York. (1964).

[25] Morizot, P.; Ostorero, J.; Plurien, P. J. Chem. Phys. 70 (1973) 1582.

[26] Nagarajan, G. Bull. Soc. Chim. Belges 72 (1963) 276.

[27] White, D.; Hu, J.H.; Johnston, H.L. J. Chem. Phys. 21 (1953) 1149.

[28] Westrum, E.F. Personal communication.

[29] Weast, R.C.: editor, Handbook of Chemistry and Physics, CRC, Boca Raton, Florida (1979-1980).

[30] Rossini, F.D. In Experimental Thermochemistry chap. 14. Rossini, F.D.: editor. Interscience: New York. (1956).

[31] Miedema, A.R.; Boom, R.; De Boer, F.R. J. Less-Common Met. 41 (1975) 283.

[32] Srikrishnan, V.; Ficalora, P.J. Met. Trans. 5 (1974) 1471.

[33] Brewer, L. Personal communication.

[34] Wijbenga, G.; Cordfunke, E.H.P.; Johnson, G.K. J. Chem. Thermodynamics. To be published.

[35] Brewer, L.; Bromley, L.A.; Gilles, P.W.; Lofgren, N.L. In The Chemistry and Metallurgy of Miscellaneous Materials: Thermodynamics chap. 6. Quill, L.L.; editor. McGraw-Hill: New York. (1950). pp. 76-192.

CHAPTER IV

EMF MEASUREMENTS

IV.1. EMF TECHNIQUES

IV.1.1. Introduction

In this chapter the set up of the EMF techniques to measure the thermodynamic properties of the compounds URu_3, URh_3 and UF_3 at high temperatures will be discussed. Attention will be payed to the principle of the measurements, developments in handling particular problems for the different systems and possible sources of error.

IV.1.2. Description of EMF apparatus and method of measurement

For measuring thermodynamic equilibria in solids, which are sensitive to oxygen, moisture and other non-inert gasses, the EMF equipment as described below can be used. Schematic diagrams of the EMF apparatus and the electrochemical cells are shown in fig. 4.1.
The EMF measurements were performed with reversible galvanic cells using CaF_2 as electrolyte [1]. The electrochemical cell consisted of a series of pellets in a quartz tube (f), contacts (Ni/Mo or W), a reference electrode, CaF_2 electrolyte, a URh_3 or URu_3 electrode and, again, Ni/Mo contacts. The temperature of the cell was measured with a Pt, Pt/10% Rh thermocouple (d), calibrated at the melting temperatures of tin, zinc, antimony and silver. The thermocouple was surrounded by a thin quartz tube (e) which was sealed into the EMF apparatus by a Viton O-ring. In this way, the electrodes, electrolyte and contacts could be pressed tightly against the quartz holder (f) along with the moveable thermocouple tube. After assembling, the cell was placed in a quartz tube (h), all the stopcocks were closed, the equipment was taken out of the dry box and connected with the gas purification system. Before a series of experiments was started, the EMF apparatus was leak tested with a helium or Freon leak detector.
Since the measurements have to be carried out in an inert atmosphere, a slow stream of purified argon was passed through the EMF apparatus during operation.

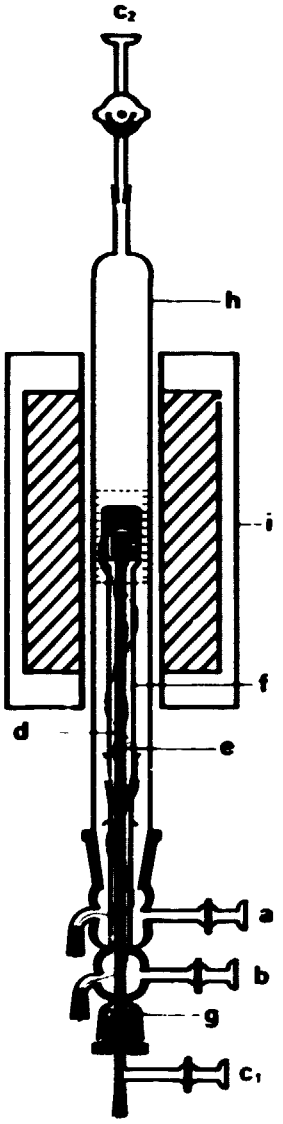

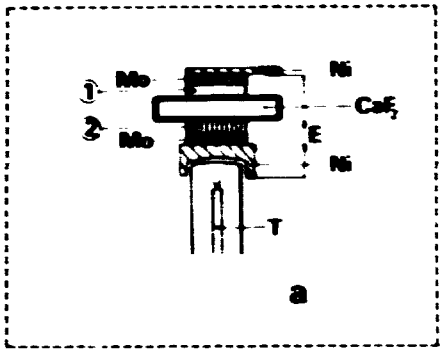

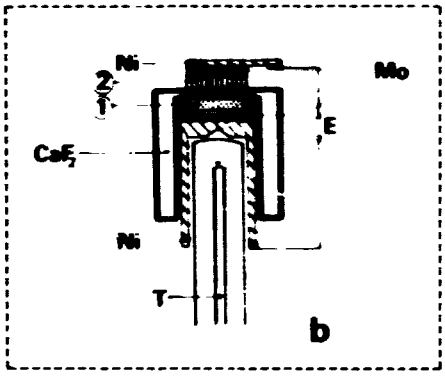

Fig. 4.1. EMF apparatus and electrochemical cells.

a,b argon inlet

c_1,c_2 argon outlet

d thermocouple (Pt, Pt/10% Rh)

e small moveable quartz tube

f quartz holder

g viton O ring

h quartz tube

i furnace

1 UF_4, URh_3, Rh-, respectively, UF_3, URu_3, Ru-electrode

2 Ni, NiF_2 reference electrode

CaF_2 Calcium fluoride crucible or single crystal

Mo inert molybdenum ring and contacts

Ni nickel contacts

T thermocouple

A Freon leak test is performed as follows: the EMF apparatus is evacuated and sprayed with Freon. If the apparatus is leaking, Freon is detected by way of a Freon sensitive detector and a change in resistance is shown on a recorder. Another method to test equipment for leaks is filling the apparatus with helium just above atmospheric pressure. All critical points are checked with a helium detector with a small hole in it. Traces of helium are then detected by way of a mass spectrometer (centronic Leak Detector - LD600) and an audiogenerator (sensitivity $1:10^7$).
During the measurements, the oxygen and H_2O concentrations in the cell were constantly monitored. The concentrations of oxygen and H_2O were below 1 ppm.

IV.1.2.1. Gas purification system
Before entering the EMF apparatus, the inert gas (argon) has to be extremely well purified. The purification system consisted of a column of BTS-catalyst heated to 110 °C, a column of activated molecular sieve and a column of finely divided powdered uranium heated to 220 °C. The last column is very reactive and will also pick up traces of N_2 and H_2 from the inert gas stream.
At the argon outlet of the EMF equipment the oxygen and moisture concentrations were monitored. Oxygen can be measured with a standard EMF cell: $Pt(O_2)/ZrO_2/(Ni,NiO)Pt$, and moisture with a panametric-cell connected with a hygrometer (model 1000 or 2000).

IV.1.2.2. Furnace control and data processing
The EMF cell was heated with a resistance-heated furnace, connected with a temperature controller. Temperature control to within 1 K was achieved using a null-balance controller. In a later stage a programmable furnace temperature controller was used. The temperature distribution in the furnace was determined, by measuring the temperature in the furnace as a function of the distance of the center. This measurement was performed in an unloaded EMF apparatus, by moving the thermocouple axially up and down from the geometrical center of the furnace. In the actual measurements the electrochemical cells were placed in the zone of constant temperature. The length of this zone was 2 cm, sufficient to cause no temperature gradient in the electrochemical cells.

The cell potentials of the EMF cell as well as of the thermocouple were measured simultaneously with a digital voltmeter (Solartron, type A210), connected to a Solartron data transfer unit.

IV.1.2.3. Fabrication of electrodes, electrolytes and contacts

The electrodes and electrolytes (see fig. 4.1.) were fabricated as follows. In order to avoid loss of contact between the pellets in the EMF cell during operation, Ni/NiF_2 reference electrodes have to be sintered prior to use.

Nickel powder was first dried in purified argon by slowly heating the powder up to 500 °C. The reference electrodes were prepared by intimate mixing of nickel powder and nickel fluoride (mixing ratio 3:1), pressed pellets were made (8 mm in diameter) and sintered in argon at 800 °C for two hours. After sintering, the pellets were polished. The other electrodes, mixtures of UF_4 + URh_3 + Rh; UF_3 + URu_3 + Ru and U + UF_3 were pressed into 8 mm-diameter pellets. Sintering before use of these electrodes was not required.

During the measurements with different types of cells, using CaF_2 as electrolyte, both CaF_2 crucibles and single crystals have been used. The CaF_2 crucibles were made from compacts of CaF_2 powder (extra pure, BDH Chemicals Limited), which were pressed into pellets with a diameter of 2.0 cm and length ± 3.5 cm. A hole (diameter 1.2 cm) was drilled into these pellets and the bottoms of the CaF_2 crucibles were carefully flattened with a special tool. The crucibles were made gas-tight by sintering in argon at 1340 °C, somewhat below the melting point of CaF_2. The resulting density was 96.5% of the theoretical density. The thickness of crucible bottoms as well as single crystals was about 0.1 cm.

The contacts were made of molybdenum (or tungsten) and nickel connected with nickel wires (fig. 4.1.).

IV.1.2.4. Diffusion in calcium fluoride

Calcium fluoride has been used extensively as the solid electrolyte in galvanic cells for the past decades [1]. EMF cells have been designed to determine the free energy of formation of various compounds.

Single crystals of CaF_2 as well as sintered crystals and crucibles of CaF_2 are becoming more and more popular as electrolytes as can be seen

from the large amount of work done with these crystals recently on the systems: Th-Ru [4], Th-Rh [5], Th-Os and Th-Ir [6], as well as Th-Pd [7]. Also work has been done on the systems: U-Fe, U-Cu, U-Co [8,9], and U-Os, U-Ir [10], using CaF_2 electrolytes.
Ure [11] has originally studied the mechanism of conduction in CaF_2 stabilized with NaF and YF_3, by transference number measurements and diffusion measurements. It was concluded that the conduction was ionic and the F^- ion carried all of the current. In the range 500 °C - 900 °C no electronic conduction was found in CaF_2 [12]. The reaction in the electrolyte is as follows:

$$Ca(g) + 2F^- = CaF_2 + 2e^- \qquad (4\text{-}1)$$

from which the electronic conduction (σ_e) in CaF_2 can be derived as a function of the activity (a_{Ca}) of calcium:

$$\sigma_e = k.\ (a_{Ca})^{0.5} \qquad (4\text{-}2)$$

It is important to note that the electronic conduction can be neglected, as long as the molar free enthalpy of solution of fluorine ($\Delta\bar{G}_{F(sol)}$) in the electrodes is smaller compared to $\Delta\bar{G}_{F(sol)}$ in CaF_2. Also more recently [13] conductivity and EMF measurements, performed with undoped CaF_2 single crystals, have lead to the conclusion that the transference number for F^- ions in CaF_2 is 1 over the entire temperature range studied (550 °C - 800 °C). Measurements of the total conductivity (σ_{ac}) for CaF_2 with an a-c bridge as a function of the partial pressure of fluorine (p_{F_2}) do not indicate any electronic conductivity for CaF_2 at very low partial pressures of fluorine (p_{F_2} 10^{-45} atm) [13]. Adding other fluorides, for instance YF_3, increases the number of F^- vacancies and, hence, the conductivity for fluoride ions. No direct measurements have been made to determine whether CaF_2 (doped) becomes an electronic conductor at very low fluorine potentials. Measurements can be undertaken over wide ranges of fluorine activity and temperature (600 °C - 900 °C), with fluorine chemical potentials of Ni,NiF_2: ΔG^o_f(600 °C) = -261 kJ per fluorine atom [2] up to Th,ThF_4: ΔG^o_f(600 °C) = -456 kJ per fluorine atom [3]. Note that for Ca,CaF_2: ΔG^o_f(600 °C) = -538 kJ per fluorine atom [3].

During our EMF measurements it was noticed that the kind and the thickness of the solid CaF_2 electrolyte influences the length of time in which an EMF cell reaches equilibrium at a constant temperature. The increase of the EMF (mV) as a function of time (hours) was measured, just after the start of the measurements, with the cell:
- $Ni,NiF_2/CaF_2/UF_4,URh_3,Rh$ -, using polycrystalline, sintered CaF_2 crucibles, with varying bottom thickness, as electrolyte. The results for 1.0, 1.8 and 3.6 mm bottoms at a cell temperature of 650 °C are

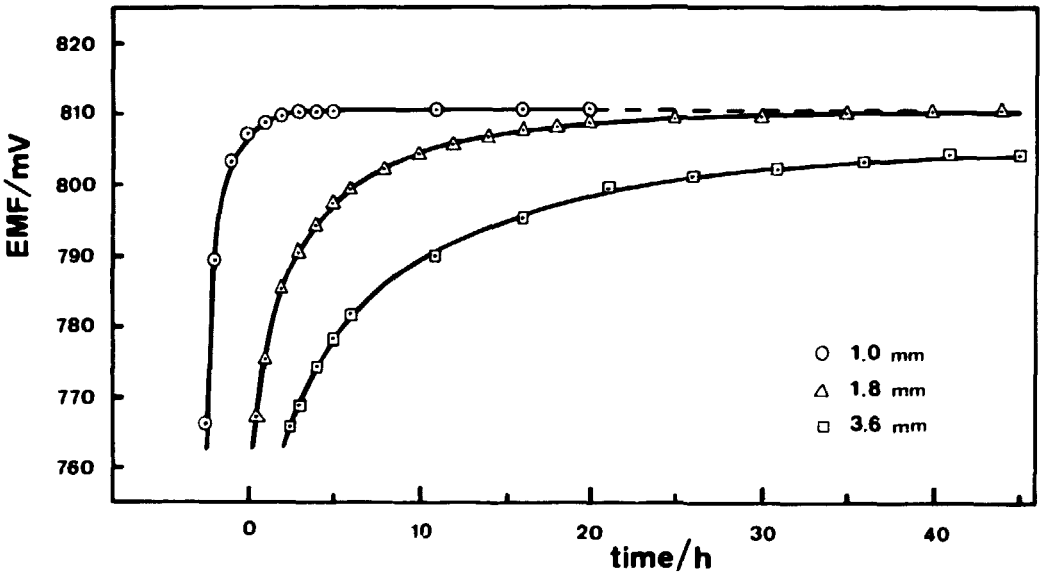

Fig. 4.2. EMF/mV as a function of the time after the start of an EMF measurement. On the time t = 0 the temperature of the cell had reached equilibrium (650 °C).

given in fig. 4.2. On the time t = 0 the temperature of the cell had reached equilibrium. It appears from the measurements that with a CaF_2 electrolyte having a bottom thickness of 1 mm, the EMF of the cell is in equilibrium at 650 °C only after about 11 hours. A CaF_2 crucible with a bottom thickness of 1.8 mm gives a constant cell EMF after 36 hours. There is a relation between the thickness of an electrolyte (d), the time (t) to reach equilibrium and the diffusion coefficient (D) of the transporting ion in the electrolyte (in this case F^-). Therefore the diffusion coefficient D_{F^-} at 650 °C for our particulary sintered CaF_2 electrolyte can be calculated. Since $\frac{d}{\sqrt{D.t}}$ is constant at constant

temperature, it follows from the measurements:

$$D_{F^-}(650\ °C) = \frac{(d_1)^2}{t_1} = \frac{(d_2)^2}{t_2} = 2.5 \times 10^{-7}\ cm^2sec^{-1}. \qquad (4\text{-}3)$$

Theoretically it would take six days for a cell with a CaF_2 electrolyte with a bottom thickness of 3.6 mm to reach equilibrium at 650 °C. For a CaF_2 single crystal it was found in the literature (14) that:

$$D_{F^-} = 50\ \exp(-2.0/kT) \qquad (350\ °C - 940\ °C) \qquad (4\text{-}4)$$

which means that at 650 °C: $D_{F^-} = 6 \times 10^{-10}\ cm^2/sec^{-1}$.
Diffusion of F^- ions in sintered crystals is much more rapid compared to single crystals of CaF_2, because of the contribution of grain boundary diffusion.

IV.1.2.5. Measurements of asymmetry potentials

An advantage of the use of CaF_2 electrolytes is the fact that studies may be made using electrodes containing metals which have a large solubility of oxygen, and hence would be unsuitable in oxide electrolyte studies.
Asymmetry potentials were measured using the simple cell:

$$Ni\ /\ Mo\ /\ Ni,NiF_2\ /\ CaF_2\ /\ Ni,NiF_2\ /\ Mo\ /\ Ni$$

Usually the asymmetry potential of EMF cells may not exceed ± 2 mV. From the results we concluded that a higher oxygen content in one of the electrodes (0.412 mass percent) does have influence on the asymmetry potential at temperatures below 750 °C, but the difference is not significant. In our actual measurements Ni,NiF_2 electrodes were used with an oxygen content of 0.143 mass percent.

IV.1.2.6. Sources of error in EMF techniques

A short discussion of possible sources of error in our particular EMF measurements is necessary because most problems in EMF measurements arise from experimental difficulties.

- The gas purification system must work well. It is necessary to pay close attention to the gaseous atmosphere which is in contact with the electrodes and electrolyte. The principal gas (argon) must be rigorously de-oxidised and dried before use, and even then it is

useful to protect the most sensitive electrode by locking the electrode in the CaF_2 crucible. Oxidation of the electrodes will result in loss of contact between electrode and electrolyte, and therefore give a wrong EMF.

- When sintering of one of the electrodes or both of them takes place during the measurements, loss of contact will be the result. Presintering of the electrodes is necessary then.
- A small leak in the system will cause slow oxidation, poor contacts and sometimes a rather slow drop in EMF. This can be checked after dismantling the EMF-cell in the dry box, and studying the surfaces of the electrodes and electrolyte very carefully by means of X-ray diffraction. The X-ray diffraction results will answer the question whether there is a reaction between the electrodes and the electrolyte or oxidation. It is therefore necessary to study both surfaces, of the electrode as well as of the electrolyte, because the diffusion of one of the components in the cell can go in two directions.
- Deterioration of the electrical contacts at high temperatures or after using the cell for a long period of time, will cause an instable EMF.

REFERENCES

[1] Markin, T.L. In: Electromotive Force Measurements in High Temperature Systems. (C B. Alcock: editor), Proc. of a Symposium 1967, American Elsevier Publishing Co., Inc.: New York (1968) p. 91.

[2] Mah, A.D; Pankratz, L.B. Contributions to the Data on Theoretical Metallurgy, XVI, Bull. Bureau of Mines, 668, (1976).

[3] Kubaschewski, O.; Alcock, C.B. Metallurgical Thermochemistry. Pergamon Press (1979).

[4] Kleykamp, H.; Murabayashi, M. J. Less Common Metals 35 (1974) 227.

[5] Murabayashi, M.; Kleykamp, H. J. Less Common Metals 39 (1975) 235.

[6] Kleykamp, H. J. Less Common Metals 63 (1979) P25.

[7] Schaller, H.J. Z. Naturforsch. 34a (1979) 464.

[8] Yoshihara, K.; Kanno, M. J. Inorg. Nucl. Chem. 36 (1974) 309.

[9] Kanno, M. J. Nucl. Mater. 51 (1974) 24.

[10] Holleck, H.; Kleykamp, H.; Franco, J.I. Z. Metallkde 66 (1975) 298.

[11] Ure, R.W. J. Chem. Phys. 26 (1957) 1363.

[12] Wagner, C. J. Electrochem. Soc. 115 (1968) 933.

[13] Hinze, J.W.; Patterson, J.W. J. Electrochem. Soc. 120 (1973) 96.

[14] Matzke, Hj. J. Mater. Sci. 5 (1970) 831.

IV.2. DETERMINATION OF THE GIBBS ENERGIES OF FORMATION OF URh_3 AND URu_3 BY SOLID STATE EMF MEASUREMENTS [a]

IV.2.1. Introduction

Intermetallics of the type $(U,Pu)Me_3$, where Me = ruthenium, rhodium and palladium, are formed during fission of actinides in fast breeder reactors by reaction of platinum metal fission products with ceramic $(U,Pu)O_2$ or (U,Pu)(C,N) fuel. Plutonium fission, in particular, gives a high yield of light platinum metals. Bramman et al. [1] first reported the presence of $(U,Pu)(Ru,Rh,Pd)_3$ inclusions in irradiated oxide fuel. The appearance of these intermetallic phases is surprising because their formation implies the reduction of the very stable uranium and plutonium oxides and, consequently, a high thermodynamic stability for the UMe_3 compounds. Indeed, Brewer [2] predicted unusual thermodynamic stability for intermetallic compounds of the platinum group metals.

Holleck and Kleykamp [3,4], and Naraine and Bell [5], who measured Gibbs energies of formation by EMF measurements, found a high stability for URh_3. In addition, Schmidt [6] measured the Gibbs energies of URh_3 by means of a "coupled reduction". However, the different sets of measurements do not agree at all. In the case of URu_3 only EMF measurements by Holleck and Kleykamp are available [19]. Because of the uncertainties in the published measurements, we decided to redetermine the Gibbs energies of formation of URh_3 and URu_3.

IV.2.2. Experimental

IV.2.2.1. Materials

Starting materials for the preparation of URh_3 and URu_3 were rhodium and ruthenium powder of high purity (99.99%, Johnson & Matthey Chemicals, Limited), and uranium nitride (UN).

UN was prepared by the reaction of finely divided uranium powder with nitrogen [7]. At 980 K uranium sesquinitride (U_2N_{3+x}) is formed,

---

[a] This chapter has been submitted for publication as an article with the same title in The Journal of Chemical Thermodynamics, by G. Wijbenga and E.H.P. Cordfunke.

followed by decomposition in vacuum or inert atmosphere to UN at 1700 K. Before use the rhodium, ruthenium and nickel powders were dried in vacuum at about 800 K to remove any adsorbed moisture. URh_3 and URu_3 were prepared by heating mixtures of UN with rhodium and ruthenium in the stoichiometric compositions at 1380 K and 1580 K, respectively. A high-frequency induction furnace was used for the heating of samples. The equipment consisted of a pyrex tube with a water cooled copper concentrator containing a TaC crucible on an alundum bar. The tube was assembled in the glove box, placed within the induction coil of the furnace and connected with the gas purification system. After the pyrex tube had been flushed sufficiently with purified argon, the sample in the TaC crucible was heated. The temperature was measured with an optical pyrometer on a black-body hole in the TaC crucible (accuracy about 5 K in the temperature range 1200 K - 1800 K). The reaction products were ground and reheated. This was done until the reaction was complete as indicated by the X-ray diffraction patterns. The X-ray diffraction results for URh_3 and URu_3 are given in table 4.1.

Table 4.1. The X-ray diffraction results for URh_3 and URu_3

compound	symmetry	lattice parameter of UMe_3 observed	lattice parameter of UMe_3 literature
$URh_{3.0000}$	fcc (Cu_3Au)	a_o = 399.15 pm	a_o = 399.1 pm ref. 8
URh_3 + Rh*)	fcc	a_o = 399.11 pm	
$URu_{2.9996}$	fcc	a_o = 397.9 pm	a_o = 398.0 pm ref. 9
URu_3 + Ru + UF_3*)	fcc	a_o = 398.3 pm	

*) The X-ray diffraction patterns of these mixtures were used to diagnose extraneous reactions in the electrodes.

Since the UN starting material contained a certain amount of UO_2, the URh_3 and URu_3 preparations were purified by washing in an acidic solution (HNO_3/H_2O = 1) to remove UO_2. URh_3 and URu_3 are insoluble in this acidic solution. The purified preparations were dried in vacuum

Table 4.2. Analytical results of the compounds used for the EMF measurements: mass fraction w and molar mass M.

compound	M / mol	10^2 w (U) found	10^2 w (U) calc.	10^2 w (Rh,Ru,Ni) found	10^2 w (Rh,Ru,Ni) calc.	10^2 w (F) found	10^2 w (F) calc.	10^2 w (N) found	10^2 w (N) calc.	10^2 w (O)	10^2 w (C)
UN	252.038	94.38	94.44					5.41	5.557	0.128	0.0130
URh_3	546.746		43.54		56.46					*)0.062	0.0300
URu_3	541.239		43.98		56.02						
NiF_2	96.707			60.7	60.7	37.9	39.3			1.016	
UF_4	314.023	75.5	75.8			23.3	24.2			0.480	
UF_3	295.024	80.5	80.7			19.1	19.3			0.156	

*) Before removing UO_2.

at 800 K.

Before use, the UF_4 and NiF_2 electrode materials were dried in a mixture of hydrogen fluoride (HF) and argon at 900 K and 1000 K, respectively. The UF_3 was prepared by heating at 1325 K a mixture of uranium powder and UF_4 at the proper stoichiometric ratio. The results of the chemical analyses of the compounds, prepared for the EMF measurements, are given in table 4.2.

IV.2.2.2. EMF apparatus

The EMF measurements were performed with reversible galvanic cells using CaF_2 as the electrolyte [10]. Schematic diagrams of the EMF apparatus and the electrochemical cell have been given elsewhere [7]. The EMF measurements have to be carried out in an inert atmosphere. Therefore, a slow stream of purified argon was passed through the EMF apparatus during operation.

The electrochemical cell consisted of a series of pellets in a quartz holder, Ni/Mo contacts, a reference electrode, CaF_2 electrolyte, a URh_3 or URu_3 electrode and, again, Ni/Mo contacts. The temperature of the cell was measured with a Pt, Pt/10% Rh thermocouple, calibrated at the melting temperatures of tin, zinc, antimony and silver. The thermocouple was surrounded by a thin quartz tube which was sealed into the EMF apparatus by a Viton O-ring. In this way the electrodes, electrolyte and contacts could be pressed tightly against the quartz holder along with the moveable thermocouple tube. After assembling, the entire cell was placed in a large quartz tube, all the stopcocks were closed, the equipment was taken out of the box and connected with the gas purification system. This consisted of a column of BTS heated to 385 K, a column of activated molecular sieve and a column of powdered uranium heated to 500 K. Before a series of experiments was started, the EMF apparatus was leak tested with a helium or Freon leak detector. During the measurements, the oxygen and H_2O concentrations in the cell were constantly monitored.

The electrodes and electrolytes were fabricated as follows:

The reference electrode was a pressed pellet of an intimate mixture of nickel fluoride and nickel powder sintered at 1075 K. After sintering, the pellet was polished. As the other electrode mixtures of UF_4 + Rh + URh_3, or UF_3 + Ru + URu_3, were pressed into 8 mm-diameter pellets. The

CaF_2 electrolyte was a cylindrical crucible placed over the UF_4,URh_3,Rh electrode to prevent evaporation of the UF_4 from the electrode, and to protect the electrodes from oxygen. The CaF_2 crucibles were made from compacts of CaF_2 powder (extra pure, BDH Chemicals Limited), which was pressed into pellets with a diameter of 2.0 cm and length ~ 3.5 cm. A hole (diameter 1.2 cm) was drilled into these pellets and the bottoms of the CaF_2 crucibles were carefully flattened with a special tool. The crucibles were made gas-tight by sintering in argon at 1615 K, somewhat below the melting point of CaF_2. The resulting density was 96.5 per cent of the theoretical density. The thickness of the crucible bottom was about 1 mm which was sufficient to enable the cell to reach equilibrium in a short time as diffusion measurements showed. Some of the measurements were done with single crystal CaF_2 pellets. However, these cells were instable due to lack of mechanical strength and evaporation of UF_4.

The contacts were made from molybdenum and nickel connected with nickel wires. A ring of molybdenum, which fitted exactly around the URh_3 electrode, minimized the space for vaporization in particular of UF_4. The cylindrical nickel contact fitted snugly within the CaF_2 crucible.

The entire EMF-cell was heated with a resistance-heated furnace. The electrochemical cell was placed in the zone of constant temperature. The length of this zone was 2 cm, sufficient to cause no temperature gradient over the electrochemical cell. Temperature control to ± 1 K was achieved using a null-balance controller. Cell potentials were measured with a digital voltmeter (Solartron, type A 210), connected to a data transfer unit (Solartron).

Since the UF_4,URh_3,Rh electrode is very sensitive to oxygen, the measurements had to be performed in an inert atmosphere with an extremely low H_2O/oxygen content. The argon gas flowing out of the cell contained H_2O and oxygen at concentrations below 1 ppm. Provided the atmosphere was inert, and the contacts were good, the electrochemical cell could be kept in operation for several months.

The measurements were performed in the temperature range 950 - 1180 K. In this range, there is no electronic conduction in CaF_2 [11]. Only deteriorating electrical contacts and reactions with the electrodes and electrolyte determine the temperature limits between which measurements can be performed.

IV.2.3. Results

URh_3

It was first attempted to determine the Gibbs energies of formation of URh_3 by measuring the EMF of the simple cell:

$$Ni,Mo \;/\; Ni,NiF_2 \;/\; CaF_2 \;/\; UF_3,\ URh_3,Rh \;/\; Mo,Ni,$$

However, it was found that UF_3 reacted with Rh in the electrode to give a mixture of UF_4, Rh and URh_3. Therefore, a mixture of these compounds was used as the electrode, to give the cell:

$$(-)\ Ni,Mo/\ Ni,NiF_2 \;/\; CaF_2 \;/\; UF_4,URh_3,Rh \;/\; Mo,Ni\ (+)$$

Several series of measurements were performed, and good agreement was found between the different sets of measurements (table 4.3.).
The equilibrium cell voltages at constant cell temperatures were reached within eight hours. When the thickness of the electrolyte between the reference and URh_3 electrode was more than 1 mm, it took much more time to reach equilibrium. Measurements were made at constant temperatures, both heating and cooling with no significant difference in the measured values.

The overall cell reaction, on passing 4 Faradays, is:

$$2\ Ni + UF_4 + 3\ Rh = 2\ NiF_2 + URh_3$$

The standard molar Gibbs energy of formation of URh_3 can be calculated from:

$$\Delta G_f^o(URh_3) = \Delta G_f^o(UF_4) - 2\ \Delta G_f^o(NiF_2) + 4\ FE_{cell} \qquad (\cdot 5)$$

where E_{cell} denotes the measured cell EMF.
The value for F used was: 96484.56 $JV^{-1}eq^{-1}$ [21]. The Gibbs energy of formation of NiF_2 as a function of temperature is well established [12]:

$$\Delta G_f^o(NiF_2)/kJ.mol^{-1} = -653.499 + 0.151293\ T \qquad (800\text{-}1100\ K) \quad (4\text{-}6)$$

Table 4.3. EMF-measurements with galvanic cells of the type: Ni, NiF_2 / CaF_2 / UF_4, URh_3, Rh; standard Gibbs energies of formation, and "third law" enthalpies of formation of URh_3.

T/K	EMF/mV	$\Delta G_f^\circ(URh_3)$/kJ mol^{-1}	$\Delta H_f^\circ(298.15\ K)$/kJ mol^{-1}
948.6	815.7	- 307.35	- 301.36
966.8	816.5	- 307.40	- 301.47
968.3	816.6	- 307.39	- 301.46
982.9	818.0	- 307.15	- 301.24
991.1	818.2	- 307.24	- 301.36
992.5	817.5	- 307.54	- 301.66
997.3	818.6	- 307.21	- 301.35
999.2	819.2	- 307.02	- 301.16
1000.8	818.4	- 307.36	- 301.51
1006.7	820.0	- 306.86	- 301.03
1008.2	820.3	- 306.78	- 300.95
1024.5	821.5	- 306.65	- 300.88
1027.4	821.5	- 306.70	- 300.95
1031.5	821.0	- 306.98	- 301.21
1036.4	820.3	- 307.34	- 301.61
1038.6	820.3	- 307.39	- 301.66
1044.2	824.3	- 305.96	- 300.25
1044.8	821.8	- 306.94	- 301.23
1065.5	825.4	- 305.97	- 300.41
1067.7	823.0	- 306.93	- 301.40
1089.0	825.6	- 306.36	- 300.99
1113.2	828.3	- 305.81	- 300.66

$\Delta H_f^c(URh_3, 298.15\ K) = -(301.16 \pm 0.17)$kJ mol^{-1}

An evaluation of the thermodynamic data for UF_4 (s) at room temperature, using $\Delta H^\circ_{f,298.15}$ [13], $S^\circ_{298.15}$ [14,15] and Cp [14,16,17] gave for the Gibbs energy of formation of UF_4:

$$\Delta G^\circ_f(UF_4)/kJ.mol^{-1} = -1909.958 + 0.282353\ T \qquad (900\text{–}1100\ K) \quad (4\text{–}7)$$

From equations (4-5), (4-6) and (4-7) the standard molar Gibbs energy of formation of URh_3 can be calculated for each temperature in table 4.3. to give:

$$\Delta G^\circ_f(URh_3)/kJ\ mol^{-1} = -316.369 + 0.309257\ T \qquad (950\text{–}1115\ K)$$

To calculate ΔH°_f (298.15 K) for URh_3 a "third law" analysis was performed for all experimental EMF temperatures in table 4.3. Values for $\{H^\circ(T) - H^\circ(298.15)\}$ and $S^\circ(T)$ of URh_3 [18], U [17] and Rh [22] were used to calculate $\Delta\{H^\circ(T) - H^\circ(298.15)\}$ and $\Delta S^\circ(T)$ for the reaction:

$$U(c) + 3Rh(c) \rightarrow URh_3(c)$$

They were calculated at the experimental EMF temperatures by means of a Newton interpolation method. The enthalpy of formation of URh_3 at 298.15 K was calculated at all experimental EMF temperatures from:

$$\Delta H^\circ_f(298.15\ K) = -\Delta\{H^\circ(T) - H^\circ(298.15)\} + T\ \Delta S^\circ(T) + \Delta G^\circ_f(T) \quad (4\text{–}8)$$

The results are given in table 4.3.; the average value for $\Delta H^\circ_f(URh_3, 298.15\ K)$ was calculated from this to be $-(301.16 \pm 0.17)kJ\ mol^{-1}$.

URu_3

The Gibbs energy of URu_3 has been measured with the same type of electrochemical cell as URh_3. The electrode was a pressed pellet of UF_3, URu_3 and Ru. No reaction was found in this electrode. Since UF_3 is less volatile than UF_4 at the same temperatures, the CaF_2 electrolyte was used in the form of a thin pellet. After the first experiments, cracks were found in the electrolyte, resulting in poor contacts with the electrodes. For this reason, a CaF_2 crucible, which had a very high mechanical strength, was again employed as described before: no cracks

were observed in the crucible after the experiments.
The EMF values of the reversible cell:

$$(-)\ Ni,Mo\ /\ Ni,NiF_2\ /\ CaF_2\ /\ UF_3,URu_3,Ru\ /\ Mo,Ni\ (+)$$

have been listed in table 4.4.
The overall cell reaction on passing 6 Faradays, is:

$$3\ Ni + 2\ UF_3 + 6\ Ru = 3\ NiF_2 + 2\ URu_3$$

The standard molar Gibbs energy of formation of URu_3 can be calculated from:

$$2\ \Delta G_f^\circ\ (URu_3) = 2\ \Delta G_f^\circ\ (UF_3) - 3\ \Delta G_f^\circ\ (NiF_2) + 6\ FE_{cell} \qquad (4\text{-}9)$$

where E_{cell} denotes the measured cell EMF.
An evaluation of the thermodynamic data for $UF_3(s)$ at room temperature, using $\Delta H^\circ_{f,298.15}$ [13], $S^\circ_{298.15}$ [14,15,18] and Cp [14,16,17,18] gave the Gibbs energy of formation of UF_3:

$$\Delta G_f^\circ(UF_3)/kJ\ mol^{-1} = -1500.500 + 0.213924\ T \quad (1000\text{-}1200\ K) \quad (4\text{-}10)$$

From equations (4-6), (4-9) and (4-10) the standard molar Gibbs energy of formation of URu_3 can be calculated for each temperature in table 4.4. The results obtained were calculated by least squares:

$$\Delta G_f^\circ\ (URu_3)/kJ\ mol^{-1} = -178.543 + 0.016290\ T \quad (1090\text{-}1180\ K)$$

To calculate ΔH_f° (298.15 K) for URu_3 a "third law" analysis was performed for all experimental EMF temperatures in table 4.4. Values for $\{H^\circ(T) - H^\circ(298.15)\}$ and $S^\circ(T)$ of URu_3 [18], U [17] and Ru [22] were used to calculate $\Delta\{H^\circ(T) - H^\circ(298.15)\}$ and $\Delta S^\circ(T)$ for the reaction:

$$3\ Ru(c) + U(c) \rightarrow URu_3(c)$$

The enthalpy of formation of URu_3 at 298.15 K was calculated at all experimental EMF temperatures using equation (4-8). The average value for $\Delta H_f^\circ(URu_3, 298.15\ K)$ was calculated to be: $-(150.83 \pm 0.30)\ kJ\ mol^{-1}$.

Table 4.4. Results of EMF-measurements for galvanic cells of the type: Ni, NiF_2 / CaF_2 / UF_3, URu_3, Ru: standard Gibbs energies of formation, and "third law" enthalpies of formation of URu_3.

T/K	EMF/mV	$\Delta G_f^o(URu_3)$/kJ mol^{-1}	$\Delta H_f^o(298.15K)$/kJ mol^{-1}
1091.2	1290.6	- 160.89	- 151.66
1103.8	1292.9	- 160.38	- 151.18
1112.7	1292.7	- 160.56	- 151.36
1116.8	1294.5	- 160.09	- 150.89
1123.8	1294.2	- 160.27	- 151.08
1130.0	1293.8	- 160.46	- 151.28
1133.3	1294.5	- 160.31	- 151.11
1133.7	1295.3	- 160.08	- 150.90
1144.1	1297.8	- 159.49	- 150.31
1149.2	1296.4	- 159.96	- 150.80
1157.4	1299.1	- 159.29	- 150.13
1165.2	1297.7	- 159.80	- 150.63
1168.4	1300.0	- 159.17	- 150.03
1178.4	1298.6	- 159.70	- 150.56

$\Delta H_f^o(URu_3, 298.15\ K) = -(150.83 \pm 0.30)$ kJ mol^{-1}

IV.2.4. Discussion

The results of the measurements by different authors are shown in fig. 4.3. For URh_3 our results differ from those published before. This is especially so with Naraine and Bell's values [5]; no explanation can be given for the considerable discrepancies with our measurements.
Holleck and Kleykamp [3], because of formation of UF_4 in their electrodes (as discussed before), obviously measured the EMF of the cell:

$$U,UF_3 \ / \ CaF_2 \ / \ UF_3,UF_4$$

The overall cell reaction, on passing 3 Faradays, is:

$$4\ UF_3(c) \rightarrow 3\ UF_4(c) + U(c)$$

Indeed, the ΔG^o-values, derived from their EMF measurements ($= -3\ F.E_{cell}$), are almost identical with the Gibbs energies of the UF_3/UF_4 equilibrium as can be calculated from the Gibbs energies of formation of $UF_3(c)$ and $UF_4(c)$; this is illustrated in figure 4.3.
Schmidt [4] derived values for the Gibbs energy of formation of URh_3 in a different way, namely by means of "coupled reductions":

$$x\ Rh + UO_2 + 2H_2 = URh_x + 2H_2O$$

The results of Schmidt do not agree with ours. Like in Naraine and Bell's results, their entropies of formation of URh_3 are much too high, indicating that the measurements are in error.
For URu_3 the situation is much better. The Gibbs energies of formation of URu_3, found by Holleck and Kleykamp and later corrected by the authors [19], are in fair agreement with our results (figure 4.3.).

The values of the Gibbs energies of formation of URh_3 and URu_3 demonstrate the great thermodynamic stability of these compounds, as predicted by the Engel-Brewer theory. Intermetallic compounds formed by combining transition metals form the left of the periodic table with metals form the right of the table (e.g. $HfPt_3$) are usually very stable [2,20]. From our results, it can be concluded that URh_3 is much more stable than URu_3; this is in agreement with the Engel-Brewer theory.

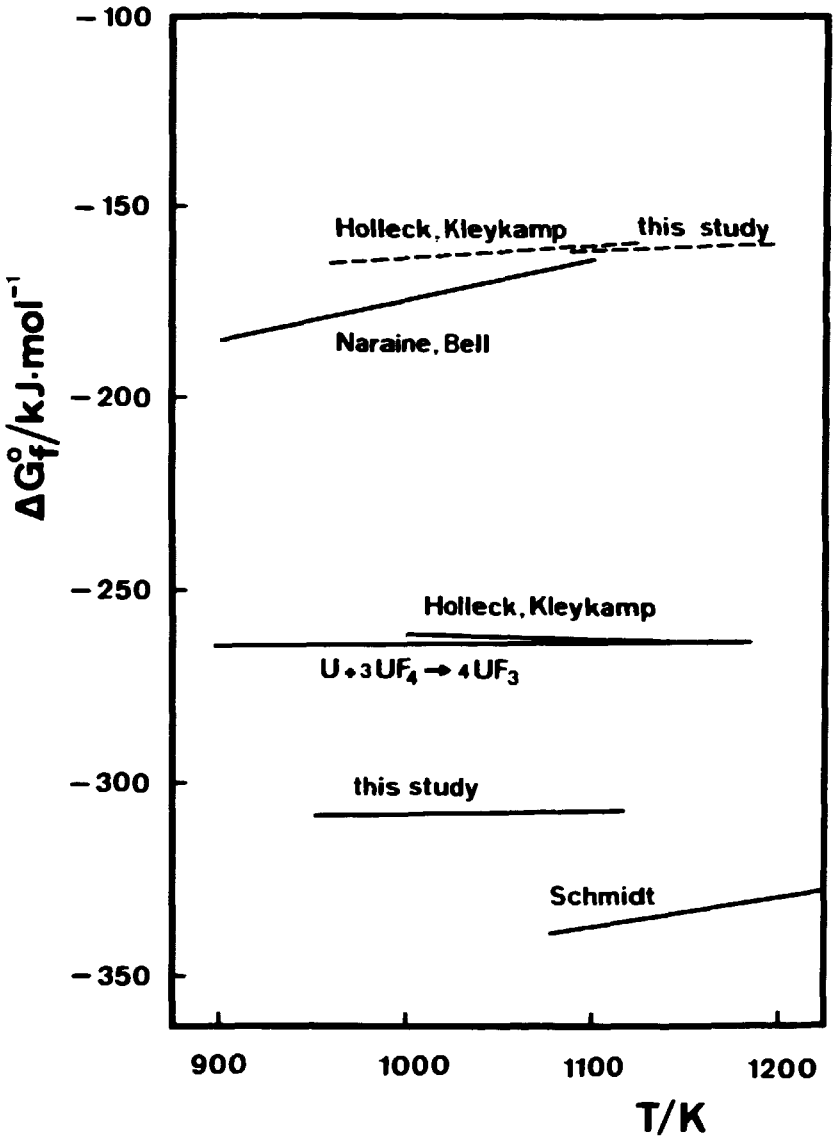

Fig. 4.3. Gibbs energies of formation of URh_3 and URu_3 as a function of temperature by various authors.
Full lines: URh_3; dotted lines: URu_3.

REFERENCES

[1] Bramman, J.I.: Sharpe, R.M.; Thom, D.; Yates, G. J. Nucl. Mater. 25 (1968) 201.

[2] Brewer, L. Acta Met. 15 (1967) 553.

[3] Holleck, H.; Kleykamp, H. J. Nucl. Mater. 45 (1972-73) 47.

[4] Holleck, H.; Kleykamp, H. J. Nucl. Mater. 35 (1970) 158.

[5] Naraine, M.G.; Bell, H.B. J. Nucl. Mater. 50 (1974) 83.

[6] Schmidt, N. KFK-1987, Karlsruhe (1974).

[7] Wijbenga, G. thesis; to be published (1981).

[8] Dwight, A.E.; Downey, J.W.; Conner, R.A.Jr. Acta Crystallogr. 14 (1961) 75.

[9] Heal, T.J.; Williams, G.I. Acta Crystallogr. 8 (1955) 494.

[10] Alcock, C.B. (editor) EMF Measurements in High Temperature Systems, Inst. Min. Met., London (1968).

[11] Wagner, C. J. Electrochem. Soc. 115 (1968) 933.

[12] Mah, A.D.: Pankratz, L.B. Contributions to the Data on Theoretical Metallurgy, XVI, Bull. Bureau Mines, (1976) 668.

[13] Cordfunke, E.H.P.; Ouweltjes, W. J. Chem. Thermodynamics, 13 (1981) 193.

[14] Rand, M.H.; Kubaschewski, O. The Thermochemical Properties of Uranium Compounds, Oliver & Boyd, Edinburgh and London, (1963).

[15] Technical Note 270-3; Selected Values of Chemical Thermodynamic Properties. N.B.S. (1968).

[16] Barin, I.; Knacke, O. Thermochemical properties of Inorganic substances. Springer-Verlag, Berlin (1973).

[17] Oetting, F.L.; Rand, M.H.; Ackermann, R.J. The Chemical Thermodynamics of Actinide Elements and Compounds, part 1, IAEA, Vienna (1976).

[18] Cordfunke, E.H.P.; Muis, R.P.; Wijbenga, G.; Burriel, R.: Zainel, H.; To. M.; Westrum, E.F. J. Chem. Thermodynamics, to be published.

[19] Holleck, H.; Kleykamp, H. Z. Metallk., 66 (1975) 298.

[20] Brewer, L. High-Strength Materials ed. F. Zackay (Wiley, New York, (1965) p. 12.

[21] Codata Bulletin 11, (1973).

[22] Barin, I.; Knacke, O.; Kubaschewski, O. Thermochemical properties of inorganic substances. Supplement, Springer-Verlag (1977).

IV.3. GIBBS ENERGY OF FORMATION OF UF_3

IV.3.1. Introduction

In chapter III.2. the determination of the enthalpy of formation of UF_3 by fluorine bomb calorimetry has been described. Cordfunke and Ouweltjes [1] determined $\Delta H_f^o(UF_3,c,298.15\ K)$ by solution calorimetry. From these results, combined with $S^o_{298.15}$ and C_p^o (see chapter VI.2.), $\Delta G_f^o(UF_3)$ at higher temperatures can be derived.
In this chapter the integral values for $\Delta G_f^o(UF_3)$ will be compared with the partial Gibbs energies of formation of UF_3, obtained by solid state EMF measurements, in the temperature range 950 - 1170 K.

IV.3.2. Experimental

IV.3.2.1. Materials

Uranium powder was prepared by hydriding metallic uranium at 300 °C, followed by dehydriding at 450 °C. This process was repeated several times to obtain finely divided powder.
NiF_2 and UF_4 were dried in a mixture of HF and argon at 600 °C and 700 °C, respectively.
Nickel powder was heated at 500 °C in vacuum to remove any adsorbed moisture. The UF_3 was prepared by heating in argon at 1050 °C a mixture of uranium powder and UF_4 at the stoichiometric ratio.
The results of the chemical analysis of the compounds prepared for the EMF measurements are given in table 4.5.

Table 4.5. Analytical results of the compounds used for the EMF measurements: mass fraction w and molar mass M.

compound	$\frac{M}{mol}$	10^2 w (U),(Ni) found	10^2 w (U),(Ni) calculated	10^2 w (F) found	10^2 w (F) calculated	10^2 w (O)	10^2 w (C)
U	238.029	99.6	100.00	-	-	0.165	0.043
UF_3	295.024	80.5	80.7	19.1	19.3	0.287	-
NiF_2	96.707	60.7	60.7	37.9	39.3	1.016	-

IV.3.3. Results

The EMF measurements were performed with reversible galvanic cells using CaF_2 as the electrolyte. The description of the EMF apparatus and schematic diagrams of the equipment have been given in chapter IV.1.
As the reference electrode, a pressed pellet of an intimate mixture of nickel fluoride and nickel powder, sintered at 800 °C, was used. As the other electrode, mixtures of uranium and UF_3 were pressed into pellets and sintered at 700 °C.
After sintering all pellets were polished. For the CaF_2 electrolyte a sintered cylindrical crucible was used, as described before, and placed over the U,UF_3 electrode to protect the electrode from any oxygen contamination. The fabrication of the CaF_2 crucibles has been described in detail in chapter IV.1.
The contacts were made from tungsten and nickel connected with nickel wires.
The Gibbs energies of formation of UF_3, were measured using the cell:

$$(+)\ Ni,W\ /\ Ni,NiF_2\ /\ CaF_2\ /\ UF_3,U\ /\ W,Ni\ (-),$$

Three series of measurements were performed in the temperature range 950 - 1170 K, and good agreement was found between the different sets of measurements (tables 4.5. and 4.7.). The different series of measurements are shown in fig. 4.4.

The equilibrium cell voltages at constant cell temperatures were reached within 8 hours at temperatures above 1000 K; however, at lower temperatures equilibrium in the cell took over 24 hours. Measurements were made at constant temperatures, both heating and cooling, with no significant difference in the measured values.
The argon gas flowing out of the cell contained H_2O and oxygen at concentrations below 1 ppm, as measured by a panametric-cell connected with a hygrometer and a standard EMF-cell: $Pt(O_2)\,|\,ZrO_2\,|\,(Ni,NiO)Pt$.
Reaction of the very sensitive U,UF_3 electrode with impurities in the gas atmosphere of the EMF cell was minimized by locking the electrode in the CaF_2 crucible, as described.
The results obtained in the measurements are plotted as a temperature versus EMF graph (fig. 4.4.).

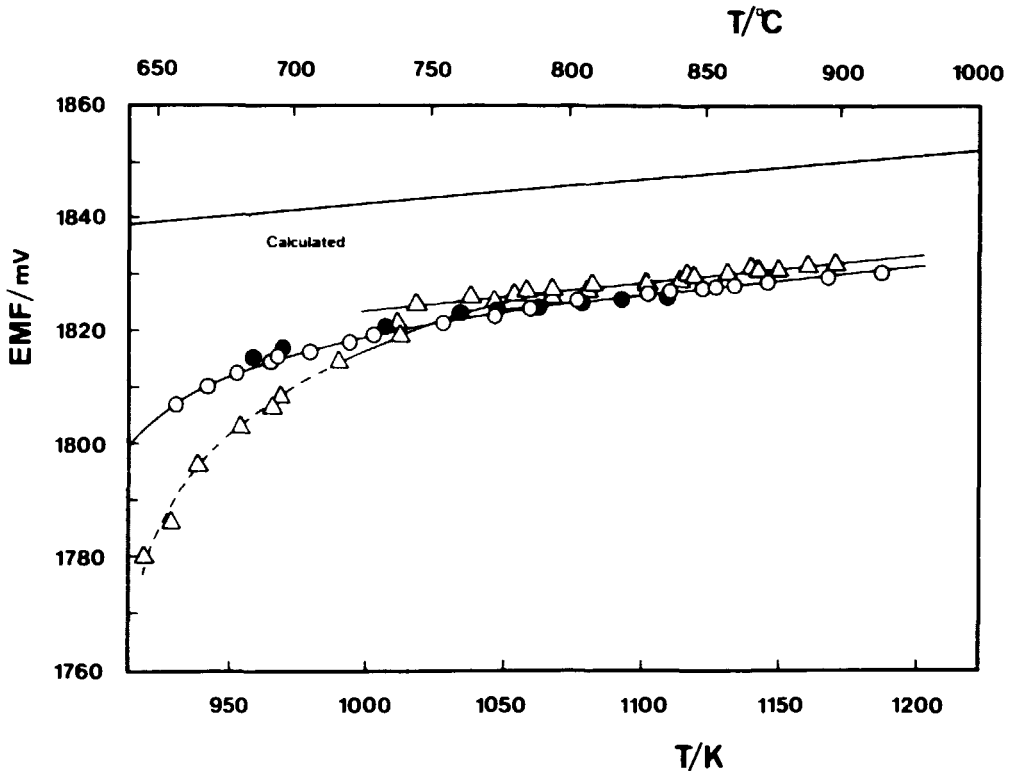

Fig. 4.4. Graph of EMF measurements as a function of temperature of the cell: Ni,NiF_2 / CaF_2 / U,UF_3.
Results from three separate cells are shown.

The overall cell reaction, on passing 6 Faradays, is:

$$3\ Ni + 2\ UF_3 \rightarrow 3\ NiF_2 + 2\ U$$

The standard molar Gibbs energy of formation of UF_3 can be calculated from:

$$2\ \Delta G_f^o(UF_3) = 3\ \Delta G_f^o(NiF_2) - 6\ FE_{cell} \qquad (4\text{-}11)$$

where E_{cell} denotes the measured cell EMF.
The Gibbs energy of formation of NiF_2 as a function of temperature is well established [2]:

$$\Delta G_f^o(NiF_2)/kJmol^{-1} = -653.499 + 0.151293\ T \quad (800 - 1100\ K) \qquad (4\text{-}6)$$

From equations (4-11) and (4-6) the standard molar Gibbs energies of formation of UF_3 can be calculated for each temperature in tables 4.6. and 4.7. The value for F used was 96484.56 J $V^{-1}eq^{-1}$ [3].

$$\overline{\Delta G}^{o}_{f}(UF_3)/kJmol^{-1} = -1480.61 + 0.200528\ T \quad (1000 - 1049\ K) \quad (4\text{-}12)$$

and

$$\overline{\Delta G}^{o}_{f}(UF_3)/kJmol^{-1} = -1492.40 + 0.211622\ T \quad (1049 - 1170\ K) \quad (4\text{-}13)$$

IV.3.4. Discussion

The values for $\overline{\Delta G}^{o}_{f}(UF_3)$, obtained from the EMF measurements, will now be compared with $\Delta G^{o}_{f}(UF_3)$, obtained from the thermodynamic data of $UF_3(s)$.
In chapter IV.2. it has been derived:

$$\Delta G^{o}_{f}(UF_3)/kJmol^{-1} = -1500.500 + 0.213924\ T \quad (1000 - 1200\ K) \quad (4\text{-}10)$$

With this result the EMF of the cell: Ni,NiF_2 / CaF_2 / U,UF_3, can be calculated using the equations (4-11), (4-6) and (4-10).
The resulting EMF as a function of T is plotted in fig. 4.4.
The values of $\overline{\Delta G}^{o}_{f}(UF_3)$, obtained via the EMF method (equations (4.12) and (4-13)), are more positive compared to $\Delta G^{o}_{f}(UF_3)$ determined calorimetrically (equation (4.10)). This difference arises from the fact that EMF measurements are methods of deriving partial molar functions, while calorimetric methods provide the integral values.
If we make the assumption that the main reason for the difference between $\overline{\Delta G}^{o}_{f}(UF_3)$ and $\Delta G^{o}_{f}(UF_3)$ is the solubility of impurities in uranium, we can calculate the activity of uranium.
From the equation:

$$\Delta G^{o}_{f}(UF_3) = \overline{\Delta G}^{o}_{f}(UF_3) + \overline{\Delta G}_{U}, \quad (4\text{-}14)$$

the Gibbs energy ($\overline{\Delta G}_{U}$) of impurities in solution in uranium can be derived, from which the activity of uranium (a_U) follows:

$$\overline{\Delta G}_{U} = RT \ln a_{U} \quad (4\text{-}15)$$

Table 4.6. Results of EMF measurements for galvanic cells of the type: Ni,NiF_2 / CaF_2 / U,UF_3, and measured standard Gibbs energies of formation of UF_3.

T/K	EMF/mV	$\Delta G_f^o(UF_3)$/kJmol^{-1}
953.0	1812.3	- 1288.6
959.1	1815.5	- 1288.1
966.4	1814.4	- 1286.1
967.5	1815.9	- 1286.3
970.2	1817.0	- 1286.0
980.0	1816.6	- 1283.7
988.8	1818.0	- 1282.1
1003.1	1819.4	- 1279.2
1007.2	1821.2	- 1278.8
1011.8	1821.5	- 1277.9
1013.0	1819.1	- 1276.9
1019.1	1824.5	- 1277.1
1027.8	1821.4	- 1274.2
1028.4	1821.2	- 1274.0
1034.4	1823.1	- 1273.2
1037.7	1825.9	- 1273.[illegible]
1047.0	1824.5	- 1270.8
1047.1	1823.4	- 1270.4
1047.5	1823.0	- 1270.2

Table 7. Results of EMF measurements for galvanic cells of the type: Ni,NiF_2 / CaF_2 / U,UF_3, and measured standard Gibbs energies of formation of UF_3.

T/K	EMF/mV	$\Delta G_f^o(UF_3)$/kJmol^{-1}
1054.2	1826.7	- 1269.8
1058.2	1824.0	- 1268.1
1058.7	1827.0	- 1268.8
1062.6	1824.2	- 1267.1
1067.3	1826.2	- 1266.6
1067.5	1827.3	- 1266.9
1077.1	1825.5	- 1264.2
1078.0	1825.1	- 1263.9
1081.4	1827.2	- 1263.7
1081.8	1828.0	- 1263.9
1092.7	1825.4	- 1260.6
1102.0	1826.9	- 1259.0
1102.1	1828.4	- 1259.4
1109.1	1826.0	- 1257.1
1110.0	1827.5	- 1257.3
1113.9	1829.0	- 1256.9
1116.8	1829.6	- 1256.4
1118.8	1829.6	- 1255.9
1122.3	1827.7	- 1254.6
1127.1	1828.2	- 1253.6
1131.5	1830.1	- 1253.2
1134.2	1828.3	- 1252.1
1140.6	1830.6	- 1251.3
1142.8	1830.6	- 1250.8
1146.5	1828.7	- 1249.4
1149.7	1831.0	- 1249.3
1160.9	1831.5	- 1246.9
1161.2	1831.5	- 1246.9
1168.5	1829.8	- 1244.7
1170.2	1832.0	- 1245.0

The results of the activity of uranium as a function of the EMF are presented in fig. 4.5.

From fig. 4.5. it can be seen that the activity of uranium is much smaller than 1. A possible reason could also be a small non-stoichiometry range of UF_3. However, this has not been seen on the X-ray diagrams.

It should be pointed out that, although several authors have used U,UF_3 electrodes as reference electrodes in their EMF cells [4,5,6], our measurements indicate that U,UF_3 is not a very suitable reference electrode, due to the activity of uranium.

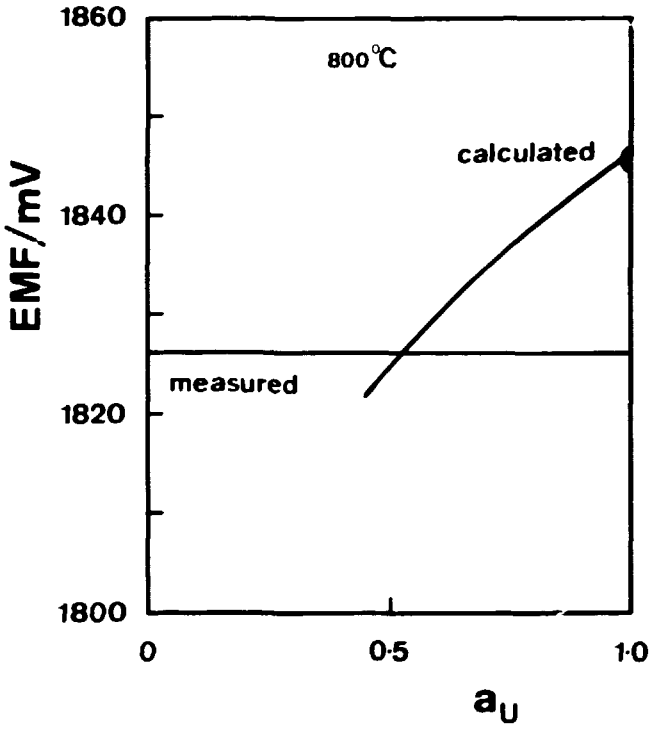

Fig. 4.5. Activity of uranium (a_U), calculated from the difference between $\Delta G_f^o(UF_3)$ using the thermodynamic data at 298.15 K and $C_p(T)$, and $\overline{\Delta G_f^o}(UF_3)$ using the measured EMF values.

REFERENCES

[1] Cordfunke, E.H.P.; Ouweltjes, W. J. Chem. Thermodynamics 13 (1981) 193.

[2] Mah, A.D.; Pankratz, L.B. Contributions to the Data on Theoretical Metallurgy, XVI, Bull. Bureau Mines, (1976) 668.

[3] Codata Bulletin 11, (1973).

[4] Holleck, H.; Kleykamp, H. J. Nucl. Mater 35 (1970) 158.

[5] Alcock, C.B. (editor) EMF Measurements in High Temperature Systems, Inst. Min. Met., London (1968).

[6] Yoshihara, K.; Kanno, M. J. Inorg. Nucl. Chem. 36 (1974) 309.

CHAPTER V

ESTIMATION PROCEDURES OF THERMOCHEMICAL DATA OF ACTINIDE-NOBLE METAL COMPOUNDS

V.1. INTRODUCTION

In nuclear industry knowledge of phase relationships and thermodynamic properties is required to deal effectively with possible material problems. These problems include the interaction of nuclear fuel with alloy claddings and fission products.

There has been a growing interest in predictive models of inorganic materials behaviour, not only for this reason, but also because of increasing metal needs and energy shortages expected at the end of this century. Experimentally determined thermochemical data such as enthalpies of formation and spectroscopic data are very valuable for deciding which predictive model is suitable for which group of compounds.

In this chapter a short description will be given of the major predictive models for transition metals and alloys : the Engel-Brewer theory [1,2,3], the model of Miedema, de Boer and Boom [4,5,6], and the model of Watson and Bennett [33,34]. These models may serve as a basis for ordering and predicting the thermodynamic properties of alloys and pure metal phases. As a result we can understand and predict the phase diagrams and thus the reactivity of a metal, intermetallic compound or alloy in any chemical environment.

As an example, the prediction of certain very stable intermetallic compounds by Brewer [7] has indicated the possibility of reactions between common ceramics such as zirconia, or thoria, as well as refractory oxides such as UO_2, or PuO_2, and the platinum metals. Combinations of refractory oxides and noble metals were formerly thought to be stable at high temperatures. However, they appear to react readily under reducing conditions [8]. Predictive models for alloy stability can be a considerable help in making the proper decisions concerning the use of high-temperature materials in technology.

V.2. DESCRIPTION OF THE PREDICTIVE MODELS

V.2.1. The Engel-Brewer theory

Brewer has published several papers [1-3, 7, 9-16] on the stabilities of transition metal alloys. The essentials of the Engel-Brewer theory will be briefly presented here.

The application of the valence bond model to metals and the recognition of d electron bonding are Pauling's important contributions to the development of the Engel-Brewer theory [17]. W. Hume-Rothery [19] developed the correlation between electronic configuration and crystal structure of normal metals, and N. Engel [18] extended this concept to transition metals. Later on Engel applied the correlation between crystal structure and valence electron concentration more extensively to both elements and alloys [20,21].

A summary of the fundamental rules of the Engel-Brewer theory will be given here:

1. The valence bond model is applicable to metals. Bonding is created through incompletely filled orbitals in the bonding valence state so that stability is determined by the number of unpaired bonding electrons and efficiency of overlap of their charge clouds.
2. In metals and alloys the correlation between the number of s,p electrons per atom in the bonding valence state, and the crystal structure is as follows. If n is the total number of valence electrons, then a $d^{n-1}s$ electronic configuration (less than 1.5 s,p electrons/atom) is related with a body-centered cubic, $d^{n-2}sp$ (1.7-2.1 s,p electrons/atom) with a hexagonal close-packed, and $d^{n-3}sp^2$ (2.5-3 s,p electrons/atom) with a face-centered cubic structure.
3. In metals the d electrons are somewhat localized because of their fairly small orbits [30], the s,p electrons are quite delocalized. Accordingly, the roles of d versus s,p electrons in determining structure are different. Only the concentration of s,p electrons determines structure. The d electrons have relatively poor overlap with orbitals of nearest neighbours; however, overlap increases from 3d to 4d to 5d. Some d bonding will be lost if the number of d electrons exceeds five because this necessitates the internal pairing of d electrons in the bonding valence state.

In the following sections the rules of the Engel-Brewer theory will be applied in the description of the interactions between the platinum metals and the actinides : thorium, uranium, and plutonium considering both the pure metals and the alloys.

V.2.1.1. Application of the Engel-Brewer theory to noble metals and actinides

Noble metals

The application of the valence bond model to metals will be explained with palladium as an example [14,15,22]. The ground state of a gaseous Pd-atom is d^{10} (fig. 5.1). If the average internuclear distance, r, of a mole of gaseous Pd-atoms is reduced, the interatomic potential follows a shallow curve; there are only weak Van der Waals interactions. Solid Pd has the fcc structure with the $d^{7.5}sp^{1.5}$ configuration, which can be considered as a blend of d^8sp and d^7sp^2 configurations. If the promotion energy of about 586 kJ mol^{-1} [23] is used to excite the gaseous atoms from d^{10} to $d^{7.5}sp^{1.5}$ and the excited gaseous Pd-atoms

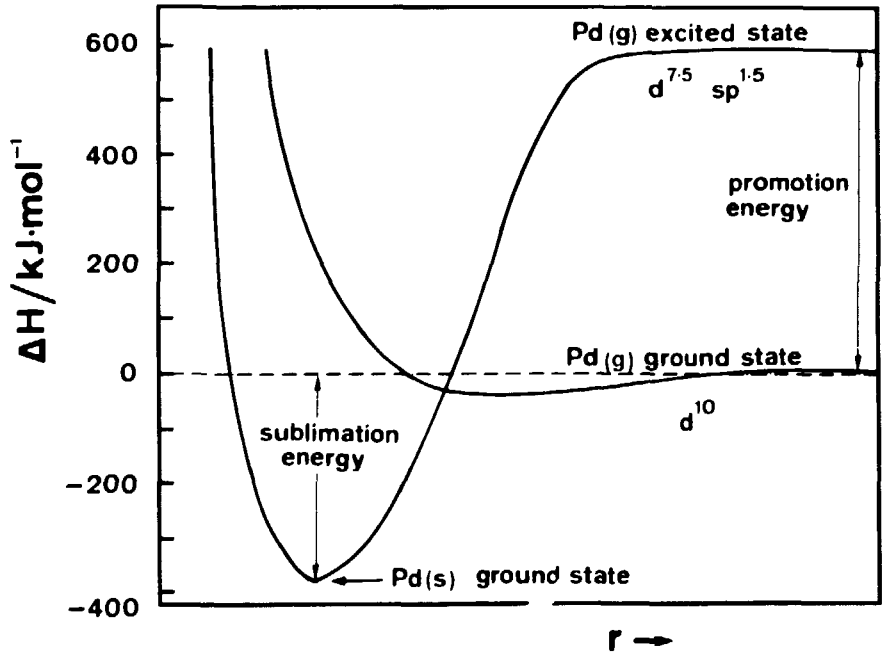

Fig. 5.1. Potential energies of d^{10} and $d^{7.5}sp^{1.5}$ configurations of Pd as a function of internuclear distance.

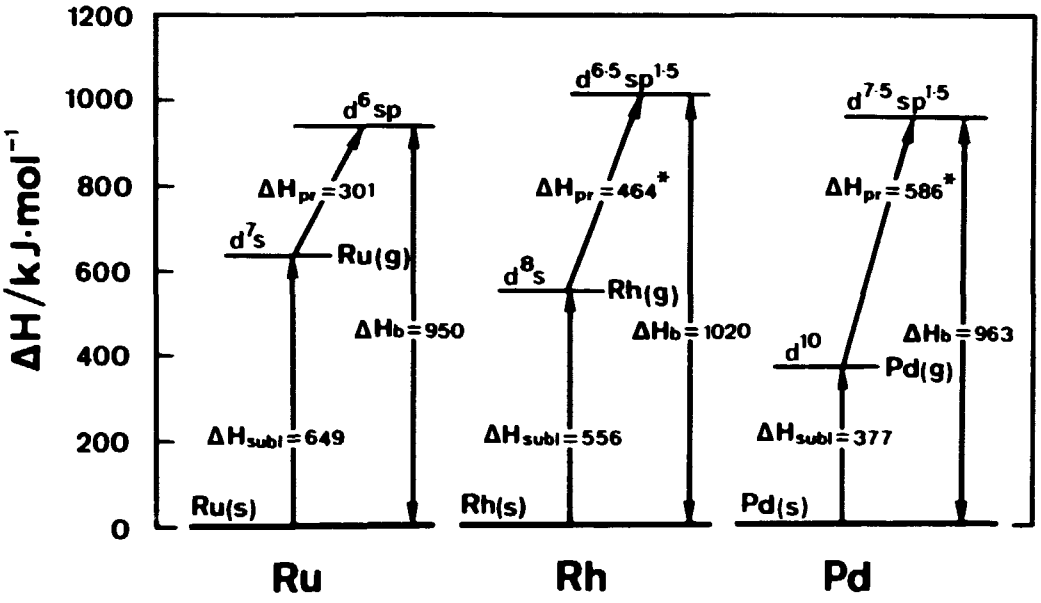

Fig. 5.2. Sublimation and promotion energies for Ru, Rh and Pd.
* = Brewer's estimate.

are allowed to approach one another, the result will be a very deep potential curve. This curve schematically represents the potential energy of a mole of Pd-atoms in the $d^{7.5}\ sp^{1.5}$ configuration. Interaction of Pd-atoms in the $d^{7.5}\ sp^{1.5}$ configuration is much stronger because there are five electrons per atom available for bonding. As the internuclear distance is reduced, the energy of the $d^{7.5}\ sp^{1.5}$ configuration drops far below that of d^{10}; and the cohesion in Pd metal is due to five (or more) bonding electrons per atom.
The net enthalpy of sublimation (or cohesive enthalpy) from solid to gaseous ground state of Pd metal is the enthalpy released when atoms in the bonding valence state condense, the bonding enthalpy of gaseous $d^{7.5}\ sp^{1.5}$ Pd of 963 kJ mol^{-1}, minus the promotion energy to the $d^{7.5}\ sp^{1.5}$ state of Pd gas of 586 kJ mol^{-1}, or 377 kJ mol^{-1}.
As presented here, the valence bond model is a thermodynamic cycle in which bonding has been shown in simple steps. The rule is that promotion may only take place if the bonding enthalpy is sufficient to pay off the promotion energy.
In fig. 5.2. sublimation (ΔH_{subl}), promotion (ΔH_{pr}) and bonding (ΔH_b) enthalpies are given for ruthenium, rhodium and palladium in energy diagrams. The values for the promotion energies of Rh and Pd are recent

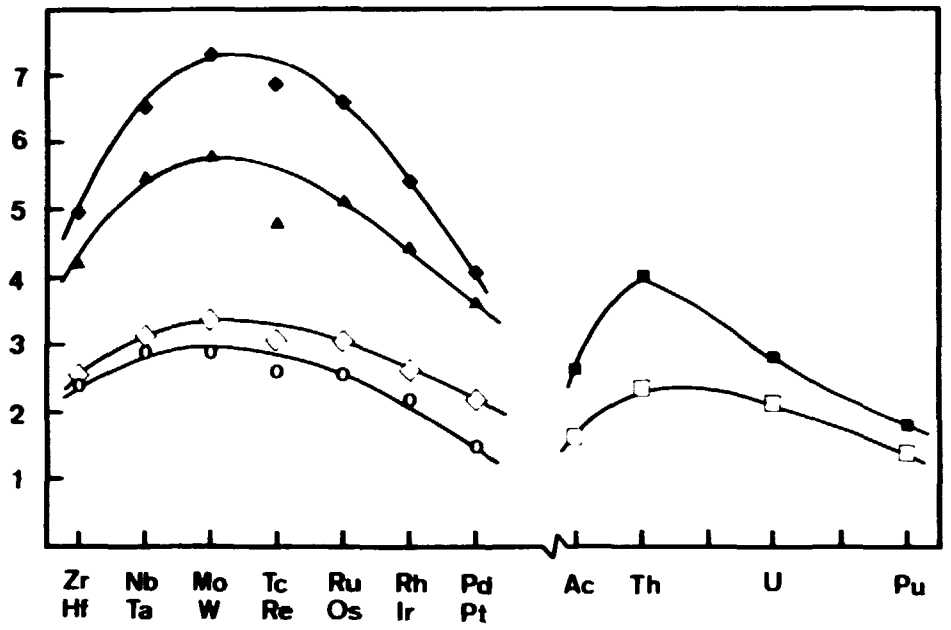

Fig. 5.3. Properties of the second and third series transition metals and the actinides Ac, Th, U and Pu.
(▲ ◆ ■ : melting point ÷ 500 K).
(o ◇ □ : sublimation enthalpy ÷ 250 kJ mol^{-1}).

estimates of Brewer [23].

The shape of the melting curves in fig. 5.3. can be explained also by application of the valence bond theory [3,24]. In the first half of the second transition series, increasing the number of electrons increases the number of bonds.
Niobium has one more electron than zirconium. This electron is in an unoccupied orbital. Thus, niobium has one more bond than zirconium and as a result it has a higher melting point and sublimation enthalpy (see also table 5.1.). Bonding effectiveness also plays a role, e.g. compare Nb and Mo. In the second half of the second transition series, increasing the number of electrons decreases the number of bonds.
Palladium has one more electron than rhodium. This electron goes into an occupied orbital. According to the Pauli principle, two electrons sharing the same orbital will spin pair and will be unavailable for bonding. Thus palladium has a lower melting point than rhodium.
The VI B metals molybdenum and tungsten have the highest melting points

of the second and third transition series elements, due to their d^5s configurations in the solid with the optimum five *d* orbitals with spin unpaired electrons available for bonding. It is interesting to see the role of 5d electrons compared to 4d electons in fig. 5.3. Apparently, the 5d electrons bond more strongly than 4d electrons (compare also fig. 5.4). In fig. 5.3. plots of the sublimation enthalpies of the second and third transition series elements have been presented. The similarity of the curves suggests that the same valence effects play a role in the different transition metal series.

The melting points and sublimation enthalpies of the actinides Ac, Th, U and Pu are presented in table 5.1. and in fig. 5.3.

We can make use of spectroscopic data in a quantitative manner by using the experimental promotion energies required to achieve the electronic configurations under consideration, together with experimental enthalpies of sublimation, to determine the bonding energies that result when gaseous atoms are condensed to the solid metal (table 5.1.). Fig. 5.4. illustrates the experimental data for bonding energies of metals of the second and third transition series [3,9]. Fig. 5.4. gives bonding energies, not energies of gaseous valence state configurations which is what is usually meant by the term "energy of configurations". It follows from fig. 5.4. that the difference in energy between the 4d configurations for Ru, Rh and Pd, and the 5d configurations for Os, Ir and Pt lays within the range of 29 to 46 kJ per electron mol.

The bonding energy of an electron is largely independent of the particular structure, and one can draw a curve that can be used for predicting the bonding in yet unobserved phases of these metals with either the bcc or hcp structures. Since the spectroscopic data for the $d^{n-2}sp$ [3,9] configuration of Rh and Pd are incomplete, estimates were given for the d bonding energies for the hcp structures of Rh and Pd in fig. 5.4.

Actinides

The extension of the Engel-Brewer theory to the actinide metals is complicated because it is necessary to consider also the role of f electrons. For a long time, the necessary spectroscopic data have been lacking as spectra of elements involving s, p, d and f electrons have been extremely difficult to analyse [10]. Sufficient data are now known

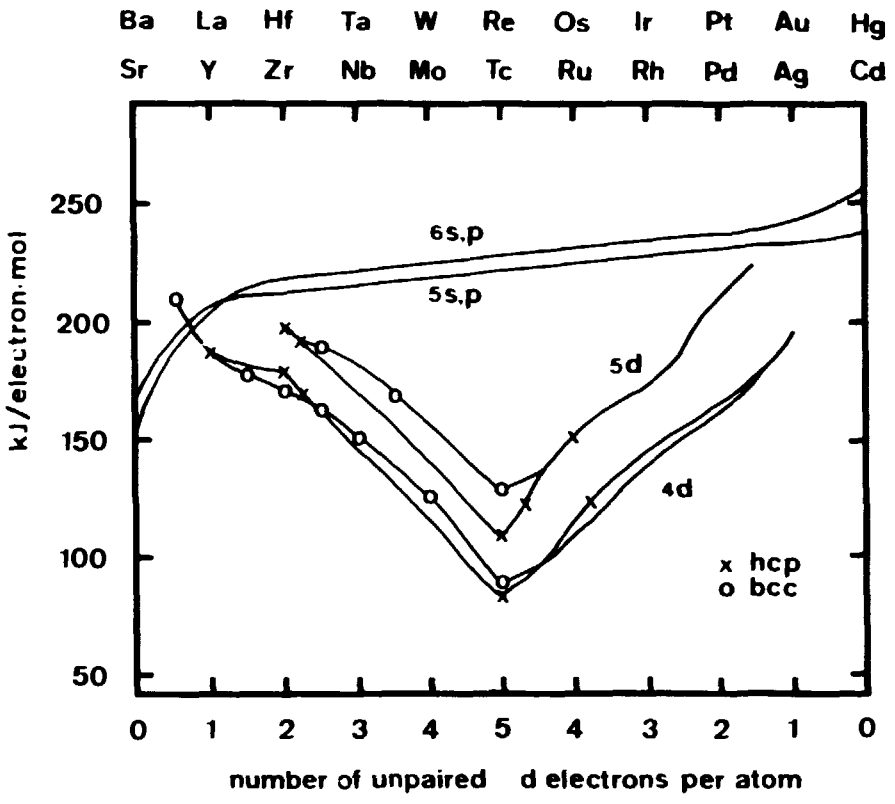

Fig. 5.4. Valence-state bonding enthalpy of metals in kJ mol^{-1} per bonding electron. Top curves : bonding enthalpy of 5s,5p and 6s,6p electrons, versus element. Bottom curves : bonding enthalpy of 4d and 5d electrons, versus number of unpaired d electrons [3].
x : experimental points derived from hcp structures
o : experimental points derived from bcc structures

to allow tabulation of promotion energies of the important electronic configurations of thorium, uranium and plutonium.
Table 5.2. lists possible configurations that could make important contributions to the bonding in the bcc-fcc phases of Th, U and Pu [11]. Important configurations for uranium are f^3d^2s, f^3dsp, f^2d^3s, f^3d^3, fd^4s, f^2d^2sp and f^3sp^2. The promotion energies are given in kJ mol^{-1} above the ground electronic states of the gaseous atoms $6d^27s^2$ of Th, $5f^36d^17s^2$ of U and $5f^67s^2$ of Pu. For bcc thorium the electronic configuration is predominantly f^0d^3s with a promotion energy of 66.5 kJ mol^{-1} and with four electrons for bonding.

Plutonium (bcc) with a configuration f^5d^2s with three bonding electrons and a promotion energy of 178.2 kJ is less strongly bound.
There are no spectroscopic data available to verify the electronic configurations of the fcc phases but the Engel theory indicates that the fcc phases will have more s and p electrons and fewer d electrons than the bcc phases. In bcc thorium the configurations fd^2s, and f^2ds would be of little importance. For plutonium the configurations f^6ds and f^5d^2s, and also f^6sp and f^5dsp have similar promotion energies, but the configurations f^5d^2s and f^5dsp with three bonding electrons would be most important. The configurations f^4d^3s and f^4d^2sp are estimated to have promotion energies that are too high to be offset by the additional bonding energy.
The sublimation energies of Th, U and Pu are given in table 5.1. The difference in sublimation enthalpies between Pu and Th of almost 251 kJ mol^{-1} is due to the Pu f^5d^2s configuration which has a promotion energy of 111.7 kJ above the Th d^3s configuration and has one less bonding electron.
In fig. 5.5. bonding enthalpies and cohesive enthalpies are compared for the second and third series transition metals, as well as for the lanthanides and actinides. The high enthalpies of sublimation of the early actinides compared to the corresponding lanthanides is to be attributed to the more ready promotion of f to d electrons which allows use of more than three bonding electrons for Th and U and the use of three bonding electrons for Pu (see fig. 5.5. and 5.6.).
Going from La to Sm (fig. 5.5.) the bonding energies of these metals (d^2s, trivalent state) hardly increase, which means that the 4f electrons of the lanthanides do not contribute significantly to bonding, however, we must allow for contributions of 5f electrons to the bonding of the metals U and Pu [11].
The ground states of the gaseous actinides Ac, Pa, U, Np, and Cm are trivalent, Th has a tetravalent state and Pu, Am, Bk and Cf have divalent ground states.
The sublimation enthalpies of the actinides Pa to Am are much larger than the corresponding lanthanides but decrease more rapidly. Possible reasons are: promotion of f to d electrons (Th and Pa have the d^3s-state in the metal; U, Np and Pu the d^2s-state), or contribution of 5f electrons to the bonding, which is decreasing going from U to Pu.

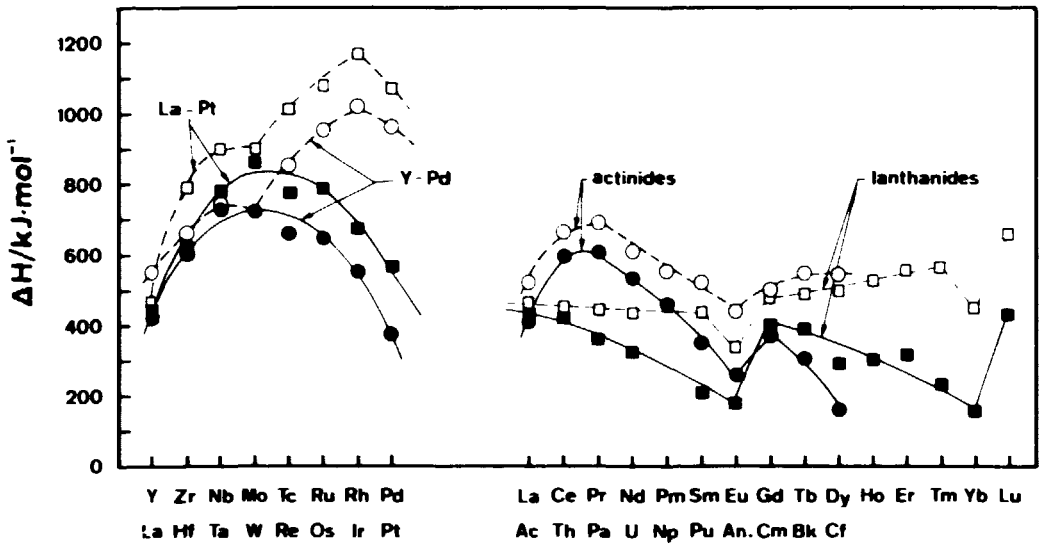

Fig. 5.5. Sublimation and bonding enthalpies of the second and third series transition metals and the lanthanides and actinides.
● ■ Sublimation enthalpies.
○ □ Bonding enthalpies.

The calculation of the known points in fig. 5.6. can be illustrated for uranium. The ground electronic state of gaseous uranium is f^3ds^2 and from table 5.2. we see that the f^3d^2s level of gaseous uranium is 74.9 kJ higher in energy. The enthalpy of sublimation of uranium is 536 kJ mol^{-1} (see table 5.1.). The bonding enthalpy of f^3d^2s atoms to form bcc metallic uranium is then 536 + 74.9 = 611 kJ mol^{-1}.
In fig. 5.6. the valence-state bonding energies of the actinides Th, U and Pu in the bcc structure are given for the configurations $f^{n-2}ds$ through $f^{n-6}d^5s$. Only in uranium all f electrons can promote to the d level up to the optimum of five bonding d electrons, the promotion energies are not too high to be offset by the additional bonding energies.

V.2.1.2. Estimates of enthalpies of formation of actinide-noble metal compounds with the Engel-Brewer theory

When thorium, uranium and plutonium or any of the metals with unused 4d, 5d or 6d orbitals are mixed with the transition metals Ru to Pd or Os to Pt, which have an excess of 4d and 5d electrons, one would expect an extreme decrease in Gibbs energy for any of the structures [13,25].

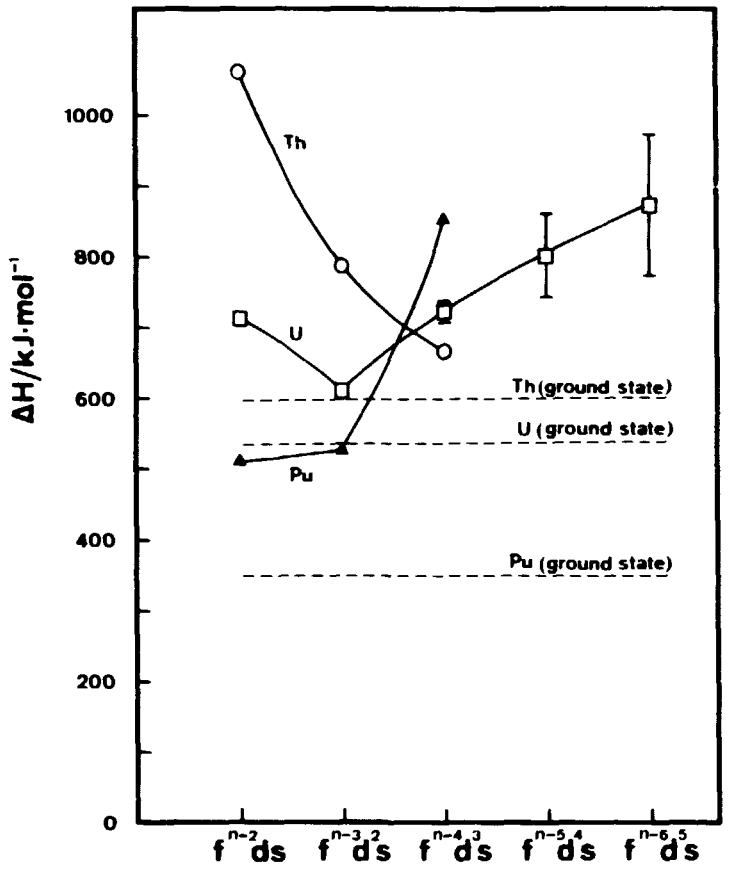

Fig. 5.6. Valence state bonding energy of the actinides Th, U and Pu in the bcc structure.

As an illustration the possible electronic configurations of $ThPd_3$ and $ThRh_3$ are presented in fig. 5.7. In pure palladium the d orbitals occupied with a pair of d electrons are non-bonding because they cannot overlap with d orbitals of neighbouring atoms. In fcc Pd, each Pd atom has a maximum of 2-2.5 d electrons that can be donated to the vacant orbitals in bcc d^3s thorium. Since $ThPd_3$ has the hcp structure, the following can happen. The non-bonding d electrons of the Pd atoms will be divided over the d and s,p levels of $ThPd_3$.
The gain in bonding electrons in $ThPd_3$ compared to the elements will be approximately 0.75 electrons per atom according to the model in fig. 5.7. There will also be a pay-off in promotion energy of Pd. The qualitative prediction can be made that $ThPd_3$ will be a very stable intermetallic compound; its enthalpy of formation being comparable with

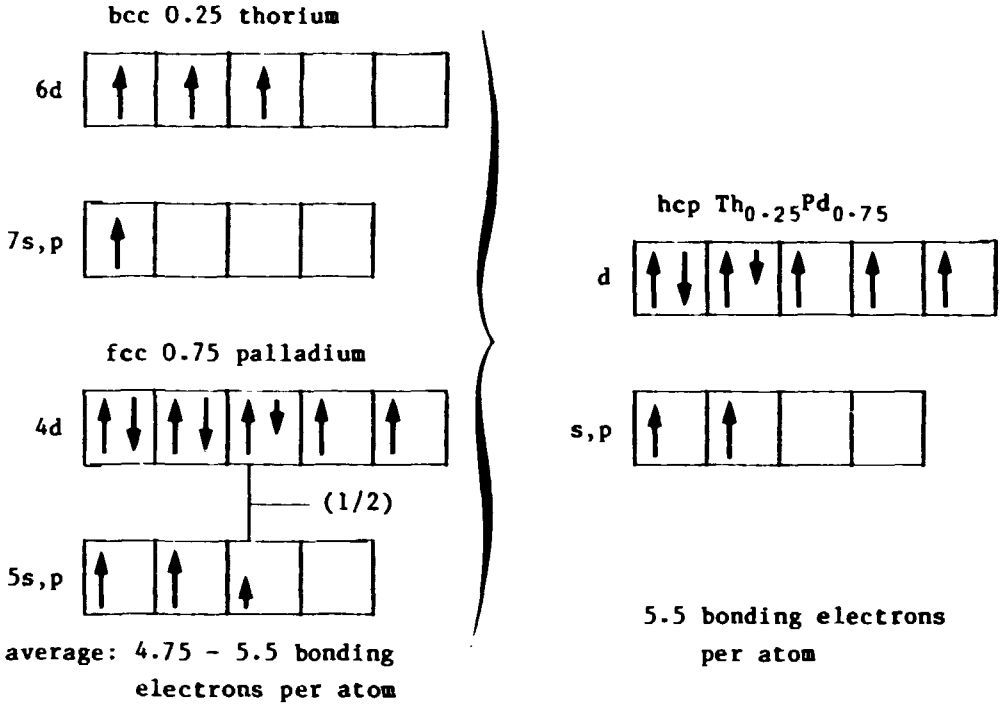

Fig. 5.7. Electronic configurations of Th, Pd, Rh, $Th_{0.25}Pd_{0.75}$ and $Th_{0.25}Rh_{0.75}$.

$ZrPt_3$ and $HfPt_3$. Zirconium and hafnium also have the d^3s configuration in the pure metal.

The gain in bonding electrons in $ThRh_3$ compared to the elements (see fig. 5.7.) will be about 1.5 - 2.25 electrons per atom, and the enthalpy of formation of $ThRh_3$ will be comparable with the enthalpy of formation (table 5.4.) of $ZrRh_3$. If we consider the compound hcp $ThPd_3$ with more d electrons in Pd to be uncoupled compared to Rh, complete uncoupling of the d electrons in $ThPd_3$ will not occur because Th already has three d electrons and the f level of $ThPd_3$ will not accept electrons. Thus, some d bonding in $ThPd_3$ will be lost. However, it is also not sure whether complete uncoupling of d electrons in $ThRh_3$ will take place. There will be a gain in bonding electrons in $PuPd_3$ compared to the elements. The stability of $PuPd_3$ will therefore be comparable with the stability of UPd_3, or less because it is possible that some d electrons will "sink" in the f level of $PuPd_3$ and contribute less to the total bonding energy of the compound. It is expected that the intermetallic compounds of Th, U and Pu with Os, Ir and Pt will be more stable compared to the corresponding compounds of Th, U and Pu with Ru, Rh and Pd due to the larger contribution of 5d electrons in bonding compared to 4d electrons.

An approximate calculation for the enthalpy of formation of URh_3 can be made as follows.

The enthalpies of sublimation (ΔH_{subl}) of U and Rh are given in table 5.1. and shown in fig. 5.5. Rh has a maximum of 9 (d and s,p) electrons and U a maximum of 6 (f,d and s,p) electrons, which can be made available for bonding in the intermetallic compound URh_3. If we consider that all the electrons in the incomplete filled energy levels of Rh and U are spread uniformly over all the atoms in URh_3, the average electron per atom value is:

$$(0.25)6\ e + (0.75)9\ e = 8.25\ e$$

With this electron per atom number (value in between Ru and Rh in the noble-metal rich compound URh_3) corresponds an enthalpy of sublimation :

$$\left(0.75\Delta H_{subl}\ (Ru) + 0.25\Delta H_{subl}\ (Rh)\right) = 626.3\ kJ\ per\ g\ atom, \quad (5\text{-}1)$$

which can be considered as the hypothetical value for $\Delta H_{subl}(URh_3)$. The excess enthalpy of the intermetallic compound URh_3 as compared to the elements Rh and U would be:

$$[0.25\{\Delta H_{subl}(URh_3) - \Delta H_{subl}(U)\} + 0.75\{\Delta H_{subl}(URh_3) - \Delta H_{subl}(Rh)\}] \quad (5\text{-}2)$$

is 76.6 kJ per gram atom or 306 kJ mol^{-1}.
Using the same procedure the enthalpies of formation of URu_3, UPd_3, UIr_3 and UPt_3 will be -138, -556, -490 and -452 kJ mol^{-1}, respectively. In fact these calculations have to be corrected for other factors such as electronic promotion energies and size effects. The results for uranium are expected to be the best because the atomic radii of U, Ru, Rh and Pd are very close: 1.38 Å, 1.34 Å, 1.34 Å and 1.37 Å, respectively. The results of Th, U and Pu noble-metal compounds are given in table 5.3.
For the intermetallic compounds of Th, U and Pu with the platinum metals Pd and Pt, the results are presented in a graph in fig. 5.8. The choice of 6 bonding electrons in uranium (including f-electrons) to calculate the estimates in table 5.3. was arbitrary, however, the $\Delta H^{o}_{f,298.15}$ values were excellent agreement with the experimental values. The choice of 4 bonding electrons in thorium is logical, but 8 bonding electrons in Pu are may be too many. The estimated uncertainty for $PuPd_3$ is therefore large (± 80 kJ mol^{-1}).
Using the same procedure, estimates of the enthalpies of formation of Zr, Nb, Hf and Ta noble-metal compounds were made and given in table 5.4. The results of the intermetallic compounds of Hf with the platinum metals Pd, Pt, Ir and Os are presented in a graph (fig. 5.9.). The thick solid lines are estimates following Brewer's model. It has to be noted that these estimates are expected to be most accurate for AB_3-compounds (noble metal rich), especially for Th, U and Pu. The distribution of electrons around AB_3 will then be least disturbed compared to the pure noble metal.

V.2.2. The cellular model of Miedema et al.

Miedema, de Boer and Boom have shown extensively in several papers [4,5,6,26] that a relatively simple atomic model can account semi-quantitatively for the enthalpy of formation, $\Delta H^{o}_{f,298.15}$ of a wide

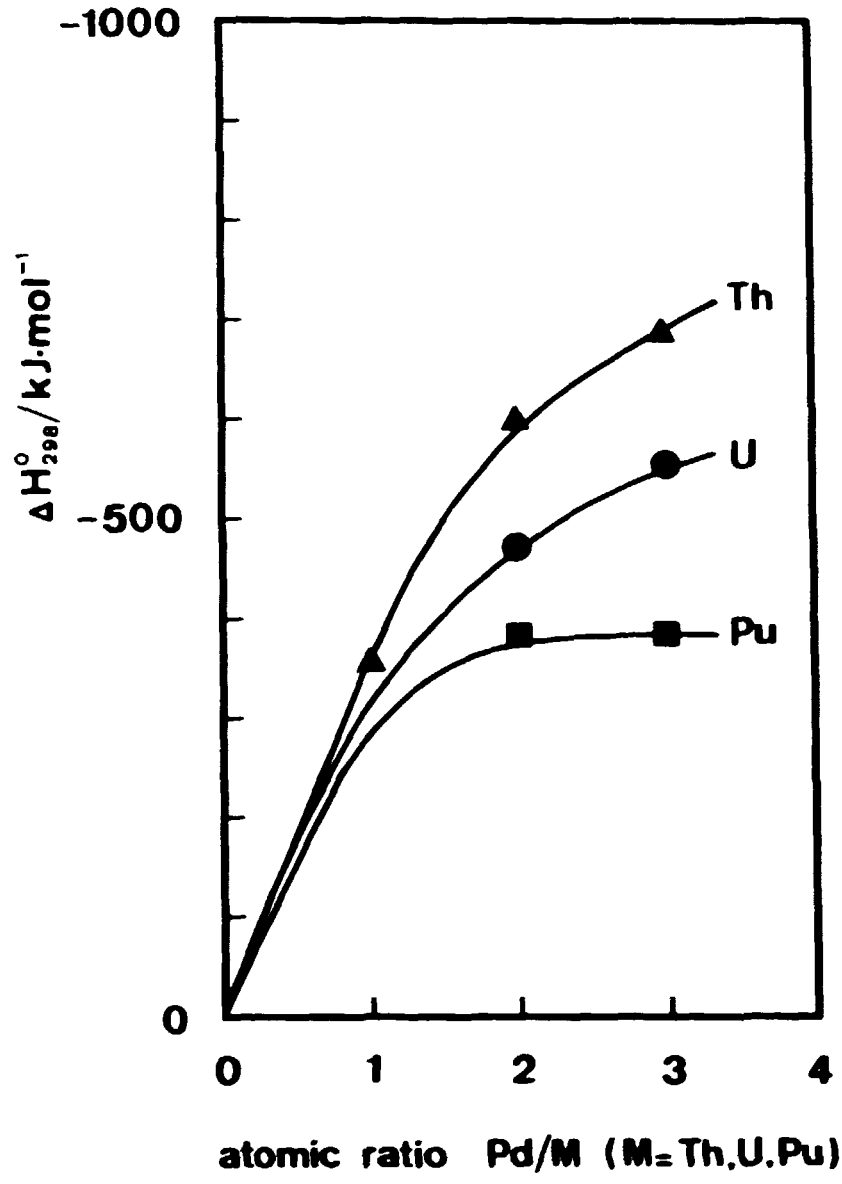

Fig. 5.8. Estimated enthalpies of formation of MPd_x compounds as a function of the atomic ratio Pd/M, (M=Th, U, Pu).

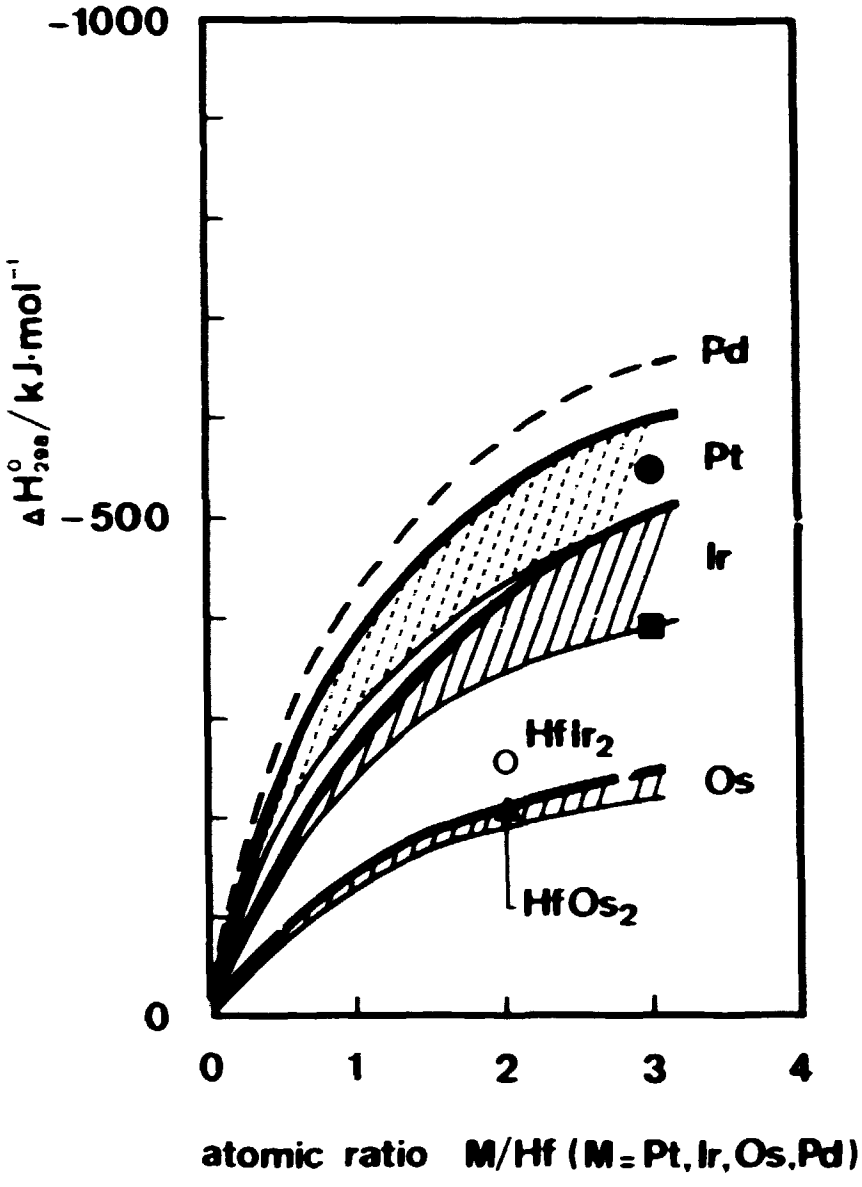

Fig. 5.9. Estimated and experimental enthalpies of formation of HfM_x compounds as a function of the atomic ratio M/Hf(M=Pt, Ir, Os, Pd).

——— : Estimated results of Brewer.

——— : Estimated results of Watson.

● : Srikrishnan, Ficalora [39].

○ ▲ : Kaufman, Bernstein [37].

■ : Choudary et al. [38].

variety of liquid alloys and intermetallic compounds.
According to Miedema et al. a binary alloy is constructed from Wigner-Seitz atomic cells similar to those in the pure metallic elements. The atomic cells of two metals have approximately the same volume in the alloy and in the pure metals.
Since an alloy or intermetallic compound is not only a mechanical mixture of two metals an alloying energy originates from the change in boundary conditions when dissimilar atoms come into contact. This energy effect is derived from two contributions.
The first term is negative, arising from the difference in chemical potential, Q^*, for electrons in the two types of atomic cells. The second term reflects the discontinuity in the density of electrons, n_{ws}, at the boundary between dissimilar atomic cells. This term gives a positive contribution to the enthalpy of formation of the alloy.
When the binary alloy systems contain at least one transition metal, the following formula is applicable:

$$\Delta H \approx [- Pe(\Delta Q^*)^2 + Q_o(\Delta n_{ws}^{1/3})^2 - R] \qquad (5-3)$$

where Q^* and $n_{ws}^{1/3}$ are, respectively, the electronegativity and electron density parameters which characterize a metallic element, e is the charge on the electron and the values of P, Q_o and R are constant for large groups of alloy systems.
R represents a large contribution that arises from an effective d-p hybridisation energy (relative to the pure d-metal). It is gained when a d-type transition metal acquires p-electron-type neighbouring atoms. Both terms Q^* and $n_{ws}^{1/3}$ lead to a redistribution of electrons and thus to a change in the volumes of the atomic cells.
As energy effects arise at the contact surface between dissimilar atomic cells its concentration dependence will be that of this surface area. It is therefore useful to introduce a term for the "surface concentration" of metals [5]. The formula, used for calculating ΔH_f of alloys from two transition metals, is slightly different from the formula above [5].
The model has been used to calculate the enthalpy of formation of binary alloys that contain thorium [5], uranium [5], plutonium [27] and the platinum metals Ru, Rh, Pd, Os, Ir and Pt. Values of $\Delta H^o_{298.15}$

predicted for intermetallic actinide-noble metal compounds are given in table 5.3.
Enthalpies of formation of intermetallic compounds of Zr, Nb, Hf and Ta with the noble-metals using Miedema's model are given in table 5.4.

V.2.3. An electron band theory model

From point of view of the physics of metals, the regular variation of cohesion with the filling of the d-band, peaking to a maximum for the refactory metals in the middle of the series is well-known [36].

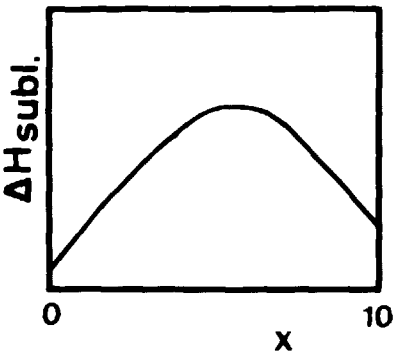

Fig. 5.10.
Cohesive energy per atom ΔH_{subl} versus the atomic number of the transitional series (2^{nd} and 3^{rd} series)

It is especially clear in the second and third series where no magnetic complications occur in the solid state (fig. 5.10.). The magnitude of the cohesion peak shows that it must be related to d-band formation in the solid. The cohesive or sublimation enthalpy ΔH_{subl} per atom can be given by:

$$\Delta H_{subl}(N) = AN(10-N) + BN \qquad (5-4)$$

if one assumes that N (the number of d-electrons per atom) increases linearly from 0 to 10 through a series. This would correspond to a rectangular d-band of width W = 20A.
Watson and Bennett [34] have used the electron band theory model to predict enthalpies of formation of transition metal alloys. The model involves the chemical concept due to Friedel [36] of the transition element d electron levels broadening into a band where bonding energy is to be gained if the band is partially occupied. The model is illustrated in fig. 5.11. It assumes a rectangular density of states, i.e. the number of electron states within any unit energy interval is constant across the band. If an electron is put into the bands, there is a

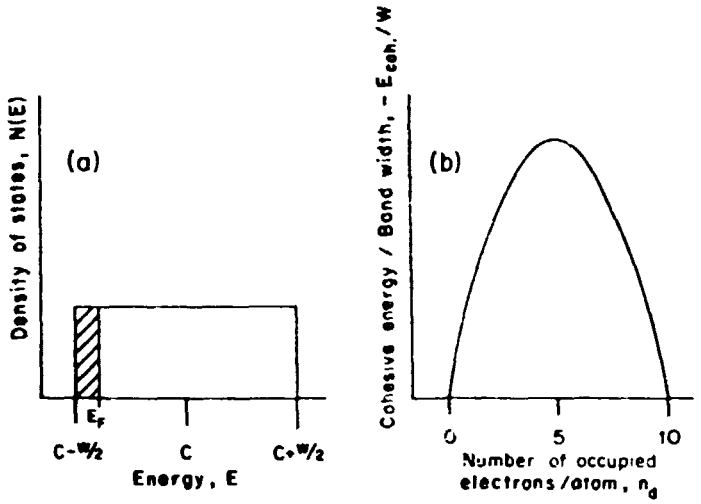

Fig. 5.11 a) Schematic of the rectangular band model of Friedel [36].
b) Cohesive energy predicted by this model for transition elements.

bonding energy gain which is the difference between the energy of the occupied levels and the band center of gravity C (see also fig. 5.4.). Once the band is half filled, adding another electron involves filling antibonding levels above C and a consequent loss of bonding energy. The band filling energy is:

$$H = \frac{N\,(10-N)}{20}\,W \tag{5-5}$$

where N and W are the d band occupancy and bandwidth, respectively. Pettifor [40] and Varma [41] applied the Friedel model to alloys. In addition to the band broadening term, one must account for changes in the position of the band centers of gravity. For a 50-50 alloy the enthalpy of formation will be:

$$\Delta H = N_{AB}C_{AB} - \frac{N_{AB}\,(10-N_{AB})}{20}\,W_{AB}$$

$$- \frac{1}{2}\left\{N_A C_A + N_B C_B - \frac{N_A\,(10-N_A)}{20}\,W_A - \frac{N_B\,(10-N_B)}{20}\,W_B\right\} \tag{5-6}$$

where N_A, N_B and N_{AB} are the numbers of occupied d band levels in metals A and B and the alloy respectively, C and W being their centers of gravity and bandwidths.

Watson and Bennett [31,32,34] have taken into account also effects due to d electron transfer, conduction electron screening and volume effects. They have set up a data base of predicted values for the enthalpy of formation of 270 50-50 transition metal alloys.
Their results [33,34] were used to estimate the enthalpies of formation of AB_3-compounds of Zr, Nb, Hf and Ta, and the noble metals as given in table 5.4. The relation:

$$\Delta H(AB_3)\ [\text{kJ mol}^{-1}] = 3.2\ F\ (\Delta H(50\text{-}50)\ [\text{eV atom}^{-1}]) \qquad (5\text{-}7)$$

was used to calculate the values in table 5.4.
The results are presented in a graph in fig. 5.9. for intermetallic compounds of Hf with the platinum metals Pt, Ir and Os.
The thin solid lines are estimates following Watson's results.

V.3. DISCUSSION

It follows from table 5.3. that there is a very good agreement between the estimates of $\Delta H^{o}_{298.15}$ of uranium compounds with the platinum metals, using Brewer's model and the experimentally determined values. For this reason the model was applied to plutonium and thorium compounds with the platinum metals. Miedema's predictions for the enthalpies of formation of URh_3, UPd_3 and UIr_3 are too positive compared with the experimental values. Since there are hardly any data on plutonium compounds with the platinum metals, we expect Brewer's estimates to be most reliable especially for $PuRh_3$, $PuPd_3$, $PuIr_3$ and $PuPt_3$. It can be concluded that the Engel-Brewer model is very well applicable to the intermetallic compounds of the actinides Th, U and Pu and the platinum metals.

Miedema's predictions of ΔH^{o}_{298} are generally too positive for this group of compounds. One possible reason is that the uranium atom has a variable atomic configuration as far as the number of 5f electrons is concerned. This will effect n_{ws} and, possibly also Q*.

Another reason can be the use of incorrect values for the electronegativity parameters (Q*) of the platinum metals. The values for Q* and n_{ws} are almost the same for Ru, Rh and Pd in Miedema's model [5], while the values for Q* increase considerably going from Ru to Pd, using an estimation procedure based on d-band properties [31].

Miedema has adjusted the electronegativity parameters Q* and the electron density parameters n_{ws} using work-function and bulk-modulus data. Watson and Bennett have estimated electronegativities for the transition metals based on their d-band properties [31].

Four predictive models are compared in table 5.4. and some experimental data. It can be seen that for the compounds $MtRu_x$, $MtOs_x$ and $MtRh_3$ (Mt = Zr, Nb, Hf and Ta) all the models are in good agreement. It is interesting that the tendencies in the predicted $\Delta H^{o}_{298.15}$ values using the models of Brewer and Watson are the same, except for $MtPd_3$-compounds.

It has to be noted that there is a deviation of the regular variation of cohesion with the filling of the d-band going from Rh to Pd (table 5.1.; fig. 5.5.). Palladium has a relatively low cohesive enthalpy compared to platinum, due to its d^{10} configuration in the gaseous state.

This could explain the difference between Brewer's and Watson's results for $\Delta H^{o}_{298.15}$ of $MtPd_3$-compounds. If we take the average values for $\Delta H^{o}_{298.15}$ of Brewer and Watson, most estimates are within 15 percent of the average, and there is a very good agreement with the experimental data, especially the very negative enthalpies of formation of $ZrPt_3$ and $HfPt_3$. This is illustrated in fig. 5.9., in which $\Delta H^{o}_{298.15}$ is given as a function of the atomic ratio M/Hf (M = Pt, Ir, Os, Pd). It is clearly seen that the experimental results for $HfPt_3$ and $HfIr_3$ fall within the shaded areas between the predicted lines. Kaufman and Bernstein [37] have derived the ΔH^{o}_{f}-values as given in table 5.4. from the binary phase diagrams. They use the regular solution approach but they also have taken into account electronic contributions in AB_x alloy formation. However, their estimates for the $\Delta H^{o}_{f,298.15}$ values of $MtPd_3$, $MtIr_3$ and $MtPt_3$ compounds are too positive in comparison with the experimental data. This means that their assumption that A-A interaction and B-B interaction in the intermetallic compound is the same as in the pure metal may be incorrect.

Miedema's [5] predicted ΔH^{o}_{f} values in table 5.4. for the zirconium-noble metal compounds show the same tendency as Brewer's values. However, the values predicted for the $MtPt_3$ compounds are somewhat low, for reasons mentioned earlier. We believe that some of Miedema's concepts about bonding especially in intermetallic compounds having incomplete filled d and/or f-shells are too much simplified.

It is well known [17,35] that metallic bonds are closely related to covalent electron-pair bonds. The total bonding energies in metals and intermetallic compounds can be so high, because each atom in an intermetallic compound or metal forms covalent bonds by sharing electrons with its nearest neighbours. Brewer's model is based on the insight of creating more covalent bonds in the intermetallic compounds compared to the pure metals.

In Miedema's model, charge is transferred from electropositive metals Zr or Hf to Rh or Pd atoms, thus reducing the number of Zr and Hf d-electrons and filling the Rh and Pd d levels. First of all it is questionable if this will happen and secondly, in the scope of the above, the direction in which the charge goes is not really important in bonding. It is important in metallic bonding and as a result in the enthalpy of formation of intermetallic compounds that there is sharing

of charge between the atoms.

The role of electronegativity should be amplified as there is considerable confusion in the literature [50]. Essentially, it is not realized by some that the transfer of a pair of electrons in a generalized Lewis Acid-Base reaction is determined by the availability of a non-bonding pair of electrons and a vacant orbital. Thus Ga with a vacant p orbital accepts a non-bonding pair of electrons from As to form essentially a diamond lattice with four bonds around each atom even though gallium is much more electropositive than arsenic. The electronegativity difference will play a role in the distribution of the electrons in the bond between Ga and As but the driving force for formation of the bond does not have anything to do with electronegativity. Another example would be chromiumcarbonyl, $Cr(CO)_6$. Chromium is certainly much more electropositive than CO, but it is well recognized that the bonding involves transfer of non-bonding electrons of CO to incompletely filled orbitals of Cr to completely fill the 3d, 4s and 4p orbitals.

Miedema has tried to cover much load with his prediction model. It is of course true that his predictions are very valuable in liquid alloy formation and also in solid alloy formation containing one transition metal, as long as there are enough experimental data available to verify the model for certain groups of compounds. In the case of intermetallic compounds from elements of the transition series and in particular Th, U and Pu it is questionable if Miedema's model is applicable, since the difference between some experimental data and the estimated ΔH_f^o values is more than 50 per cent.

Table 5.1. Bonding properties of transition metals

Element	Electronic configuration in gaseous ground state	Electronic configuration in metallic ground state	Number of bonding d electrons in solid state	Melting point (K)	Sublimation enthalpy (kJ mol^{-1}) [28,29,42]	Promotion enthalpy (kJ mol^{-1}) [2,23,11]
Zr	$4d^2 5s^2$	$4d^3 5s$	3	2125	603.3	59
Nb	$4d^3 5s^2$	$4d^4 5s$	4	2741	730.1	13
Mo	$4d^5 5s$	$4d^5 5s$	5	2890	725.1	0
Ru	$4d^7 5s$	$4d^6 5sp$	4	2583	650.2	301
Rh	$4d^8 5s$	$4d^{6.5} 5sp^{1.5}$	3.5	2239	554.4	464
Pd	$4d^{10}$	$4d^{7.5} 5sp^{1.5}$	2.5	1825	375.7	586
Hf	$5d^2 6d^2$	$5d^3 6s$	3	2495	620.9	167
Ta	$5d^3 6s^2$	$5d^4 6s$	4	3269	782.0	117
W	$5d^4 6s^2$	$5d^5 6s$	5	3683	858.6	38
Os	$5d^6 6s^2$	$5d^6 6sp$	4	3318	788.3	293
Ir	$5d^7 6s^2$	$5d^{6.5} 6sp^{1.5}$	3.5	2727	669.9	498
Pt	$5d^9 6s$	$5d^{7.5} 6sp^{1.5}$	2.5	2045	563.6	506
Ac	$6d^1 7s^2$	$6d^2 7s$	2	1323	410.0	110.0
Th	$5f^0 6d^2 7s^2$	$5f^0 6d^3 7s$	3	2023	597.9	66.5
U	$5f^3 6d^1 7s^2$	$5f^3 6d^2 7s$	2	1408	535.6	74.9
Pu	$5f^6 6d^0 7s^2$	$5f^5 6d^2 7s$	2	913	347.3	178.2

Table 5.2. Electronic configurations and promotion energies of Th, U and Pu [11]

	Electronic configuration	Promotion energy (kJ mol^{-1}) thorium n = 4	uranium n = 6	plutonium n = 8
1	$f^{n-3}ds^2$	93.3	0.0	75.3
2	$f^{n-3}d^2s$	186.6	74.9	178.2
3	$f^{n-3}d^3$	(372) ± 38	(251) ± 46	(322) ± 59
4	$f^{n-2}sp$	(502) ± 38	272.4	185.4
5	$f^{n-5}d^4s$	-	(264) ± 59	-
6	$f^{n-4}ds^2p$	128.9	(289) ± 13	(561) ± 25
7	$f^{n-4}d^2sp$	172.8	(297) ± 13	(611) ± 13
8	$f^{n-2}dp$	(657) ± 38	408.4	285.8
9	$f^{n-4}d^3p$	259.8	(377) ± 25	(695) ± 38
10	$f^{n-2}s^2$	(335) ± 38	84.1	0.0
11	$f^{n-4}d^2s^2$	0.0	137.7	431.0
12	$f^{n-3}s^2p$	220.5	161.1	212.5
13	$f^{n-3}dsp$	264.0	174.9	248.9
14	$f^{n-4}d^3s$	66.5	(184) ± 13	(506) ± 13
15	$f^{n-2}ds$	(464) ± 38	177.4	161.9
16	$f^{n-6}d^5s$	-	(335) ± 96	-
17	$f^{n-3}d^2p$	(464) ± 42	(364)	(456) ± 25
18	$f^{n-2}d^2$	(682) ± 46	(406) ± 38	(372) ± 59
19	$f^{n-2}p^2$	(715) ± 59	(490) ± 25	(431) ± 25
20	$f^{n-3}sp^2$	(276) ± 71	(264) ± 63	(360) ± 59

Values between brackets are estimates.

Table 5.3. Enthalpies of formation of actinide-noble metal compounds

Compound	Estimated $\Delta H^{o}_{298.15}$ (kJ mol^{-1})		Experimental $\Delta H^{o}_{298.15}$(kJ mol^{-1})	References
	Brewer	Miedema		
URu_3	-138	-146	-151 ± 1	43
URh_3	-306	-159	-301 ± 1	43
UPd_3	-556	-251	-550 ± 33	44
UOs_2	-172	-126	-167 ± 17	45
UIr_2	-364	-159	-218	45
UIr_3	-490	-213	-418 ± 42	46
UPt_3	-452			
$PuRu_2$	-226	-117	- 96	47
$PuRh_3$	-301	-167		
$PuPd_3$	-385	-234		
$PuOs_2$	-331	-100		
$PuIr_3$	-439	-201		
$PuPt_3$	-431	-251		
$ThRu_2$	- 71	-176	-151	47
$ThRh_3$	-351	-305	-335	48
$ThPd_3$	-686			
$ThOs_2$	-105	-159	-105	49
$ThIr_3$	-531	-301	-314	49
$ThPt_3$	-628			

Table 5.4. Enthalpies of formation of Zr, Nb, Hf and Ta - noble metal compounds

Compound	Estimated $\Delta H^{o}_{298.15}$ (kJ mol^{-1})				Experimental	
	Brewer [29]	Watson [34] Bennett	Miedema [5]	Kaufman [37] Bernstein	$\Delta H^{o}_{298.15}$ (kJ mol^{-1})	Ref.
$ZrRu_2$	-142	-189	-230	-197	-180±13[1])	13
$ZrRh_3$	-347	-265	-314	-293		
$ZrPd_3$	-678	-325	-452	-285		
$ZrOs_2$	-230	-175	-218	-197		
$ZrIr_3$	-527	-389	-310	-276	-360±38[2])	38
$ZrPt_3$	-623	-475	-393	-285	-510±38	39
$NbRu_3$	-	-158		-180		
$NbRh_3$	-209	-183		-167		
$NbPd_3$	-456	-186		-155		
NbOs	-117	-102				
$NbIr_3$	-414	-289	-209	-167	-276±67[2])	38
$NbPt_3$	-377	-308	-251	-167		
$HfRu_2$	-126	-193		-205		
$HfRh_3$	-326	-277		-293		
$HfPd_3$	-661	-348		-285		
$HfOs_2$	-209	-172		-201		
$HfIr_3$	-510	-396	-272	-285	-393±42[2])	38
$HfPt_3$	-607	-496	-351	-276	-552±42	39
TaRu	-	-114		-113		
$TaRh_3$	-155	-219		-167		
$TaPd_3$	-406	-244		-167		
TaOs	- 63	-109		-113		
$TaIr_3$	-360	-316		-167	-301±67[2])	38
$TaPt_3$	-326	-364	-238	-167		

[1]) ΔG^{o}_{f} at 1800 K.

[2]) Extrapolated values from measurements on $TiIr_3$.

REFERENCES

[1] Brewer, L. In Electronic Structure and Alloy Chemistry of the Transition Elements. Beck, P.A.: editor. Interscience, N.Y. (1963) p. 211.

[2] Brewer, L. In High-Strength Materials, Proc. of Second Berkeley International Materials Conference, June 1964; Zackay, V.F.: editor. John Wiley, N.Y. (1965) p. 12.

[3] Brewer, L. In Phase Stability in Metals and Alloys, Rudman, P.; Stringer, J.; Jaffee, R.I.: editors. McGraw-Hill, N.Y. (1967). pp. 39-61, 241-9, 344-6 and 560-8.

[4] Miedema, A.R. J. Less Common Met., 32 (1973) 117.

[5] Miedema, A.R.; de Boer, F.R.; Boom, R. J. Less Common Met., 41 (1975) 283.

[6] Miedema, A.R. J. Less Common Met., 46 (1976) 67.

[7] Brewer, L. Acta. Met., 15 (1967) 553.

[8] Darling, A.S.; Selman, G.L.; Rushforth, R. Platinum Metals Rev. 14 (1970) 54 and 95.

[9] Brewer, L. Science, 161 (1968) 115.

[10] Brewer, L. In Plutonium 1970 and other Actinides, TMS Nuclear Metallurgy Series, Vol. 17. Miner, W.N.: editor. Metallurgical Soc. AIME, N.Y., (1970) pp. 650-658.

[11] Brewer, L. J. Opt. Soc. Am. 61 (1971) 1101.

[12] Brewer, L. J. Electrochem. Soc. 119 (1972) 7-12C.

[13] Brewer, L.; Wengert, P.R. Metallurgical Transactions 4 (1973) 83.

[14] Brewer, L. Amer. Institute of Physics Conference Proceedings, Magnetism and Magnetic Materials - 1972. Wolf, H.C.: editor. (1973) No. 10, part 1, p.1.

[15] Brewer, L. J. Nucl. Mater. 51 (1974) 2.

[16] Brewer, L. Review Chimie Minerale. 11 (1974) 616.

[17] Pauling, L. The Nature of the Chemical Bond (Cornell University Press, Ithaca, N.Y. 3rd Ed. and ezrlier editions) (1960).

[18] Engel, N. Powder Metallurgy Bulletin 7 (1954) 8.

[19] Hume-Rothery, W.; Smallman, R.E.; Haworth, C.W. The Structure of Metals and Alloys, 5th Ed., Institute of Metals, London (1969).

[20] Engel, N. Trans. Am. Soc. Metals 57 (1964) 610.

[21] Engel, N. Acta Met. 15 (1967) 557 and 565.

[22] Bullard, G.L. Ph. D. Thesis, University of California, Berkeley, LBL-7691, May (1979) pp. 145.

[23] Brewer, L. private communication 1980.

[24] Goodman, D.A. Ph. D. Thesis, University of California, Berkeley, LBL-10633, May (1980) pp. 72.

[25] Wengert. P.L. Ph. D. Thesis, University of California, Berkeley, UCRL-18727, April 1969 pp. 118. Available from University Microfilms, Ann Arbor, Michigan; order no. 70-6258.

[26] Miedema, A.R.; de Boer, F.R.; Boom, R. Calphad 1 (1977) 341.

[27] Miedema, A.R. In Plutonium and Other Actinides: Blank, H.; Lindner, R.: editors. North-Holland Publishing Company, Amsterdam, (1976), pp. 3-20.

[28] Oetting, F.L.; Rand, M.H.; Ackermann, R.J. The Chemical Thermodynamics of Actinide Elements and Compounds, Part 1 IAEA: Vienna (1976).

[29] Brewer, L. In C. Kittel; Introduction to Solid State Physics 5th edition, John Wiley, 1976, p. 74. After LBL report 3720, (1975).

[30] Brewer, L. The Consequences of partial delocalization of d-electron orbitals in transition metals. LBL report 3102, 1974. Submitted to Inorganic Chemistry.

[31] Watson, R.E.; Bennett, L.H. Phys. Rev. B. 18 (1978) 6439.

[32] Watson, R.E.; Bennett, L.H. Phys. Rev. Lett. 43 (1979) 1130.

[33] Bennett, L.H.; Watson, R.E. Calphad 4 (1980).

[34] Watson, R.E.; Bennet, L.H. Calphad 4 (1980).

[35] Moore, W.J. Physical Chemistry 4th edition. Longman: London. (1970).

[36] Friedel, J. In The Physics of Metals chap. 8. Ziman, J.M.: editor. Cambridge University Press: Cambridge. (1969).

[37] Kaufman, L.; Bernstein, H. Computer Calculation of Phase Diagrams. Academic Press: New York. (1970).

[38] Choudary, U.V.; Gingerich, K.A.; Cornwell, L.R. J. Less Common Met. 50 (1976) 201.

[39] Srikrishnan, V.; Ficalora, P.J. Metall. Trans. 5 (1974) 1471.

[40] Pettifor, D.G. Solid State Comm. 28 (1978) 621. Phys. Rev. Lett. 42 (1979) 846.

[41] Varma, C.M. Solid State Comm. 31 (1979) 295.

[42] Hultgren, R.; Orr, R.L.; Anderson, P.D.; Kelley, K.K. Selected Values of Thermodynamic Properties of Metals and Alloys. J. Wiley: New York. (1963).

[43] Wijbenga, G.; Cordfunke, E.H.P. to be published.

[44] Wijbenga, G. J. Chem. Thermodynamics, to be published.

[45] Holleck, H.; Kleykamp, H.; Franco, J.I. Z. Metallkde 66 (1975) 298.

[46] Cordfunke, E.H.P. Personal communication.

[47] Kleykamp, H.; Murabayashi, M. J. Less Common Met. 35 (1974) 227.

[48] Murabayashi, M.; Kleykamp, H. J. Less Common Met. 39 (1975) 235.

[49] Kleykamp, H. J. Less Common Met. 63 (1979) p.25.

[50] Mogutnov, B.M.; Shvartsman, L.A. Russian Journal of Physical Chemistry, (3)54 (1980) 328.

CHAPTER VI

THE THERMOCHEMICAL PROPERTIES OF THE UMe_3 COMPOUNDS (Me = Ru, Rh and Pd)

VI.1. INTRODUCTION

The tabulation of the thermochemical data of the UMe_3 compounds will be presented in this chapter. Apart from the enthalpies of formation, given in chapter III and IV, the heat capacities and standard entropies of the UMe_3 compounds are required to calculate the thermodynamic functions. Low-temperature heat capacities of the UMe_3 compounds have been measured from 5 to 350 K using adiabatic calorimetry by E.F. Westrum Jr. at the University of Michigan, Ann Arbor, United States. The cryogenic calorimetric technique, using liquid hydrogen and helium as refrigerants, has been described in detail elsewhere [1,2,3]. The experimental procedure consists of a careful measurement of the small, stepwise temperature rise caused in an insulated sample by an accurately measured energy input. The resulting heat capacity data of UPd_3, URh_3 and URu_3 have already been published [3,4]. These heat capacity data are extrapolated to 0 K, applying the Debye theory, to determine the "third law" entropies towards 0 K. The heat capacities and standard entropies at 298.15 K for the UMe_3 compounds are shown in table 6.1. High-temperature enthalpy-increment values for the UMe_3 compounds were measured from 390-890 K at The Netherlands Energy Research Foundation ECN, Petten.

Measurements were made in a diphenyl ether drop-calorimeter developed by Cordfunke et al. [5]. The procedures used will be described below. The combined results of the high and low-temperature heat-capacity data have been reported [3,4].

Table 6.1. Heat capacity and standard entropy of UMe_3 compounds at 298.15 K

Compound	Cp^o(298.15 K)/J $K^{-1}mol^{-1}$	S^o(298.15 K)/J $K^{-1}mol^{-1}$
URu_3	101.42	144.60
URh_3	103.05	152.26
UPd_3	102.09	176.36

VI.2. HIGH-TEMPERATURE HEAT-CAPACITIES OF UMe_3 COMPOUNDS [a]

VI.2.1. Introduction

The enthalpy increments of the UMe_3 compounds (Me = Pd, Rh, Ru) have not yet been measured before. Only estimated molar heat capacity equations are reported for URh_3 and URu_3 by Barin et al. [6]. In this chapter the experimental determination of the enthalpy increments of the UMe_3 compounds in the temperature range 390-890 K will be described.

VI.2.2. Experimental

VI.2.2.1. Materials

Starting materials for the preparation of the UMe_3 compounds were palladium, rhodium and ruthenium powders of high purity (99.99%, Johnson & Matthey Chemicals, Limited) and pure uranium nitride (UN). Before use, the platinum metal powders were dried in vacuum at 500 °C to remove adsorbed moisture. UPd_3, URh_3 and URu_3 were prepared by heating mixtures in the correct stoichiometric ratio's of UN and palladium, rhodium and ruthenium at 1080 °C, 1100 °C and 1300 °C, respectively, as described in chapter II.

The preparations were carried out in purified argon. Chemical analyses of UN and the UMe_3 compounds are given in table 6.2.

For the preparations of the UMe_3 compounds a mass correction was made for the oxygen in UN. The X-ray diffraction patterns agree with previous patterns [7,8].

The URh_3 and URu_3 samples were purified by washing in an acidic solution (HNO_3/H_2O=1) to remove UO_2. The UMe_3 compounds may be rich in Me, due to a higher oxygen content in UN than determined by the chemical analysis.

---

[a] This chapter has in part been submitted for publication as:
Thermodynamics of Uranium Intermetallic Compounds:
I. Heat capacities of URu_3 and URh_3 from 5 to 850 K and
II. Heat capacities of UPd_3 from 8 to 850 K, in The Journal of Chemical Thermodynamics, by E.H.P. Cordfunke; R.P. Muis; G. Wijbenga; R. Burriel; M.W.K. To; H. Zainel and E.F. Westrum Jr.

Table 6.2. Analytical results for UPd_3, URh_3, URu_3 and UN, mass fraction w.

compound	10^2 w (U) found	calculated	10^2 w (Pd,Rh,Ru) found	calculated	10^2 w (O)	10^2 w (N) found	calculated	10^2 w (C)
UN	94.38	94.44	-	-	0.128	5.41	5.557	0.013
UPd_3	42.48	42.72	57.27	57.28	0.066	0.014		0.021
URh_3	- *	43.54	-	56.46	0.062	-		0.030
URu_3	- *	43.98	-	56.02	-	-		-

* URh_3 and URu_3 are insoluble in acidic solutions, such as HCl, HNO_3 and H_2SO_4.

For the drop-calorimetric studies, spherical vitreous silica ampoules with a 0.6 mm wall thickness and 20 mm diameter were used to contain the samples. The ampoules were about 4.2 cm^3 in volume, and weighed 1 to 1.5 g empty. For loading purposes, each ampoule was fitted with a filling tube sealed with a stopcock.

VI.2.2.2. Description of the apparatus

The drop-calorimetric system was an improved version of the diphenyl ether calorimeter developed by Cordfunke et al. [5]. The basic components of the system are:

a. a well-stirred, thermostatted water jacket held at the melting point of diphenyl ether to keep solid and liquid diphenyl ether in equilibrium. The temperature was controlled at 26.910 ± 0.002 °C,
b. a furnace with an alundum core heated with kanthal windings,
c. a copper diaphragm to isolate the calorimeter from the furnace except during a drop experiment, and
d. a drop mechanism for transfer of the ampoule from the furnace to the calorimeter.

Both the calorimeter and furnace were operated under a 100 mm argon pressure to improve conduction. Temperature measurements in the furnace were made with Pt,Pt/10% Rh thermocouples to ± 0.1 K. These were calibrated according to the NBS-procedure [9].

VI.2.2.3. Procedure

Heat from the sample and ampoule, when dropped into the calorimeter, melted solid diphenyl ether in equilibrium with its liquid in a closed system. The resulting volume increase of the ether is determined by weighing the displaced mercury. The initial and final period can be considered as straight lines. The relation of heat imput to mass of mercury, resulting from the volume change of the diphenyl ether, is a constant for the apparatus. The energy equivalent of the calorimeter was determined by means of calibrations with spherical pieces of α-quartz of which the enthalpies were taken from the JANAF tables [10]. A calibration factor of (79.977 ± 0.063) $Jg^{-1}Hg$ was obtained.

The displaced mercury was weighed, and corrections were made for heat input from the surroundings by measuring the height difference of mercury in the capillary during the experiment. For the correction of the mercury weight, the final period has to be extrapolated to the time the sample felt into the calorimeter. The corrected amount of mercury thus obtained is a measure for the change in enthalpy $\{H(T) - H(T')\}$ in cooling from the furnace temperature (T) to the calorimeter temperature (T').

A correction was made for (T'-298.15 K), using the Cp value at 298.15 K. The enthalpy increment of the quartz glas was determined in a series of drops [5], and can be represented as a function of temperature by the polynomial:

$$\{H^{o}(T) - H^{o}(298.15\ K)\}/Jmol^{-1} = 14.779\ (T/K) + 1.3118 \times 10^{-3}\ (T/K)^{2} + 5.1719 \times 10^{+5}\ (T/K)^{-1} - 6258$$

The difference between the values of $\{H^{o}(T) - H^{o}(298.15\ K)\}$ for loaded and empty quartz glass ampoules can then be calculated after a correction for (T'-298.15 K).

As a check on the accuracy of the calorimetric system the enthalpy of α-Al_2O_3 synthetic sapphire (National Bureau of Standards, Standard Reference Material 720) was determined. The results agreed with the certificate value [11] to within 0.25 per cent.

The UMe_3 compounds were weighed into the silica ampoules in a glove box filled with flowing high-purity argon, and sealed outside the glove box. The ampoules contained argon at 0.1 atm pressure. In our experiments more than 85 percent of the measured heat was due to the sample.

VI.2.3. Results

UPd_3

The experimental enthalpy increments for UPd_3 are given in table 6.3. The molar enthalpies for UPd_3 can be represented over the temperature range 298.15 to 875 K, with the following polynomial:

$$\{H^o(T) - H^o(298.15\ K)\}/Jmol^{-1} = 98.6872\ (T/K) + 5.70572 \times 10^{-3}\ (T/K)^2 - 29930.7 \quad (6\text{-}1)$$

This polynomial was constrained to apply to 298.15 K, in other words, $H_T - H_{298.15} = 0$ at T = 298.15 K and Cp = Cp(298.15 K). This constraint was also applied to the results for URh_3 and URu_3. The enthalpies, calculated from equation (6-1), are given in table 6.3.

URh_3

For URh_3 the experimental enthalpy increment results are given in table 6.4. Measurements were made in the temperature range 423 to 842 K. The following equation represents the results over the range 298.15 - 842 K:

$$\{H^o(T) - H^o(298.15\ K)\}/Jmol^{-1} = 104.2824\ (T/K) + 9.20145 \times 10^{-3}\ (T/K)^2 + 597098.6\ (T/K)^{-1} - 33912.6 \quad (6\text{-}2)$$

URu_3

The experimental results for URu_3 cover the temperature range 406-890 K (see table 6.5.). The results can be represented by the following equation:

$$\{H^o(T) - H^o(298.15\ K)\}Jmol^{-1} = 101.2273\ (T/K) + 9.22739 \times 10^{-3}\ (T/K)^2 + 471997.0\ (T/K)^{-1} - 32580.8 \quad (6\text{-}3)$$

Previous determinations of the high temperature enthalpy-increments of the UMe_3 compounds are not available.

Values of the smoothed thermodynamic properties as derived from the fitted polynomial expressions have been presented elsewhere [3,4].

The heat capacity curves of the UMe_3 compounds obtained from the combined high and low-temperature experimental data are shown in fig. 6.1.

Table 6.3. Enthalpy increments of UPd_3

$\frac{T}{K}$	$\frac{H^o(T) - H^o(298.15\ K)}{J\ mol^{-1}}$		$\frac{100\delta}{H_{measured}}$ %
	measured	calculated	
392.0	9620	9631	.114
435.0	14035	14078	.306
443.5	14924	14959	.235
451.1	15805	15748	.361
536.8	24619	24689	.284
595.8	30752	30893	.459
660.6	37694	37752	.154
697.9	41660	41722	.149
740.8	46388	46308	.172
780.3	50518	50549	.061
812.4	54020	54009	.020
874.6	60814	60746	.112

1) The mass of the empty quartz ampoule was 1.49 g. The ampoule contained 14.65 g of UPd_3 ($M = 557.229\ g\ mol^{-1}$).
2) If $H^o(T) - H^o(298.15\ K) = H$, then $\delta = |H_{measured} - H_{calculated}|$.
3) The standard deviation of the calculated results from the experimental values is 74.9 J mol^{-1}, and the enthalpies have an uncertainty of 0.27 per cent. The differences between the experimental and the computed enthalpies did not exceed 0.46%.
4) A correction was made for the difference between the final calorimeter temperature and the standard reference temperature, 298.15 K, using Cp (298.15 K).

Table 6.4. Enthalpy increments of URh_3

$\frac{T}{K}$	$\frac{H^o(T) - H^o(298.15\ K)}{J\ mol^{-1}}$		$\frac{100\delta}{H_{measured}}$ %
	measured	calculated	
423.7	13393	13333	.448
465.2	17945	17874	.396
496.6	21376	21346	.140
528.6	24941	24912	.116
576.6	30305	30311	.020
627.0	36116	36042	.205
674.9	41430	41543	.273
717.6	46447	46491	.095
772.4	52827	52898	.134
842.0	61216	61126	.147

1) The mass of the empty quartz ampoule was 1.477 g. The ampoule contained 12.417 g of URh_3 ($M = 546.746\ g\ mol^{-1}$).

2) The standard deviation of the calculated results from the experimental values is 83.7 J mol^{-1}. The enthalpies have an uncertainty of 0.30 per cent. The largest difference between the experimental and computed enthalpies was 0.45%.

Table 6.5. Enthalpy increments of URu_3

$\frac{T}{K}$	$\frac{H^o(T) - H^o(298.15\ K)}{J\ mol^{-1}}$		$\frac{100\delta}{H_{measured}}$ %
	measured	calculated	
406.0	11217	11201	.143
427.8	13569	13516	.391
451.5	16113	16050	.391
481.4	19267	19269	.010
607.1	33083	33053	.091
629.9	35493	35593	.282
662.9	39300	39290	.025
711.8	44693	44811	.264
746.4	48844	48748	.197
764.3	50869	50795	.145
821.1	57229	57333	.182
889.7	65350	65316	.052

The mass of two empty quartz ampoules was 1.6507 g and 1.2702 g, respectively. The ampoules contained 12.8615 g and 17.4818 g of URu_3, respectively ($M = 541.239\ g\ mol^{-1}$).

The standard deviation of the calculated results from the experimental values is 80.7 J mol^{-1}. The enthalpies have an uncertainty of 0.25 per cent. The largest difference between the experimental and computed enthalpies was 0.39%.

These curves show normal behaviour in URh_3 and URu_3, and a smooth continuity in the low and high-temperature measurements at 298.15 K. In the heat capacity curve of UPd_3, anomalies are found below 8 K; this will be discussed in a separate paper [4]. A thorough discussion of both thermophysical and thermochemical aspects has also been given elsewhere [3,4].

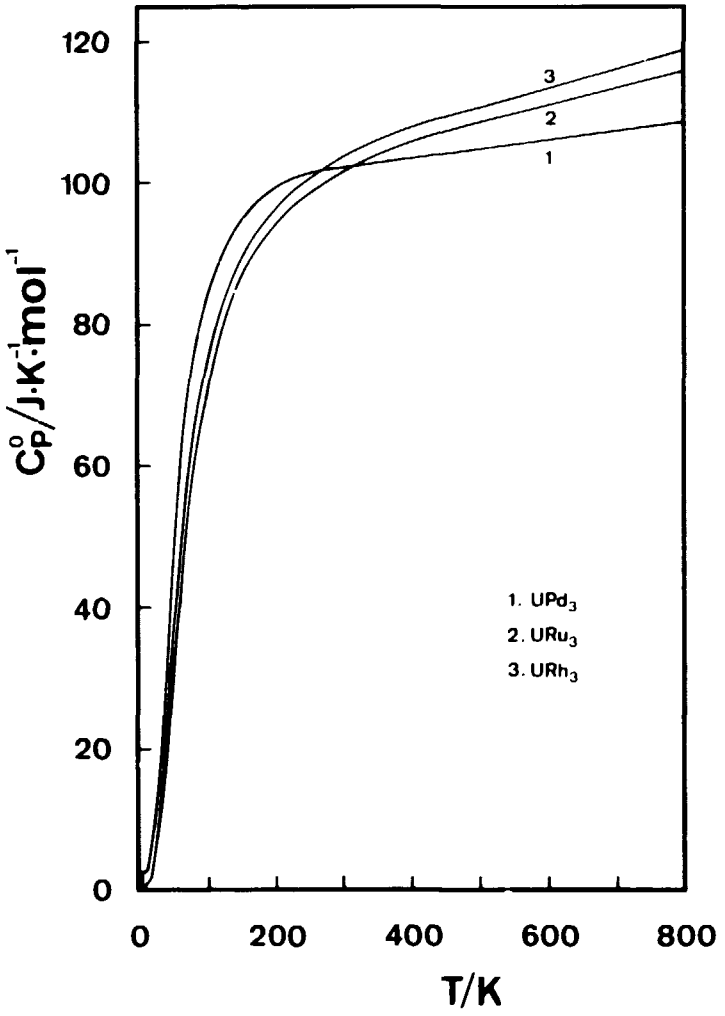

Fig. 6.1. Heat capacities of the UMe_3 compounds.

VI.3. THE THERMODYNAMIC FUNCTIONS OF UPd_3, URh_3 AND URu_3.

VI.3.1. The tabulation of the thermochemical data

The tables in this part of the thesis give the heat capacities (molar heats), entropies, enthalpy increments, enthalpies of formation and Gibbs energies of formation of the intermetallic UMe_3 compounds in the temperature range: 298.15 - 1200 K at 100 K intervals.
The calculation procedure has been as follows. The enthalpy increment polynomial (see chapter VI.2.) can be represented by:

$$H^o(T) - H^o(298.15) = aT + bT^2 + cT^{-1} + d = \int_{298.15}^{T} C_p\,dT$$

Using this formula, the heat capacity will be:

$$C_p^o = a + 2bT - cT^{-2}$$

The entropies in the tables were calculated following the relation:

$$S^o(T) = S^o(298.15) + \int_{298.15}^{T} \frac{C_p}{T}\,dT$$

or

$$S^o(T) = S^o(298.15) + \left[a\ln T + 2bT + \tfrac{1}{2}cT^{-2}\right]_{298.15}^{T}$$

The values for ΔH_f^o (UMe_3, 298.15 K) have been reported in this thesis. To calculate $\Delta H_f^o(T)$ and $\Delta G_f^o(T)$ a "third law" analysis was performed for temperatures form 298.15 - 1200 K at 100 K intervals.
Thermodynamic data for $\{H^o(T) - H^o(298.15)\}$ and $S^o(T)$ of URu_3 [3], URh_3 [3], UPd_3 [4], α-U in the standard state [12], Ru [6], Rh [6] and Pd [6] were used to calculate $\Delta\{H^o(T) - H^o(298.15)\}$ and $\Delta S^o(T)$ for the reaction:

$$U(c) + 3Me(c) \rightarrow UMe_3(c)$$

The enthalpies of formation of the UMe_3 compounds at different temperatures were calculated using:

$$\Delta H_f^o(T) = \Delta H_f^o(298.15\ K) + \Delta\{H^o(T) - H^o(298.15\ K)\}$$

The Gibbs energies of formation of the UMe_3 compounds at different temperatures were calculated according to:

$$\Delta G_f^o(T) = \Delta H_f^o(T) - T\Delta S^o(T)$$

The expression for the "third law" equation thus is:

$$\Delta G_f^o(T) = \Delta H_f^o(298.15\ K) + \int_{298.15}^{T} \Delta C_p dT - T\left[\Delta S^o(298.15\ K) + \int_{298.15}^{T} \frac{\Delta C_p}{T} dT\right] \quad (6\text{-}4)$$

The thermodynamic functions of the three UMe_3 compounds calculated with equations (6-1), (6-2), (6-3) and (6-4) are given in tables 6.6., 6.7. and 6.8. It was found that at 298.15 K $C_p^o(URh_3)$ was greater than $C_p^o(UPd_3)$, which was in turn greater than $C_p^o(URu_3)$.
For URh_3 and URu_3 molar heat equations have been estimated by Barin et al. [6]. There is a reasonable agreement between our values for $C_p^o(URu_3)$ and $S^o(URh_3)$, and the estimated values by Barin et al. [6]; the differences remain within 3 percent in the temperature range 298.15 - 1200 K. For the other functions, the agreement is poor.
The heat capacities at 298.15 K can also be compared with predictions of the heat capacities of the UMe_3 compounds calculated from the heat capacities of the elements [13]. For $U + 3Me = UMe_3$ Barin et al. [6] have assumed that: $C_p^o(U) + 3C_p^o(Me) = C_p^o(UMe_3)$ i.e., that $\Delta C_p = o$. Comparison with our experimental results show that ΔC_p is not equal to zero, $\Delta C_p(UPd_3)$ being the largest of the three compounds. Another interesting phenomenon is the function $\Delta S_T^o(UMe_3)$, which has been shown in table 6.9. at 400 K, 800 K and 1200 K. The ΔS_T^o values do not deviate much from zero which is common in the formation of intermetallic compounds, since there are no gasses involved in the reactions.
As a result the $\Delta G_f^o(UMe_3)$ function does change relatively slowly as a function of the temperature. The change in $\Delta G_f^o(UPd_3)$ in the temperature range 298.15 - 1200 K is not more than 1 percent of $\Delta G_{f,298.15}^o(UPd_3)$, and the change in $\Delta G_f^o(URu_3)$ in the temperature range 298.15 - 1200 K is about 4 percent of $\Delta G_{f,298.15}^o(URu_3)$.

Table 6.6. Thermodynamic functions of UPd_3

T	C_p°	S°	$H^\circ(T) - H^\circ(298.15)$	ΔH_f°	ΔG_f°
K	J $K^{-1}mol^{-1}$	J $K^{-1}mol^{-1}$	kJ mol^{-1}	kJ mol^{-1}	kJ mol^{-1}
298	102.09	176.36	0.00	- 550.00	- 553.76
300	102.11	176.99	0.19	- 550.00	- 553.79
400	103.25	206.52	10.46	- 550.51	- 555.00
500	104.39	229.68	20.84	- 551.29	- 556.02
600	105.53	248.81	31.33	- 552.39	- 556.88
700	106.68	265.17	41.94	- 553.82	- 557.51
800	107.82	279.49	52.67	- 555.65	- 557.93
900	108.96	292.25	63.51	- 557.93	- 558.06
942	109.44	297.23	68.09	- 559.04	- 558.05
942	109.44	297.23	68.09	- 561.83	- 558.05
1000	110.10	303.79	74.46	- 563.13	- 557.79
1049	110.65	309.07	79.87	- 564.24	- 557.50
1049	110.66	309.07	79.87	- 569.00	- 557.50
1100	111.24	314.34	85.53	- 569.93	- 556.92
1200	112.38	324.07	96.71	- 571.78	- 555.65

Table 6.7. Thermodynamic functions of URh_3

T	C_p^o	S^o	$H^o(T) - H^o(298.15)$	ΔH_f^o	ΔG_f^o
K	J $K^{-1}mol^{-1}$	J $K^{-1}mol^{-1}$	kJ mol^{-1}	kJ mol^{-1}	kJ mol^{-1}
298	103.05	152.26	0.00	- 301.16	- 303.41
300	103.17	152.89	0.19	- 301.16	- 303.42
400	107.91	183.28	10.77	- 301.11	- 304.19
500	111.09	207.72	21.72	- 301.21	- 304.95
600	113.67	228.21	32.97	- 301.60	- 305.67
700	115.95	245.91	44.45	- 302.34	- 306.29
800	118.07	261.53	56.15	- 303.53	- 306.78
900	120.11	275.55	68.06	- 305.21	- 307.09
942	120.95	281.05	73.12	- 306.07	- 307.16
942	120.95	281.05	73.12	- 308.86	- 307.16
1000	122.09	288.31	80.17	- 309.82	- 307.02
1049	123.04	294.17	86.17	- 310.66	- 306.85
1049	123.04	294.17	86.17	- 315.42	- 306.85
1100	124.03	300.04	92.47	- 316.07	- 306.44
1200	125.95	310.91	104.97	- 317.39	- 305.51

Table 6.8. Thermodynamic functions of URu_3

T / K	C_p^o / J $K^{-1}mol^{-1}$	S^o / J $K^{-1}mol^{-1}$	$H^o(T) - H^o(298.15)$ / kJ mol^{-1}	ΔH_f^o / kJ mol^{-1}	ΔG_f^o / kJ mol^{-1}
298	101.42	144.60	0.00	- 150.83	- 153.45
300	101.52	145.23	0.19	- 150.83	- 153.47
400	105.66	175.05	10.56	- 150.58	- 154.38
500	108.57	198.95	21.28	- 150.34	- 155.36
600	110.99	218.96	32.26	- 150.23	- 156.37
700	113.18	236.24	43.47	- 150.39	- 157.39
800	115.25	251.49	54.89	- 150.86	- 158.37
900	117.25	265.18	66.52	- 151.74	- 159.26
942	118.08	270.55	71.46	- 152.23	- 159.60
942	118.08	270.55	71.46	- 155.03	- 159.60
1000	119.21	277.63	78.34	- 155.48	- 159.87
1049	120.16	283.36	84.21	- 155.87	- 160.08
1049	120.16	283.36	84.21	- 160.63	- 160.08
1100	121.14	289.09	90.36	- 160.80	- 160.05
1200	123.05	299.71	102.57	- 161.15	- 159.95

Table 6.9. ΔS_T^o values of the UMe_3 compounds

Compound	ΔS_T^o(400 K) J $K^{-1}mol^{-1}$	ΔS_T^o(800 K) J $K^{-1}mol^{-1}$	ΔS_T^o(1200 K) J $K^{-1}mol^{-1}$
URu_3	+ 9.50	+ 9.39	- 1.00
URh_3	+ 7.69	+ 4.07	- 9.90
UPd_3	+ 11.21	+ 2.85	- 13.44

VI.4. PLUTONIUM ENRICHMENT IN $(U,Pu)Me_3$ INCLUSIONS

The knowledge, which is available now about the enthalpies and Gibbs energies of formation of the UMe_3 compounds, can be applied to discuss some phenomena occuring in $(U,Pu)O_{2\pm x}$ fuel.
In table 6.10. the extrapolated values for $\Delta G_f^o(UMe_3)$ at 2000 K are given, using the data in the thermodynamic tables in chapter VI.3. Values for ΔG_f^o $(PuMe_3)$ at 2000 K were estimated from the ΔH_{298}^o estimates from chapter V $(\Delta S_T^o = 0$ and $\Delta C_p^o = 0$, thus $\Delta H_{f,298.15}^o = \Delta G_f^o(T))$.
The results are summarized in table 6.10.

Table 6.10. Gibbs energies of formation of UMe_3 and $PuMe_3$-compounds

Compound	ΔG_f^o(2000 K)/kJmol^{-1}
URu_3	- 159
URh_3	- 300
UPd_3	- 548
"$PuRu_3$"	- 226
$PuRh_3$	- 301
$PuPd_3$	- 385

In $(U_{0.8}\ Pu_{0.2})O_2$ fuel metallic inclusions of the following composition have been detected: 18 at % U, 8 at % Pu, 1 at % Ru, 15 at % Rh and 59 at % Pd [14]. It has already been pointed out in chapter I, that composition and structure of these inclusions indicate solid solutions with the composition $(U,Pu)Me_3$. It is evident that the $(U,Pu)Me_3$ inclusions will be rich in palladium considering the results given in table 6.10., where the most negative Gibbs energies of formation are those for UPd_3 and $PuPd_3$ at 2000 K.
A simple thermochemical model can now be set up to predict the plutonium enrichment in $(U,Pu)Me_3$, if it is assumed that the metallic inclusions consist of solid solutions of UMe_3 and $PuMe_3$ to give $(U,Pu)Me_3$. The plutonium enrichment in this type of inclusions can then be calculated assuming ideal solid solution behaviour ($\Delta H_{mix} = 0$).

In mixed-oxide fuel the following reaction may take place (see also chapter I):

$$(U,Pu)O_{2\pm x} + 3\ Me \rightarrow (U,Pu)Me_3 + (1 \pm 0.5x)O_2$$

This reaction will only take place if:

$$\Delta G_f^o(U_{1-z},Pu_z)Me_3 < \Delta G_f^o(U_{1-y},Pu_y)O_{2\pm x} - (1 \pm 0.5x)\overline{\Delta G}_{O_2} \qquad (6\text{-}8)$$

To calculate $\Delta G_f^o(U_{1-z},Pu_z)Me_3$ we take the composition of the $(U,Pu)Me_3$ solid solution, detected by Kleykamp in $(U_{0.8}\ Pu_{0_2})O_2$ fuel [14]: 18 at % U, 8 at % Pu, 1 at % Ru, 15 at % Rh and 59 at % Pd. This solid solution thus contains 26 at % (U+Pu) and 75 at % Me. The U/(U+Pu) ratio in the solid solution is 0.69. The composition of $(U,Pu)Me_3$ can be expressed as:

$$(U_{0.69}\ Pu_{0.31})[Ru_{0.0133}\ Rh_{0.20}\ Pd_{0.7867}]_3$$

A further assumption will be made that the distribution of Me over uranium and plutonium is equal.
In the case of pure UMe_3 we can make the assumption that the solid solution as given above contains x_1 mol URu_3, x_2 mol URh_3 and x_3 mol UPd_3, in which x_1, x_2 and x_3 are 0.0133, 0.20 and 0.7867, respectively. Using this composition, the results in table 6.10., and assuming ideal solid solution behaviour of the UMe_3 compounds ($\Delta H_{mix} = 0$), have:

$$\Delta G^o\{UMe_3,2000\ K\} = x_1\ \Delta G^o(URu_3) + x_2\ \Delta G^o(URh_3) + x_3\ \Delta G^o(UPd_3) - T\Delta S_{mix} \qquad (6\text{-}5)$$

Data about ΔH_{mix} are not available. In equation (6-5) ΔS_{mix} is the entropy of mixing:

$$\Delta S_{mix} = -\ R\ \Sigma\ n_i\ \ln\ n_i \qquad (6\text{-}6)$$

Thus quation (6-5):

$$\Delta S_{mix} = - R(x_1 \ln x_1 + x_2 \ln x_2 + x_3 \ln x_3)$$

Combination of equations (6-5) and (6-6) gives for the given composition:

$$\Delta G^{o}\{UMe_3\} = - 502.6 \text{ kJ mol}^{-1}$$

Using the Gibbs energy data for the $PuMe_3$ compounds in table 6.10. and equation (6-5) we find:

$$\Delta G^{o}\{PuMe_3, 2000 \text{ K}\} = - 375.5 \text{ kJ mol}^{-1}$$

The next step will be mixing of (1-z) $\{UMe_3\}$ and $z\{PuMe_3\}$:

$$\Delta G_f^{o}\{(U_{1-z} Pu_z)Me_3\} = (1-z)\Delta G_f^{o}\{UMe_3\} + z \Delta G_f^{o}\{PuMe_3\} - T\Delta S_{mix} \quad (6-7)$$

with:

$$\Delta S_{mix} = - R\{1-z)\ln(1-z) + z \ln z\} \quad (6-6)$$

Both equations (6-6) and (6-7) are valid if $0 < z < 1$. The value for ΔS_{mix} will have its maximum when $z = 0.5$: $- 5.76 \text{ JK}^{-1} \text{ mol}^{-1}$.
According to equation (6-8) there will be formation of $(U_{1-z} Pu_z)Me_3$ when:

$$(1-z)\Delta G_f^{o}(UMe_3) + z \Delta G_f^{o}(PuMe_3) - T\Delta S_{mix} < \Delta G_f^{o}(U_{1-y}, Pu_y)O_{2\pm x} - (1\pm 0.5x) \overline{\Delta G}_{O_2} \quad (6-9)$$

$\Delta G_f^{o}[(U_{1-y} Pu_y)O_{2\pm x}]$ can be calculated from $\overline{\Delta G}_{UO_2}$ ($- 742 \text{ kJ mol}^{-1}$) and $\overline{\Delta G}_{PuO_2}$ ($- 688 \text{ kJ mol}^{-1}$) at 2000 K [15]. By using equation (1-2) in chapter I we find:

$$\Delta G^{o}[(U_{0.8} Pu_{0_2})O_2] = - 740 \text{ kJ mol}^{-1}$$

ΔS_{mix} is a function of z. For convenience we take the maximum value of ΔS_{mix} at $z = 0.5$, and corrections are applied for other values of z.

From (6-9) we calculate for z in the metallic $(U_{1-z}\ Pu_z)Me_3$ solid solution:

$$(1-z) - 502.6 + z(-375.5) - T\Delta S_{mix} < -740 - \overline{\Delta G}_{O_2}$$

or

$$z < \frac{-225.4 - \overline{\Delta G}_{O_2}}{127.1} \qquad (6\text{-}10)$$

The results have been presented in tables 6.11. and 6.12. and in fig. 6.2.

A $(U,Pu)Me_3$ solid solution detected by Bramman et al. [16] in $(U_{0.85}\ Pu_{0.15})O_2$ fuel contained 16.1 at % U, 8.4 at % Pu, 3.7 at % Ru, 17.4 at % Rh and 54.4 at % Pd. The composition of this solid solution can be expressed as:

$$(U_{0.66}\ Pu_{0.34})[Ru_{0.049}\ Rh_{0.230}\ Pd_{0.721}]_3$$

The results for ^zPu in this solid solution have been calculated using equations: (6-5), (6-9) and (6-10) and have been presented between brackets in table 6.12.

It can be concluded that the driving forces for the plutonium enrichment in the metallic $(U,Pu)Me_3$ inclusions are the oxygen potential ($\overline{\Delta G}_{O_2}$) in the fuel, and the difference between $\Delta G^o\{UMe_3\}$ and $\Delta G^o\{PuMe_3\}$.

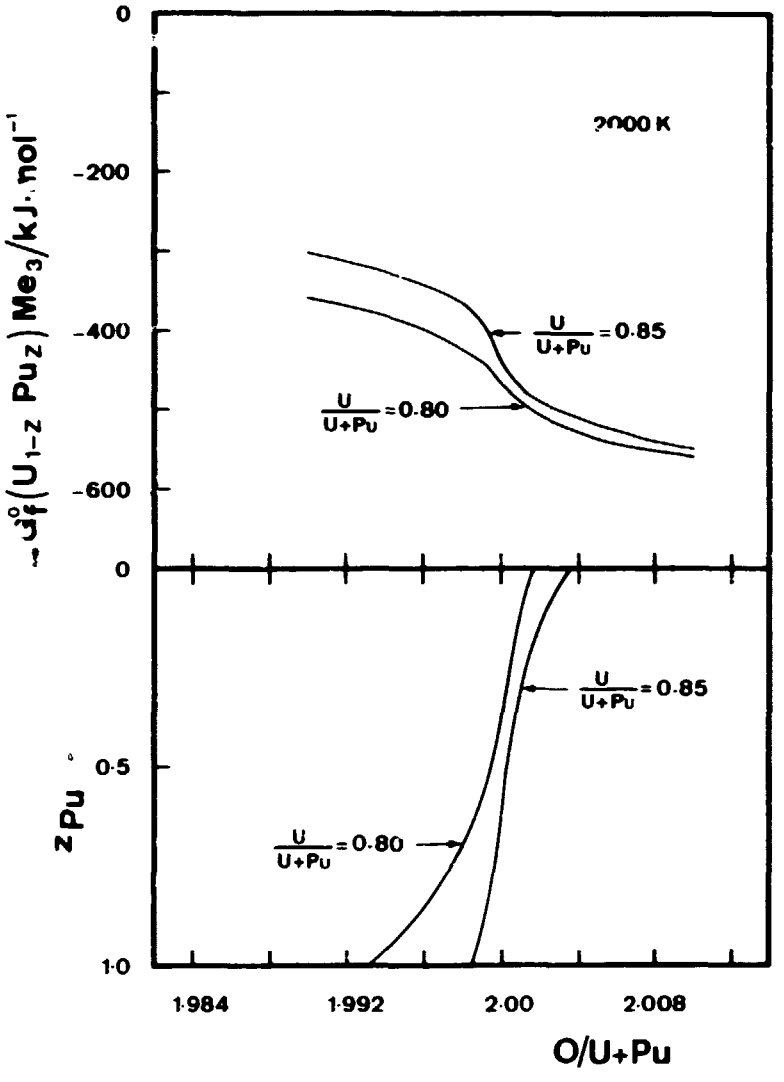

Fig. 6.2. The upper part of the graph shows the values for $\Delta G_f^o(U_{1-z}Pu_z)Me_3$ as a function of the O/(U+Pu) ratio for two different U/(U+Pu) ratios in $(U,Pu)O_{2\pm x}$ fuel (equation (6-8)). The lower part shows the value for z in the compound $(U_{1-z}Pu_z)Me$ as a function of the O/(U+Pu) ratio for the same U/(U+Pu) ratios in mixed-oxide fuel (equation (6-10)).

Table 6.11. Pu-enrichment in $(U,Pu)Me_3$ inclusions in $(U_{0.8}Pu_{0.2})O_{2\pm x}$ fuel.

$\Delta G^{\circ}\{(U_{0.8}Pu_{0.2})O_2\}$ [kJ mol^{-1}] (± 4 kJ mol^{-1})	$\frac{O}{U+Pu}$ ratio	$-\overline{\Delta G}_{O_2}$ [kJ mol^{-1}] fig. 1.7. (± 4 kJ mol^{-1})	$\Delta G_f^{\circ}(U,Pu)Me_3$ [kJ mol^{-1}] more negative than	Pu-enrichment in $(U,Pu)Me_3$ $0 < z < 1$ z =
740	1.990	381	- 359	-
740	1.992	368	- 372	-
740	1.994	356	- 384	0.96
740	1.995	347	- 393	0.90
740	1.996	339	- 401	0.85
740	1.997	331	- 409	0.80
740	1.998	318	- 422	0.71
740	1.999	301	- 439	0.59
740	2.000	272	- 468	0.36
740	2.001	247	- 493	0.12
740	2.002	230	- 510	-
740	2.003	222	- 518	-
740	2.004	209	- 531	-
740	2.005	203	- 537	-
740	2.006	197	- 543	-
740	2.008	188	- 552	-
740	2.010	180	- 560	-

Table 6.12. Pu-enrichment in $(U,Pu)Me_3$ inclusions in $(U_{0.85}Pu_{0.15})O_{2\pm x}$ fuel.

$\Delta G^\circ_f(U_{0.85}Pu_{0.15}O_2)$ [kJ mol^{-1}] (± 4 kJ mol^{-1})	$\frac{O}{U+Pu}$ ratio	$-\Delta G_{O_2}$ [kJ mol^{-1}] (± 6 kJ mol^{-1})	$\Delta G^\circ_f(Me_3)$ [kJ mol^{-1}] more negative than	Pu-enrichment in $(U,Pu)Me_3$ $0 < z < 1$ z
741	1.990	438	- 303	-
741	1.992	425	- 316	-
741	1.994	411	- 330	-
741	1.995	403	- 338	-
741	1.996	393	- 348	-
741	1.997	385	- 356	-
741	1.998	372	- 369	-
741	1.999	351	- 390	0.92 (0.88)
741	2.000	303	- 438	0.59 (0.51)
741	2.001	269	- 472	0.32 (0.17)
741	2.002	251	- 490	0.15
741	2.003	240	- 501	0.04
741	2.004	227	- 514	-
741	2.005	219	- 522	-
741	2.006	213	- 528	-
741	2 008	202	- 539	-
741	2.010	193	- 548	-

REFERENCES

[1] Westrum, E.F. Jr. J. Chem. Education 39 (1962) 443.

[2] Arko, A.J.; Brodsky, M.B.; Crabtree, G.W.; Karim, D.; Koelling, D.D.; Windmiller, L.R.; Ketterson, J.B. Phys. Rev. B 12 (1975) 4702.

[3] Cordfunke, E.H.P.; Muis, R.P.; Wijbenga, G.; Burriel, R.; Zainel, H.; To, M.; Westrum, E.F. Jr. J. Chem. Thermodynamics, submitted.

[4] Burriel, R.; To, M.; Zainel, H.; Westrum, E.F. Jr.; Cordfunke, E.H.P.; Muis, R.P.; Wijbenga, G. J. Chem. Thermodynamics, submitted.

[5] Cordfunke, E.H.P.; Muis, R.P.; Prins, G. J. Chem. Thermodynamics 11 (1979) 819.

[6] Barin, I.; Knacke, O.; Kubaschewski, O. Thermochemical Properties of Inorganic Substances; Supplement, Springer-Verlag Berlin Heidelberg (1977) 796.

[7] Heal, T.J.; Williams, G.I. Acta Crystallogr. 8 (1955) 494.

[8] Dwight, A.E.; Downey, J.W.; Conner, R.A. Jr. Acta Crystallogr. 14 (1961) 75.

[9] National Bureau of Standards, monograph 125, (1973).

[10] JANAF Thermochemical Tables; 2nd Edition NSRDS - NBS 37, Washington, (1971).

[11] Ditmars, D.A.; Douglas, T.B. J. Res. Nat. Bur. Stand. 75A (1971) 401.

[12] Oetting, F.L.; Rand, M.H.; Ackermann, R.J. The Chemical Thermodynamics of Actinide Elements and Compounds, part 1, IAEA, Vienna (1976).

[13] Hultgren, R.; Orr, R.L.; Kelley, K.K. Supplement to Selected Values of Thermodynamic Properties of Metals and Alloys, Berkely, California (1970).

[14] Kleykamp, H. In: Behaviour and Chemical State of Irradiated Ceramic Fuels. IAEA, Vienna (1974) p. 157-166.

[15] Kubaschewski, O.; Alcock, C.B. Metallurgical Thermochemistry. Pergamon Press (1979).

[16] Bramman, J.I.; Sharpe, R.M.; Thom, D.; Yates, G. J. Nucl. Mater. 25 (1968) 201.

SUMMARY

The subject of this thesis is the determination of the thermodynamic properties of the intermetallic compounds of uranium with the light platinum metals, ruthenium, rhodium and palladium. These intermetallics are formed as very stable compounds during fission in nuclear fuel by the reaction of the fission products Ru, Rh and Pd with the matrix. In (U,Pu) mixed-oxide fuel, these fission products have been identified as $(U,Pu)Me_3$ phases (Me = Pd,Rh,Ru), in which often plutonium enrichment was found compared to the Pu/U ratio in the matrix. These phases do not dissolve during reprocessing, and cause plutonium losses as has been described in chapter I.

Methods for the preparation of URu_3, URh_3 and UPd_3, experiments showing the chemical reactivities of these compounds, and studies of the stoichiometry of hexagonal UPd_3 by X-ray diffraction of solubility experiments of UN and palladium in UPd_3, are described in chapter II.

Thermodynamic properties of the UMe_3 compounds have been obtained using several experimental thermodynamic techniques: fluorine bomb calorimetry, low-temperature cryogenic calorimetry, high-temperature drop calorimetry and EMF measurements of reversible cells.

The fluorine bomb calorimetric technique is described in chapter III, followed by the determination of the enthalpies of formation of UF_4, UF_3, $Pd(PdF_6)$ and UPd_3 by fluorine bomb calorimetry and PF_3 reduction calorimetry.

In chapter IV the solid state EMF technique, using CaF_2 as the electrolyte, has been described. The Gibbs energies of formation of URh_3, URu_3 and UF_3 have been determined using this technique.

The Gibbs energies of formation of UF_3, as obtained by EMF measurements, are compared with $\Delta G^o_f(UF_3)$, calculated from the calorimetric values $C_p(T)$, $S^o_{298.15}$ and $\Delta H^o_{298.15}$. It has been concluded that U,UF_3 electrodes are not suitable as reference electrodes due to difficulties in determining the activity of uranium.

In nuclear technology there is a need for reliable thermodynamic data on fission products involving plutonium, such as $PuMe_3$ compounds. In chapter V different models to predict the stabilities of intermetallic compounds involving transition metals have been presented. A simple estimation model was used, based on the Engel-Brewer theory and the

enthalpies of sublimation of pure metals in an intermetallic compound. Comparison of the experimental data for $\Delta H_f^o(UMe_3, c, 298.15\ K)$ with estimates using this model showed excellent agreement. The model was able to predict the enthalpies of formation of the UMe_3 compounds to within 10 percent of the experimentally determined values. For this reason the model was also applied to predict the enthalpies of formation of $PuMe_3$ and $ThMe_3$ compounds. The estimates for $\Delta H_f^o(UMe_3, c, 298.15\ K)$ of Miedema et al. appeared to be too positive compared with the experimental data.

In chapter VI the tabulation of the thermochemical data of the UMe_3 compounds is presented. The results of the low-temperature heat capacity measurements from 5 to 350 K, using adiabatic cryogenic calorimetry, have been combined with the high-temperature heat-capacity measurements of the UMe_3 compounds, using diphenyl ether drop-calorimetry. The high-temperature heat capacity measurements have been described in chapter VI, and the enthalpy increments $(H^o(T) - H^o(298.15\ K))$ of the UMe_3 compounds have been expressed by polynomials. Using the enthalpy increment functions, the heat capacity and entropy functions can be calculated.

The enthalpies of formation of URh_3 and URu_3 at 298.15 K have been calculated from a "third law" analysis of these measurements. Combining these data with the $\Delta H_f^o(298.15\ K)$ data of the UMe_3 compounds, as determined in this thesis, the $\Delta H_f^o(T)$ and $\Delta G_f^o(T)$ functions can be calculated.

Finally, a thermochemical model was set up to describe plutonium enrichment in $(U,Pu)Me_3$ inclusions as a function of the O/(U + Pu) and the U/(U + Pu) ratio in oxide fuel. With this model it has been calculated that a considerable plutonium enrichment occurs in $(U,Pu)Me_3$ in a narrow stoichiometry range in $(U,Pu)O_{2\pm x}$ fuel, close to O/(U + Pu) = 2.

SAMENVATTING

Dit proefschrift behandelt de bepaling van de thermodynamische eigenschappen van de intermetallische verbindingen van uranium met de lichte platinametalen, ruthenium, rhodium en palladium. Deze intermetallische verbindingen worden in een nucleaire snelle reactor als zeer stabiele vaste oplossingen tijdens splijting door middel van de reactie van de splijtingsproducten Ru, Rh en Pd met de splijtstofmatrix gevormd. In $(U,Pu)O_2$ splijtstof werden deze splijtingsproducten geïdentificeerd als $(U,Pu)Me_3$ fasen (Me = Pd,Rh,Ru), waarin dikwijls plutoniumverrijking werd gevonden in vergelijking met de Pu/U verhouding in de matrix. Deze fasen lossen niet op tijdens het opwerkingsproces van de splijtstof, waardoor plutoniumverliezen optreden, zoals wordt beschreven in hoofdstuk I.

Methoden voor de bereiding van URu_3, URh_3 en UPd_3, experimenten ter bestudering van de chemische reactiviteit van deze verbindingen en van de stoichiometrie van hexagonaal UPd_3 met röntgendiffraktie door middel van oplosbaarheids proeven van UN en palladium in UPd_3, zijn beschreven in hoofdstuk II.

De thermodynamische eigenschappen van de UMe_3 verbindingen werden verkregen door gebruik te maken van verschillende thermodynamische technieken: fluor bomcalorimetrie, lage-temperatuur cryogene calorimetrie, hoge temperatuur valcalorimetrie en EMK metingen aan reversibele galvanische cellen. De fluor bomcalorimetrische techniek wordt beschreven in hoofdstuk III, gevolgd door de bepaling van de vormingsenthalpieën van UF_4, UF_3, $Pd(PdF_6)$ en UPd_3 met fluor bomcalorimetrie en PF_3 reductiecalorimetrie.

In hoofdstuk IV wordt de vaste-stof EMK-techniek, met CaF_2 als electroliet, beschreven. De vrije vormingsenthalpieën van URh_3, URu_3 en UF_3 werden bepaald door van deze techniek gebruik te maken. De vrije vormingsenthalpieën van UF_3, verkregen met EMK metingen, worden vergeleken met $\Delta G^o_f(UF_3)$, berekend met de calorimetrische waarden $C_p(T)$, $S^o_{298.15}$ en $\Delta H^o_{298.15}$. Er wordt geconcludeerd dat U,UF_3 electroden niet geschikt zijn als referentie-electroden omdat het moeilijk is de activiteit van uranium precies te bepalen.

In nucleaire technologie bestaat behoefte aan betrouwbare thermodynamische gegevens betreffende splijtingsproducten die plutonium bevatten,

zoals $PuMe_3$ verbindingen. In hoofdstuk V worden verschillende modellen besproken om de stabiliteiten van intermetallische verbindingen, die betrekking hebben op de overgangsmetalen, te voorspellen. Een eenvoudig voorspellingsmodel werd gebruikt, gebaseerd op de Engel-Brewer theorie en de sublimatie-enthalpieën van de zuivere metalen in een intermetallische verbinding. Vergelijking van de experimentele gegevens voor $\Delta H_f^o(UMe_3, c, 298.15\ K)$ met schattingen die van dit model gebruik maken toont een goede overeenkomst aan. Het model is in staat de vormingsenthalpieën van deze UMe_3 verbindingen binnen 10 procent van de experimenteel bepaalde waarden te voorspellen. Om deze reden werd het model ook gebruikt om de vormingsenthalpieën van $PuMe_3$ en $ThMe_3$ verbindingen te voorspellen. De schattingen van $\Delta H_f^o(UMe_3, c, 298.15\ K)$ van Miedema et al. bleken te positief te zijn vergeleken met de experimentele waarden.

In hoofdstuk VI wordt de tabellering van de thermochemische gegevens van de UMe_3 verbindingen gegeven. De resultaten van de lage-temperatuur soortelijke warmte metingen van 5 tot 350 K met behulp van adiabatische cryogene calorimetrie, werden gecombineerd met de hoge-temperatuur enthalpie-increment metingen van de UMe_3 verbindingen met behulp van diphenyl ether valcalorimetrie.

De hoge-temperatuur enthalpie-increment metingen worden beschreven in hoofdstuk VI en de enthalpie-incrementen $[H^o(T) - H^o(298.15\ K)]$ van de UMe_3 verbindingen worden beschreven met behulp van polynomen. De soortelijke warmte en entropiefuncties kunnen direct uit de enthalpie increment functies worden berekend. De vormingsenthalpieën van URh_3 en URu_3 bij 298.15 K werden met behulp van een "3de hoofdwet" analyse van deze metingen bepaald. Wanneer deze waarden gecombineerd worden met de $\Delta H_f^o(298.15\ K)$ waarden van de UMe_3 verbindingen, zoals bepaald in dit proefschrift, kunnen de $\Delta H_f^o(T)$ en de $\Delta G_f^o(T)$ functies worden berekend. Tenslotte werd een thermochemisch model opgezet om plutoniumverrijking in $(U,Pu)Me_3$ insluitsels te beschrijven als een functie van de O/(U+Pu) en de U/(U+Pu) verhouding in oxidische splijtstof. Met dit model werd berekend dat een aanzienlijke plutoniumverrijking kan plaatsvinden in $(U,Pu)Me_3$ in een klein homogeniteitsgebied bij O/(U+Pu) = 2 van de $(U,Pu)O_{2\pm x}$ splijtstof.

LIST OF SYMBOLS

Symbol	Meaning	Common Units or Value
a	activity	-
B	second virial coeffient in an equation of state in the form: $p\bar{V} = A + Bp + Cp^2 + Dp^3$	$cm^3\ mol^{-1}$
bcc	body-centered cubic structure	-
C	d-band center of gravity	eV
C_p^o	standard molar heat capacity at constant pressure	$J\ K^{-1}\ mol^{-1}$
C_v^o	standard molar heat capacity at constant volume	$J\ K^{-1}\ mol^{-1}$
c	concentration	$mol\ dm^{-3}$
D	diffusion coefficient	$cm^2\ sec^{-1}$
d	d orbitals or d electrons	
E	electromotive force (EMF)	V
e	charge on electron	$1.6021982 \cdot 10^{-19} C$
F	Faraday's constant ($=N_A e$)	$96484.57\ J\ V^{-1}\ eq^{-1}$
f	f orbitals or f electrons	-
fcc	face-centered cubic structure	-
ΔG_f^o	standard Gibbs energy of formation	$J\ mol^{-1}$
$\overline{\Delta G}_f$	partial molar Gibbs energy of formation	$J\ mol^{-1}$
$\overline{\Delta G}_{O_2}$	oxygen potential in (U,Pu) oxide fuel	$J\ mol^{-1}$
$H^o(298.15)$	standard enthalpy at 25 °C	$J\ mol^{-1}$
$H^o(T)-H^o(298.15)$	enthalpy increment	$J\ mol^{-1}$
ΔH_b	bonding enthalpy	$J\ mol^{-1}$
ΔH_{mix}	enthalpy of mixing	$J\ mol^{-1}$

Symbol	Meaning	Common Units or Value
ΔH_{pr}	promotion enthalpy	J mol^{-1}
ΔH_{subl}	enthalpy of sublimation	J mol^{-1}
ΔH_f^o	standard enthalpy of formation	J mol^{-1}
hcp	hexagonal close-packed structure	-
M	molar mass	mol
m	mass	g
N	d band electron count	-
N_A	Avogadro constant	$6.022045 \cdot 10^{23}$ mol^{-1}
n	neutron	-
n_1, n_2	mole fractions	
n_{ws}	electron density	d.u.($=10^2 kg^{0.5} cm^{-2.5}$)
p	pressure	kPa
p	p orbitals or p electrons	-
Q*	electronegativity	V
R	gas constant	8.3143 J K^{-1} mol^{-1}
$S^o_{298.15}$	standard entropy at 25 °C	J K^{-1} mol^{-1}
ΔS_{mix}	entropy of mixing	J K^{-1} mol^{-1}
s	s orbital or s electrons	
T	absolute temperature	K, °C
t	time	sec(min,hr)
t_i, t_f	time at beginning or completion of reaction	sec(min,hr)
ΔU	heat of combustion or heat of reduction	J g^{-1}
ΔU_c^o	standard heat of combustion	J g^{-1}
V	volume	cm^3, or liters
W	d bandwidth	eV
w	mass fraction	-
X_1, X_2	fission products	-
x_1, x_2, x_3	mole fractions	-
ε(calor)	energy equivalent of the calorimetric system	J K^{-1}

Symbol	Meaning	Common Units or Value
θ	temperature of calorimeter	K
θ_o	temperature of thermostatted jacket	K
ϑ_c	convergence temperature	K
$\Delta\theta_c$	corrected temperature rise in calorimetric experiment	K
μ	coefficient in an equation of state in the form: $pV = n RT(1-\mu p)$, $\mu = - B/RT$	k Pa^{-1}
ν	amount of neutrons (about 2.5) during fission of U and Pu	-
ρ	density	g cm^{-3}
σ_{ac}	total conductivity	ohm^{-1} cm^{-1}
σ_e	electronic conduction	ohm^{-1} cm^{-1}